Dissertation

submitted to the

Combined Faculties of the Natural Sciences and Mathematics

of the Ruperto-Carola-University of Heidelberg, Germany

for the degree of

Doctor of Natural Sciences

Put forward by

Armen, Hayrapetyan

born in: Yerevan (Republic of Armenia)

Oral examination: May 28th 2014

Angular momentum representation of laser-driven matter waves: twisted electrons and atoms

Referees: Prof. Dr. Stephan Fritzsche

Priv.-Doz. Dr. Jörg Evers

Zusammenfassung

Die Physik der sogenannten Vortex-Strahlen ist ein neues, sich schnell entwickelndes Forschungsfeld, das vielfältige Themen umfasst, wie Optik, Quanteninformation und Materialwissenschaften. Die Vortex-Strahlen besitzen einen wohldefinierten Bahndrehimpuls entlang ihrer Propagationsrichtung, der zu helixförmigen Wellenfronten führt. Solche getwistete Strahlen von Licht und Elektronen wurden Anfang der 1990er beziehungsweise Ende der 2000er theoretisch vorhergesagt und im Experiment beobachtet. In dieser Doktorarbeit legen wir den Schwerpunkt auf einen speziellen Typ von Vortex-Strahlen, Bessel-Strahlen genannt. Wir untersuchen getwistete Materiewellen, wie Elektronen und Atome, die in einem Laserfeld propagieren. Wir entwickeln eine exakte analytische Beschreibung dieser Teilchenzustände, indem wir die Dirac-Gleichung durch Verallgemeinerung der kürzlich beschriebenen feldfreien Elektronen-Vortex-Strahlen lösen, mit dem Ziel die Wechselwirkung zwischen Vortex-Strahlen und dem Laserfeld zu untersuchen. Hierzu überlagern wir eine Vielzahl von Dirac-Wolkow-Wellenfunktionen mit wohldefinierten Amplituden, die zu einer mono-energetischen Verteilung der Elektronen in den Vortex-Strahlen mit einem nichtverschwindenden Bahndrehimpuls führt. Außerdem unternehmen wir eine detailierte Untersuchung eines anderen Typs von Materiewellen: Bessel-Strahlen aus Zwei-Niveau-Atome, die mit dem Laser-Licht resonant wechselwirken. Insgesamt demonstrieren wir, dass die Profile von Laser-beeinflussten Elektronen- und Atom-Vortex-Strahlen ein nicht triviales Verhalten, vom Typ einer quadrierten Besselfunktion, besitzen. Wir nehmen eine Momentaufnahme dieser Strahlprofile und zeigen, dass wir in der Lage sind, ihre Intensitätverteilung durch die Einstellung des Laserfeldes zu kontrollieren und zu manipulieren.

Abstract

Physics of vortex beams is a new, fast developing research field that covers diverse topics, such as optics, quantum information, materials science. Vortex beams are known to carry well-defined orbital angular momentum along their propagation direction that gives rise to their helical wavefronts. Such twisted beams of light and electrons have been discovered both theoretically and experimentally in the beginning of 1990s and in the end of 2000s, respectively. In this thesis, we put the emphasis on a special type of vortex beams, called Bessel beams, and present a theoretical study for twisted matter waves, such as electrons and atoms, that are driven by a laser. First, in order to examine the interaction of relativistic electron vortex beams (EVBs) with a laser light we obtain exact analytical solutions for Dirac equation by generalizing recently constructed (field-)free EVBs. To do so, we superimpose a multitude of Dirac-Volkov wave functions with well-defined amplitudes that correspond to the monoenergetic distribution of electrons in vortex beams with non-zero orbital angular momentum. Second, we extend our study of EVBs to another type of matter waves and produce Bessel beams of two-level atoms that resonantly interact with a laser light. Moreover, we demonstrate that the profiles of both the laser-driven electron and atomic vortex beams obtain a non-trivial, Bessel-squared-type behavior. We take a snapshot of these profiles and show that we are able to control and manipulate the intensity distribution of beams by tuning the laser field.

for my parents

This thesis includes the following papers:

- A.G. Hayrapetyan and S. Fritzsche, *Bessel beams of laser-driven two-level atoms* Phys. Scr. **T156**, 014067 (2013).
- A.G. Hayrapetyan, O. Matula, A. Surzhykov, and S. Fritzsche, *Bessel beams of two-level atoms driven by a linearly polarized laser field*, Eur. Phys. J. D **67**, 167 (2013).
  This publication was selected as the August 2013 highlight of "The European Physical Journal D".
- A.G. Hayrapetyan, O. Matula, A. Aiello, A. Surzhykov, and S. Fritzsche, *Interaction of relativistic electron vortex beams with few-cycle laser pulses*, Phys. Rev. Lett. **112**, 134801 (2014).
  This paper is selected as "PRL Editors' Suggestion".

The following papers were prepared during my PhD, but are not included in the thesis:

- A.G. Hayrapetyan, K.K. Grigoryan, R.G. Petrosyan, and S. Fritzsche, *Propagation of sound waves through a spatially homogeneous but smoothly time-dependent medium*, Ann. Phys. **333**, 47 (2013).
- O. Matula, A.G. Hayrapetyan, V.G. Serbo, A. Surzhykov, and S. Fritzsche, *Atomic ionization of hydrogen-like ions by twisted photons: angular distribution of emitted, electrons*, J. Phys. B: At. Mol. Opt. Phys. **46**, 205002 (2013).
  This publication was chosen as an Institute of Physics Select paper ("IOPselect").
- O. Matula, A.G. Hayrapetyan, V.G. Serbo, A. Surzhykov, and S. Fritzsche, *Radiative capture of twisted electrons by bare ions*, to appear in New J. Phys.

Contents

Introduction

Vortex beams

In optics, it is well known that circularly polarized light beams carry a non-zero *spin* angular momentum (SAM) of magnitude $\pm\hbar$, in units of the reduced Planck constant $\hbar = h/(2\pi)$. Here h is the famous Planck constant and the signs "$\pm$" represent the left- and right-circular polarizations, respectively. This spin degree of freedom for photons has been demonstrated by Beth already in 1930s [1, 2]. Surprisingly, only about 60 years later Allen and coworkers discovered that the linearly polarized light may also carry a *quantized* angular momentum $\ell\hbar$, defined along the propagation direction of the beam [3]. The quantity $\ell\hbar$ is a fundamentally new degree of freedom for photons and is often called (longitudinal) *orbital* angular momentum (OAM) or *topological charge* of light. The existence of the non-zero OAM yields to helical wavefronts of light. Such a wavefront rotates around the propagation axis while the Poynting vector draws a corkscrew and results in a vortex-type distribution of the field intensity. These optical *vortex* beams have a phase singularity (called also a topological defect or a wave dislocation) at their center, where the beam intensity is zero and the phase is undetermined. Generally it is considered, moreover, that ℓ takes integer values. However, the value of ℓ is not restricted to integer numbers only: the vortex structure of the beam is still present also for fractional OAM [4].

Since the seminal article [3] there was a growing interest in the angular momentum of light and its connection to the beam trajectory [5]. Quanta of light prepared in states with well-defined OAM are often called *twisted* photons [5–7]. Nowadays, such light beams have found a range of applications in optical manipulation [8–10], quantum information [11] and atomic physics [12–14], they have also led to recognizable advances in optical tweezers [15, 16]. Moreover, twisted photons are employed to transfer the OAM to a system of atoms [17–19] and to reveal the influence of OAM on beam shifts [20–23].

In the beginning of 1920s, Uhlenbeck and Goudsmit introduced the concept that electrons possess a spin angular momentum of magnitude $\pm\hbar/2$, a fundamental degree of freedom for quantum particles with no classical analogue [24, 25]. Since then properties of the electron spin and its influence upon different elementary and complex processes have been studied extensively, both in theory [26, 27] and in experiments [28, 29]. For example, the electron spin causes the Stern-Gerlach effect for electrons bound to an atom [30], is utilized to measure the dynamics of nuclear spins that weakly couple to electrons [31, 32]. One can also analyze the spin dynamics of electrons via the electron's self-interaction with its own radiation field [33] or via the Kapitza-Dirac scattering from a standing wave of a laser [34].

In contrast to the discovery of the electron spin, the story of *electron* vortex beams (EVBs) starts very recently and stems from the original work by Bliokh and coworkers [35]. In analogy with optical vortex beams, EVBs also carry a well-defined OAM along their propagation

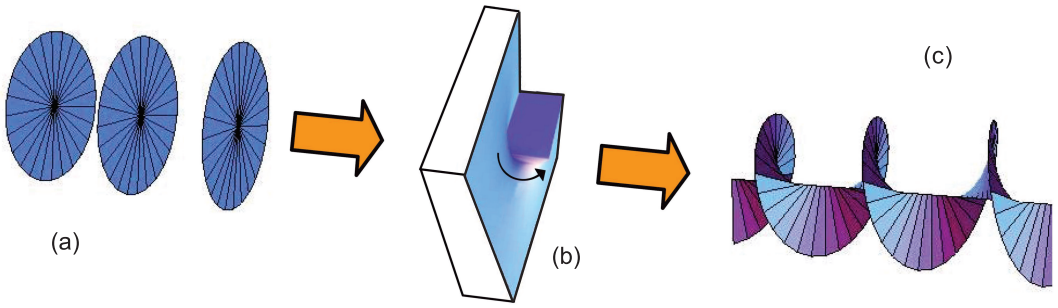

Figure 1: Generation of EVBs via a spiral phase plate, as depicted in [36]. (a) Wavefronts of plane-wave electrons, normal to their axis of propagation. (b) Spiral phase plate, thickness of which remains constant along the radial direction, while increases along the azimuthal direction (the curved arrow). (c) Wavefronts of EVB with a characteristic spiral-type shape.

direction. In Ref. [35], authors have shown that the Schrödinger equation can have a vortex-type solution describing the motion of a *twisted* electron in free space. This solution implies, moreover, that the current of the EVB coils around the electron's main (linear) momentum, a behavior, which is quite similar to the propagation of optical vortex beams with helical wavefronts.

EVBs have been experimentally generated – for the first time – in 2010, three years after their theoretical proposal, although the optical beams with phase singularities have been produced already in 1990s. Due to the short wavelength of electrons, nanoscale diffraction gratings were needed in order to create twisted electron beams with a subnanometer spot size. This technical challenge has been solved by Uchida and Tonomura [36] when they have nanofabricated a graphite thin film with continuously changing thickness. Such *spiral phase plates* were originally used in optics [37, 38] in order to generate laser beams with helical wavefronts. For 300 keV electrons in transmission electron microscope, the spiral

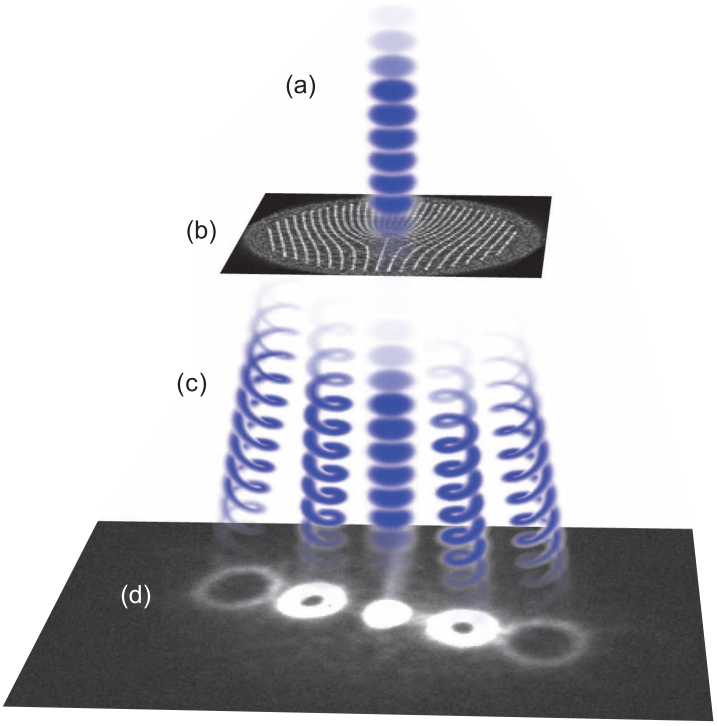

Figure 2: Production of EVBs via a computer generated "fork"-like hologram, as depicted in Ref. [40]. Spatially coherent plane-wave electrons (a) are incident on the nanofabricated "fork"-like hologram (b) where they diffract into multiple EVBs (c), that are imaged (d) using a so-called charge-coupled device. The circles show the measured electron intensity distributions corresponding to different ℓ. The depiction of plane-wave and twisted electrons simulate their wavefronts and *not* the trajectories.

phase plate has a step height of about 84 nm, as used in [36]. When the plane-wave passes through such a plate (that has some "Y"-like pattern) a helical wavefront character is imprinted on the plane-wave, where the phase singularity at the core of the beam is generated [cf. Fig. 1]. Different magnitudes of OAM $\ell\hbar$ could be obtained by changing the height or the material of the spiral phase plate. However, the experiment [36] was limited to a low magnitude of ℓ because of the absorption of electrons in the plate that otherwise would become too thick. This disadvantage has been soon eliminated in subsequent works [39, 40], where a new approach with the so-called *computer generated hologram* has been applied, again, by borrowing the analogous idea from optics [41, 42]. The advantage of this technique over spiral phase plates is that the diffracted beam automatically possesses integer ℓ. In order to create computer generated holograms one has to define (i) the target or the outcome, which is the vortex beam, and (ii) the incoming plane wave vector [cf., e.g., [39]]. These target and reference waves are further employed in an inverse interference problem to compute a virtual hologram that has a "fork"-like shape. When the hologram is ready it is then transformed into a binary mask to create EVBs. Such masks can be easily produced from a thin platinum foil (with a thickness of $\sim$ 100 nm) and provide a complete control over the beam characteristics, such as the phase and the amplitude. When the plane-wave electron is incident on the "fork"-like hologram, the diffracted beams propagate at discrete angles relative to each other and form even number sidebands with OAM $\pm\ell\hbar$ and the central band $\ell\hbar = 0$ [cf. Fig. 2]. In order to generate isolated EVBs one has to use holograms with sufficiently small grating periods, e.g., $50 \div 100$ nm. By decreasing the size of the period one can produce EVBs with various amounts of topological charge enabling to demonstrate beams with OAM up to $100\hbar$ [40]. In addition, the technique with computer generated holograms is nowadays widely used to enhance the resolution in studying magnetic and biological materials (twisted electron microscopy) [43], to further explore the Larmor and Gouy rotations of an EVB in a magnetic field [44]

In above mentioned experiments, (i) the electron beams were well-collimated such that their propagation was described within the so-called *paraxial* regime, and moreover, (ii) the spin degree of freedom – the SAM – of electrons did not manifest itself in the beam profile. In order to (theoretically) take into account the electron spin, however, one has to deal with the Dirac equation that describes the *relativistic* motion of electrons. It was again Bliokh *et al.* [45], who constructed vortex-type solutions – this time – for the Dirac equation to demonstrate that, apart from the SAM, the relativistic twisted electron carries also a non-zero OAM. The authors have shown, moreover, that for electrons with relatively high energies of about 800 keV and for the non-collimated, i.e. *non-paraxial*, regime of the beam propagation, the presence of both SAM and OAM gives rise to an *intrinsic* spin-orbit interaction (SOI) in the EVB. This SOI leads to a spin-dependent distribution of the EVB intensity, an effect that should be experimentally observable [46,47]. The idea of the intrinsic SOI dates back into 1990s when the investigations by Allen *et al.* eventually led to the discovery of the coupling that may occur between the angular momentum (either spin or orbital) and the linear momentum of a beam of light [cf., e.g., [48]]. The SOI can take various forms in different systems, but the unifying feature in all cases is the coupling between the spin and the momentum of the particle [48]. Nowadays, the SOI especially for optical vortex beams – called also "SAM-to-OAM conversion" – is quite thoroughly studied for various types of beams, such as the so-called *Laguerre-Gauss* [49] and *Bessel* beams [50]. These analytical functions and their superpositions are presently known to adequately describe the theory of vortex beams, both optical and matter.

Throughout this thesis, we put the emphasis only on Bessel beams in order to theoretically discuss twisted electrons and atoms that interact with a (*non-twisted*) light beam. A Bessel beam of any particle represents a special type of vortex beam that carries a well-defined OAM. The wave function of Bessel beams is mathematically described by means of the Bessel function of the first kind which is a solution to the so-called full Helmholtz equation. This is in contrast to the Laguerre-Gauss modes, which are a solution only to the paraxial form of the Helmholtz equation [cf., e.g., Ref. [51]]. Thus, the advantage of using of Bessel beams is that they ab initio involve both the paraxial and non-paraxial regimes of the beam propagation. The profile (which represents the transverse structure) of Bessel beams is independent of the longitudinal coordinate that is aligned along the beam propagation direction. This means that the beam do not spread out while it propagates forward, as first noted by Durnin [52]. Due to this feature, Bessel beams are also called *non-diffracting* or *diffraction-free*. The profile of the ideal Bessel beam can contain an infinite number of *concentric circles*, as seen below, meaning that an infinite area would carry an infinite power. However, Durnin and co-workers showed that one could experimentally make an approximation to a Bessel beam (a quasi-Bessel beam) which possesses the properties of the mathematical entity over a finite distance [53]. In this first experiment, authors could create a (zeroth order) Bessel beam of light that does not spread over the distance of ~ 40 cm. We refer the reader to Refs. [54–56] and [57] for further insight about how to create optical Bessel beams of higher order ℓ and with a more complex structure, respectively. Recently, moreover, non-diffracting Bessel beams of electrons have been also generated that propagate for 60 cm without a measurable spread [58]. Finally, Bessel beams have another intriguing property: they can be partially obstructed at one point, due to some external distortions, but will eventually re-form at a further point of the beam axis. This effect is called *self-healing* studied both experimentally [59–61] and theoretically [62, 63].

Scalar Bessel beams in free space: a theoretical construct

Before to start with our theory, we introduce here a recipe how to theoretically construct Bessel beams by employing the superposition principle of linear, both relativistic and non-relativistic quantum theories. We illustrate this construction for free propagating *scalar* waves by considering a particle without spin. The existence of the spin would lead to the so-called *vector* Bessel beams, as we will study quite in detail in the first part of this thesis.

A Bessel beam of any quantum particle is defined as a twisted state with its well defined energy $\mathcal{E}_0$, longitudinal momentum $p_{||0}$, absolute value of the transverse momentum $p_{\perp 0}$ as well as the quantized projection $\ell\hbar$ of the OAM on the propagation axis [cf., e.g., [45]]. Vortex beams exhibit a particular phase structure that is incorporated by the phase factor $e^{i\ell\phi}$ in the "spectrum" (or the momentum distribution) of the Bessel beam

$$\tilde{\psi}_\ell(\boldsymbol{p}) \;=\; \delta(p_\perp - p_{\perp 0}) \frac{e^{i\ell\phi}}{2\pi i^\ell p_{\perp 0}}, \tag{1}$$

where $\phi \in [0, 2\pi)$ is the azimuthal angle of $p_{\perp 0}$, ℓ is an integer, and moreover, the denominator is present for mathematical convenience. Equation (1) means that the particle has a *monoenergetic* distribution of momentum over some cone with a slant length

$$p_0 \;=\; \sqrt{{p_{||0}}^2 + p_{\perp 0}^2} \;=\; const \tag{2}$$

and a fixed polar (opening) angle θ_0 with respect to the beam propagation direction which we choose to be the z-axis [cf. Fig. 3 (a)]. The opening angle of this cone is defined as

$$p_{||0} \;=\; p_0 \cos\theta_0 \,, \quad p_{\perp 0} \;=\; p_0 \sin\theta_0 \,. \tag{3}$$

It is sufficient to write only one δ-function in Eq. (1) to indicate the conservation of energy and longitudinal and transverse components of the linear momentum. Indeed, expressions (2)-(3) and the δ-function $\delta\left(p_\perp - p_{\perp 0}\right)$ result in the conservation of longitudinal momentum, i.e. $\delta\left(p_{||} - p_{||0}\right)$. If we also take into account the known, non-relativistic

$$p_0^2 \;\;=\;\; 2m\mathcal{E}_0 \tag{4}$$

or relativistic

$$c^2 p_0^2 \;\;=\;\; \mathcal{E}_0^2 + m^2 c^4 \tag{5}$$

energy-momentum relations, the necessity is eliminated to include another $\delta\left(\mathcal{E} - \mathcal{E}_0\right)$ in the Bessel spectrum (1). In Eqs. (4)-(5), moreover, m is the mass of the particle and c is the speed of light.

Owing to the *conical* symmetry of the momentum distribution, we shall use cylindrical coordinates $\boldsymbol{p} \;=\; (p_\perp, \phi, p_{||}) \;=\; (p\sin\theta, \phi, p\cos\theta)$ in momentum space and construct Bessel beams

$$\psi_\ell\left(\boldsymbol{r}, t\right) \;\;=\;\; \int \tilde{\psi}_\ell\left(\boldsymbol{p}\right)\, \psi_p\left(\boldsymbol{r}, t\right) p_\perp \mathrm{d}p_\perp \mathrm{d}\phi \tag{6}$$

of either non-relativistic or relativistic particles as a superposition of their orthogonal wave functions ψ_p over the distribution (1). For these particles, the functions ψ_p correspondingly represent solutions of linear differential equations that are usually referred as the Schrödinger and the Dirac equations. For example, in order to examine the free propagation of scalar particles, we have to deal with the free-wave equation

$$\left(\boldsymbol{\nabla}^2 - \frac{1}{v^2}\frac{\partial^2}{\partial t^2}\right) \psi_p\left(\boldsymbol{r}, t\right) \;\;=\;\; 0 \,, \tag{7}$$

where $\boldsymbol{\nabla}^2 \equiv \Delta$ is the Laplace differential operator that is expressed via $\partial^2/\partial x^2 + \partial^2/\partial y^2 + \partial^2/\partial z^2$ in Cartesian coordinates (x, y, z). The constant v is usually associated with the velocity of propagation of the wave in free space. Furthermore, the *plane-wave* solution of the free-wave equation is given by

$$\psi_p\left(\boldsymbol{r}, t\right) \;=\; \psi^{\mathrm{PW}}\left(\boldsymbol{r}, t\right) \;=\; \sqrt{\mathcal{N}} e^{\frac{i}{\hbar}\left(\boldsymbol{p}\cdot\boldsymbol{r} - \mathcal{E}t\right)} \,, \tag{8}$$

where $\mathcal{N}$ is some normalization constant. We can employ this form in order to construct Bessel-type solutions of Eq. (7) by using cylindrical coordinates also in real space, $\boldsymbol{r} = (r, \varphi, z)$, due to the cylindrical symmetry of the beam propagation. The integral (6) can be readily calculated if we re-write the scalar product in the phase of the plane-wave, Eq. (8), as

$$\boldsymbol{p}\cdot\boldsymbol{r} \;\;=\;\; p_\perp r\cos\left(\phi - \varphi\right) + p_{||} z \tag{9}$$

and exploit the integral representation of the Bessel function, Ref. [64],

$$\int_0^{2\pi} \mathrm{d}\phi\; e^{i\ell\phi}\, e^{i\xi\cos(\phi-\varphi)} \;\;=\;\; 2\pi i^\ell e^{i\ell\varphi} J_\ell\left(\xi\right) \,. \tag{10}$$

Direct integration simply leads to the wave function of the scalar Bessel beam

$$\psi_{\ell}^{\text{free}}(\boldsymbol{r},t) \;=\; \sqrt{\mathcal{N}}e^{\frac{i}{\hbar}(p_{||0}z-\mathcal{E}_0 t)}\,e^{i\ell\varphi}J_{\ell}(\xi)\;, \tag{11}$$

where $\xi = p_{\perp 0}r/\hbar$ is the dimensionless transverse coordinate which characterizes the *width* of the beam. The wave function (11) is orthogonal. The normalization constant can be found if we integrate the squared modulus $|\psi_{\ell}^{\text{free}}|^2$, for instance, over a large, but finite cylindrical volume (see the Appendix of Ref. [65]). For our further analyzes, however, the normalization is not of a crucial interest. Thence, we will drop the pre-factor $\mathcal{N}$ and evaluate all forthcoming figures in arbitrary units. In addition, it is worth to mention that Eq. (11) can be derived also from the free-wave equation (7) if we solve it in cylindrical coordinates, by reducing to the full Helmholtz equation [51].

Equation (11) describes the main properties of scalar Bessel beams of (field-)free particles. The wave function $\psi_{\ell}(\boldsymbol{r},t)$ represents a delocalized beam that propagates freely along the z-direction, $e^{ip_{||0}z/\hbar}$, and does not spread out. Indeed, we can easily demonstrate that the distribution of the beam probability density has a simple, Bessel-squared-shape in the radial dimension

$$\rho_{\ell}^{\text{free}}(\xi) \;\equiv\; |\psi_{\ell}^{\text{free}}(\boldsymbol{r},t)|^2 \;=\mathcal{N}J_{\ell}^2(\xi)\;. \tag{12}$$

This z-independent form exhibits the diffraction-free propagation of ideal Bessel beams. The transverse distribution of the probability density, that represents concentric circles, remains invariant under the transformation $\ell \to -\ell$, i.e.

$$\rho_{\ell}^{\text{free}} \;=\; \rho_{-\ell}^{\text{free}}\,, \tag{13}$$

as also illustrated in Figs. 3 (b)-(c). Moreover, the probability density vanishes at the beam center ($\xi = 0$) for all non-zero values of the longitudinal OAM, since $J_{\ell}(0) = 0$ for $\ell \neq 0$. This reflects the vortex nature of the Bessel beam: zero intensity $\rho_{\ell}^{\text{free}} = 0$ and undetermined phase $\ell\varphi$ at $\xi = 0$.

The vortex phase factor $e^{i\ell\varphi}$ ensures that the scalar Bessel beam (11) is an eigenstate of the z-component of canonical OAM operator $\hat{\mathcal{L}}_z$ that has the form

$$\hat{\mathcal{L}}_z \;=\; (\boldsymbol{r}\times\hat{\boldsymbol{p}})_z \;=\; -i\hbar\frac{\partial}{\partial\varphi} \tag{14}$$

in the coordinate representation. Here "$\times$" means vector product and

$$\hat{\boldsymbol{p}} \;=\; -i\hbar\boldsymbol{\nabla} \;=\; -i\hbar\left(\boldsymbol{e}_x\frac{\partial}{\partial x}+\boldsymbol{e}_y\frac{\partial}{\partial y}+\boldsymbol{e}_z\frac{\partial}{\partial z}\right) \tag{15}$$

is the linear momentum operator, where $(\boldsymbol{e}_x\,,\boldsymbol{e}_y\,,\boldsymbol{e}_z)$ are the unit vectors in the Cartesian coordinate system. One can readily check that the corresponding eigenvalue of the operator $\hat{\mathcal{L}}_z$ is the longitudinal OAM $\ell\hbar$, i.e.

$$\hat{\mathcal{L}}_z\psi_{\ell}^{\text{free}} \;=\; \ell\hbar\,\psi_{\ell}^{\text{free}}\,. \tag{16}$$

This reflects the existence of the well-defined OAM along the propagation direction of the beam. As we introduced before, being a fundamentally new degree of freedom for free particles, the OAM $\ell\hbar$ of Bessel beams can nowadays be observed in experiments especially with photons [54] and, very recently, with electrons as well [58].

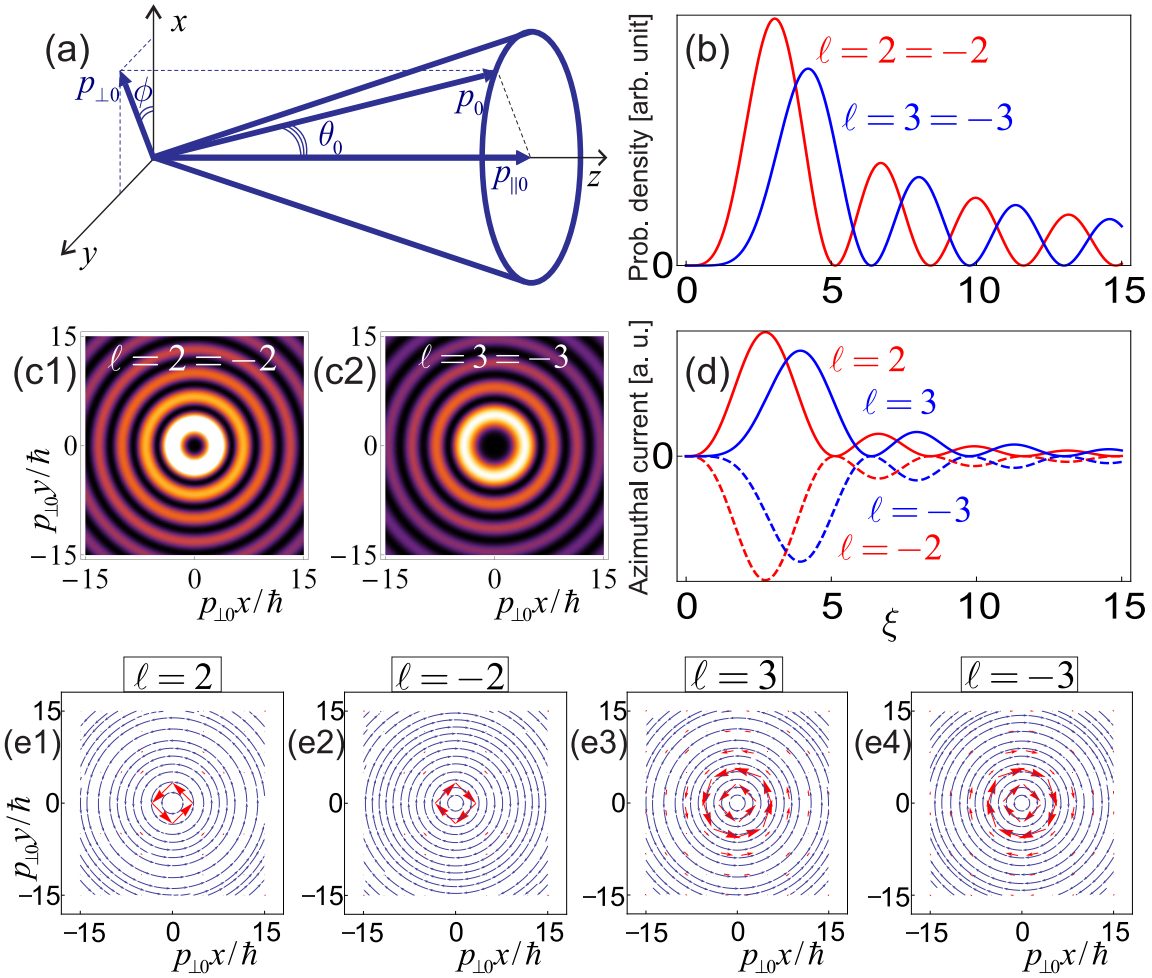

Figure 3: Basic characteristics of Bessel beams. (a) Cone of monoenergetic distribution of the linear momentum, z-axis is chosen along the beam propagation. (b) Distribution of probability density $\rho_\ell^{\rm free}$ (in arbitrary units) of a free propagating scalar Bessel beam as a function of the dimensionless transverse coordinate ξ. Red (blue) curves correspond to the particle's longitudinal OAM $2\hbar$ and $-2\hbar$ ($3\hbar$ and $-3\hbar$). (c) Snapshots of non-diffracting beam profile for different values of OAM, shown by the variation of colors from black to white within the "sunset" scale. Black and white correspond to the minimum and maximum values of the probability density. (d) Distribution of the azimuthal current $j_\ell^{(\varphi)\rm free}$ (in arbitrary units) of the field-free scalar Bessel beam as a function of ξ. Solid (dashed) lines correspond to the positive (negative) values of the OAM. (e) Streamlines and vector-plots show the direction of the transverse current of a scalar particle, $\boldsymbol{j}_\ell^{\rm tr,\,free}(x\,,y\,,t)$, evaluated for $\ell = \pm 2$ (e1-2) and $\ell = \pm 3$ (e3-4). The thickness of red vectors shows the strength of the current, the thickest vectors indicate the circles where the electronic distribution has a maximum. In Figs. (c) and (e), moreover, the beam propagates toward the reader.

In order to introduce another important feature – the *twisting* motion – of vortex beams, we further construct the current of the scalar Bessel beam defined as [66]

$$\boldsymbol{j}_{\ell}^{\text{free}} \;=\; \Re\left[(\psi_{\ell}^{\text{free}})^{*}\,\frac{\hbar}{im}\boldsymbol{\nabla}\psi_{\ell}^{\text{free}}\right],$$

where "asterisk" means complex conjugate. Since the wave function (11) is expressed in cylindrical coordinates it is now convenient to represent the differential operator $\boldsymbol{\nabla}$ as

$$\boldsymbol{\nabla} \;=\; \boldsymbol{e}_{r}\frac{\partial}{\partial r}+\boldsymbol{e}_{\varphi}\frac{1}{r}\frac{\partial}{\partial\varphi}+\boldsymbol{e}_{z}\frac{\partial}{\partial z} \;=\; \boldsymbol{e}_{r}\frac{p_{\perp 0}}{\hbar}\frac{\partial}{\partial\xi}+\boldsymbol{e}_{\varphi}\frac{p_{\perp 0}}{\hbar\xi}\frac{\partial}{\partial\varphi}+\boldsymbol{e}_{z}\frac{\partial}{\partial z},$$

where $(\boldsymbol{e}_{r}\,,\boldsymbol{e}_{\varphi}\,,\boldsymbol{e}_{z})$ are the unit vectors in the longitudinal, azimuthal and radial directions, respectively. By employing this form we can easily calculate the current of the Bessel beam and show that it acts as a sum of the *longitudinal* and *transverse* components

$$\boldsymbol{j}_{\ell}^{\text{free}}(\xi) \;=\; \boldsymbol{j}_{\ell}^{\text{long, free}}(\xi)+\boldsymbol{j}_{\ell}^{\text{tr, free}}(\xi)\,. \tag{17}$$

The longitudinal (component of) the current

$$\boldsymbol{j}_{\ell}^{\text{long, free}}(\xi) \;=\; v_{||0}\rho_{\ell}^{\text{free}}(\xi)\,\boldsymbol{e}_{z} \tag{18}$$

is responsible for the free propagation of the beam along the direction of the linear momentum $p_{||0}$, chosen to be the z-axis. This is quite similar to the plane-wave-type motion, a propagation with a velocity $v_{||0}=p_{||0}/m$ and an intensity distribution $\rho_{\ell}^{\text{free}}$. In contrast, the transverse current

$$\boldsymbol{j}_{\ell}^{\text{tr, free}}(\xi) \;=\; \frac{p_{\perp 0}\ell}{m\xi}\rho_{\ell}^{\text{free}}(\xi)\,\boldsymbol{e}_{\varphi} \;=\; \frac{\ell\hbar}{mr}\rho_{\ell}^{\text{free}}(r)\,\boldsymbol{e}_{\varphi} \tag{19}$$

gives rise to a *new* type of motion of particles inside the wave packet in the radial direction. To show this, we note that the transverse current has an azimuthal (or tangential) component

$$j_{\ell}^{(\varphi)\text{free}}(r) \;=\; \frac{\ell\hbar}{mr}\rho_{\ell}^{\text{free}}(r)\,, \tag{20}$$

proportional both to the reduced Planck constant $\hbar$ and the topological charge ℓ, but no radial component, i.e. $j_{\ell}^{(r)\text{free}}=0$. This means that the current *coils* around the "main" direction of the linear momentum along the concentric circles, as shown in Figs. 3 (e1-4). Moreover, the transverse (azimuthal) current changes its sign when $\ell\to-\ell$:

$$\boldsymbol{j}_{\ell}^{\text{tr, free}} \;=\; -\boldsymbol{j}_{-\ell}^{\text{tr, free}}\,, \quad j_{\ell}^{(\varphi)\text{free}} \;=\; -j_{-\ell}^{(\varphi)\text{free}}\,. \tag{21}$$

For positive (negative) ℓ such a rotating motion occurs counterclockwise (clockwise) with respect to the reader. This implies that the particle "trajectories" inside the Bessel beam are effectively a spiral in free space, identical to an analogue motion of scalar particles inside the Laguerre-Gauss beams [35]. A similar behavior, moreover, is characteristic for the Poynting vector of optical vortex beams that can be associated with a helical or twisted wavefront [3,5].

There is a relativistic quantum analogy that also explains the twisting motion of particles. The existence of the transverse current can be regarded as a *Zitterbewegung* of particles due to their OAM, a trembling motion of a force-free particle [35]. Such a motion vanishes in the classical limit $\hbar\to 0$ [66] and/or when $\ell\to 0$. In addition, we can recover the plane-wave behavior of particles from Eqs. (11), (12), (17)-(20) by setting limiting values for the polar angle

$\theta_0 \to 0$ (or the transverse momentum $p_{\perp 0} \to 0$) and the OAM $\ell\hbar \to 0$. We will end up with Eq. (8), and expressions $\rho^{\mathrm{PW}} = \mathcal{N}$, $\boldsymbol{j}^{\mathrm{PW}} = \boldsymbol{j}^{\mathrm{long,\,PW}} = \boldsymbol{e}_z p_0 \mathcal{N}/m$ and $\boldsymbol{j}^{\mathrm{tr,\,PW}} = \boldsymbol{e}_\varphi j^{(\varphi)\mathrm{PW}} = 0$, as one would expect.

Both the existence of the non-zero OAM and the diffraction-free propagation – that may occur, especially, in non-paraxial domain – make the Bessel beams attractive to researchers. Recent discoveries of vortex beams of electrons motivated us to further analyze the properties of electron Bessel beams and their behavior inside an electromagnetic field. Moreover, we go a step forwards and explore also another type of twisted waves, such as the *atomic* Bessel beams and their interaction with a laser light. The external electromagnetic field which we apply throughout our study acts as an additional "apparatus" that enables us to drive and, therefore, to manipulate matter vortex beams.

In this thesis, we describe Bessel beams of electrons and atoms that are driven by a laser light. **In the first part of the thesis**, we study the interaction of relativistic twisted electrons with a laser light. We pay a particular attention to the OAM-properties of such electrons and demonstrate that the spin- and orbital-degrees of freedom give rise to the intrinsic SOI inside the (vector) Bessel beam of electrons. Furthermore, we explore how this intrinsic SOI is modified within a linearly polarized, *few-cycle laser pulse*. To do so, we generalize the field-free wave functions of EVBs, as reported in Ref. [45], to the field-affected ones. Based on these generalized solutions, we calculate the probability density and the current components of Bessel beams of electrons in order to reveal the influence of the laser field on the electron beam dynamics. Particularly, we demonstrate the *shift* of the center of the field-affected EVB with respect to the center of the field-free EVB. We also show that this shift is accompanied with a finite probability for finding an electron at the *dark* center of the initially field-free beam. **In the second part of the thesis**, we extend the study of EVBs to another type of matter vortex beams and create a theoretical construct for *atomic* Bessel beams that are resonantly driven by a *monochromatic plane-wave electromagnetic field*. Such a resonant interaction allows us to approximate the atom as a *two-level* system. We furthermore assume that the two-level atom moves with a velocity far below the speed of light and determine its states in the field by taking into account the propagation direction of both atomic and laser beams. For such laser-driven two-level atoms, we construct atomic vortex beams, by using the plane-wave decomposition of the Bessel-beam atomic state. We calculate the probability density of these beams and show that it exhibits a non-trivial, Bessel-squared-type behavior. We demonstrate how one can control the profile of laser-driven Bessel beams of atoms, by tuning the parameters of the "atom + laser" system. To this end, we spatially and temporally characterize the profiles of Bessel beams of hydrogen and selected neutral alkali-metal atoms. The developed theory enables us to conclude that the two main characteristics of (laser-driven atomic) Bessel beams are fulfilled: (i) they carry a non-zero longitudinal OAM and (ii) experience a non-diffracting propagation.

Part I

Angular momentum representation of laser-driven relativistic electrons

In the first part of this thesis, we construct a relativistic theory of electron vortex beams that interact with a plane-wave electromagnetic field. For this purpose, we divide the current part into two chapters.

In chapter 1, we describe the dynamics of relativistic plane-wave electrons within an external field. To do so, in section 1.1, we start from the Dirac equation for free electrons and introduce the free-electron wave function (subsection 1.1.1) along with the so-called Dirac algebra (subsection 1.1.2), relevant for our further calculations. Next, in section 1.2, we "switch on" the laser field and examine the behavior of electrons within this field. Particularly, we introduce the Dirac equation for field-affected electrons (subsection 1.2.1) and obtain the well-known Dirac-Volkov solutions (subsection 1.2.2).

In chapter 2, we derive the theory of laser-driven relativistic electron vortex beams that carry both spin- and orbital-angular momenta defined with respect to the beam axis. In section 2.1, we introduce relativistic electron Bessel beams in free space, by deriving their wave functions (subsection 2.1.1) and calculating the 4-current (subsection 2.1.2). In section 2.2, we reveal the influence of laser light on the dynamics of such electron beams. To this end, in subsection 2.2.1, we obtain the so-called Volkov-Bessel wave functions by making use of the (Dirac-Volkov) plane-wave decomposition of the Bessel-beam electron state. Furthermore, in subsection 2.2.2, we calculate the 4-current of the laser-driven EVB in order to spatially and temporally characterize the profile of Bessel beams of electrons that couple to a few-cycle femtosecond laser pulse. By constructing the components of the 4-current, moreover, we show how the laser beam can be employed in order to control and manipulate the EVB.

We conclude each chapter with a summary.

Chapter 1

Relativistic theory of the electron-light interaction

> God used beautiful mathematics in creating the world.
>
> P.A.M. Dirac

In this chapter, we shall discuss the relativistic theory of interaction of plane-wave electrons with a plane electromagnetic wave. This *external* electromagnetic field will be regarded as "given", which means that all the radiative corrections will be neglected, such that the number of particles remains unchanged. We work in a single-particle approximation which neglects the Coulomb interaction between electrons inside the beam, thus, allowing us to use the terms "electron" and "electron beam" equivalently. Such an approximation is well suited for electron beams, for example, in transmission electron microscopes. Below, we use relativistic Gaussian units $c = 1$, $\hbar = 1$ and, for the scalar product of any two 4-vectors $a = \left(a^0, \boldsymbol{a}\right)$ and $b = \left(b^0, \boldsymbol{b}\right)$, we adopt the notations $(ab) \equiv a^\mu b_\mu \equiv a^0 b^0 - \boldsymbol{a} \cdot \boldsymbol{b}$, where $\mu \in \{0, 1, 2, 3\}$ and the "dot" means the three-dimensional scalar product. By a widely followed convention, moreover, the 4-vectors that are written with lower (upper) indices are called covariant (contravariant) vectors.

1.1 Relativistic electrons in free space

1.1.1 Dirac equation for free electrons

We consider an electron with mass m and 4-momentum $p^\mu = (\mathcal{E}, \boldsymbol{p})$ that fulfills the standard, relativistic energy-momentum relation

$$p^2 \,=\, \mathcal{E}^2 - \boldsymbol{p}^2 \,=\, m^2\,. \tag{1.1}$$

Here $\mathcal{E}$ and $\boldsymbol{p}$ are the energy and the three-dimensional momentum of the electron, respectively (see also Eq. (5)). The electron and its antiparticle – positron, being fermions, are described

via the so-called Dirac bi-spinor [68]

$$\psi \;=\; \begin{pmatrix} \psi_1 \\ \psi_2 \\ \psi_3 \\ \psi_4 \end{pmatrix} . \tag{1.2}$$

The equation that governs the dynamics of such a bi-spinor in free space is the free-(particle) Dirac equation

$$(\gamma\hat{p} - m)\,\psi \;=\; 0\,, \tag{1.3}$$

where $\hat{p}^\mu \equiv \partial^\mu = (i\partial/\partial t, -i\boldsymbol{\nabla})$ is the particle's 4-momentum operator. The 4×4 matrices $\gamma^\mu = \left(\gamma^0, \gamma^1, \gamma^2, \gamma^3\right) = \left(\gamma^0, \boldsymbol{\gamma}\right)$ are the Lorentz-invariant[1] Dirac matrices that have the following explicit form

$$\gamma^0 \;=\; \begin{pmatrix} 1 & 0 \\ 0 & -1 \end{pmatrix} , \quad \boldsymbol{\gamma} \;=\; \begin{pmatrix} 0 & \boldsymbol{\sigma} \\ -\boldsymbol{\sigma} & 0 \end{pmatrix} \tag{1.4}$$

in the so-called *standard* representation (which we will employ from now on). Here the 2×2 matrices

$$\boldsymbol{\sigma} \;=\; (\sigma_x\,, \sigma_y\,, \sigma_z) \;=\; \left(\begin{pmatrix} 0 & 1 \\ 1 & 0 \end{pmatrix} , \begin{pmatrix} 0 & -i \\ i & 0 \end{pmatrix} , \begin{pmatrix} 1 & 0 \\ 0 & -1 \end{pmatrix} \right) \tag{1.5}$$

are the well-known Pauli matrices. Moreover, the scalar 4-product in the free Dirac equation (1.3) can be expanded as

$$\gamma\hat{p} \;=\; i\gamma^0 \frac{\partial}{\partial t} + i\boldsymbol{\gamma}\cdot\boldsymbol{\nabla} \;=\; i\gamma^0 \frac{\partial}{\partial t} + i\gamma^1 \frac{\partial}{\partial x} + i\gamma^2 \frac{\partial}{\partial y} + i\gamma^3 \frac{\partial}{\partial z}\,,$$

that contains partial derivatives both with respect to space and time coordinates.

Although the equation (1.3) describes the motion of electrons and positrons, however, in this thesis, we are interested only in relativistic electron beams. Therefore, to describe the state of a free particle with a *positive* energy, i.e. the electron state, we express the solution of Eq. (1.3) in terms of a plane-wave

$$\boxed{\psi_p \;=\; \frac{1}{\sqrt{2\mathcal{E}}}\, u_p e^{-ipx}\,.} \tag{1.6}$$

Here the amplitude u_p is a constant suitably normalized bi-spinor

$$\bar{u}_p u_p \;=\; 2m\,,$$

where the "bar" denotes Dirac conjugation, $\bar{u}_p = u_p^\dagger \gamma^0$, and the "dagger" is Hermitian conjugation. The normalization of u_p is done such that the condition $\psi_p^\dagger \psi_p = 1$ is satisfied. For

[1] Lorentz invariance is a fundamental requirement in physics, meaning that the laws of physics must look the same in all reference frames [67].

the positron, moreover, one should change $p \to -p$ and, therefore, replace ψ_p with ψ_{-p} in Eq. (1.6).

If we substitute the plane-wave wave function (1.6) into the free-electron Dirac equation (1.3) and use the standard representation (1.4) of Dirac matrices, we can find the explicit form of the bi-spinor u_p

$$u_p = \begin{pmatrix} \sqrt{\mathcal{E}+m}\, w \\ \sqrt{\mathcal{E}-m}\, \dfrac{(\boldsymbol{p}\cdot\boldsymbol{\sigma})}{p} w \end{pmatrix} . \tag{1.7}$$

Here the spinor w is an arbitrary two-component matrix that has to be normalized as

$$w^\dagger w = 1 .$$

There are three possible ways to physically describe the latter spinor. It can be chosen as the *polarization* states of the electron such that w has a defined component of the electron *spin* on some axis. For example, one can choose the following spin states of the electron in the rest frame

$$\sigma_z w^{(s)} = s w^{(s)} , \tag{1.8}$$

as an eigenstate of the σ_z matrix with the eigenvectors

$$w^{(s)} = \begin{pmatrix} \alpha \\ \beta \end{pmatrix} \tag{1.9}$$

and the eigenvalues $s = \pm 1/2$, where $\{\alpha\,, \beta\} = \{0\,, 1\}$. The eigenvector $w^{(1/2)} = \begin{pmatrix} 1 \\ 0 \end{pmatrix}$ with its positive eigenvalue $s = 1/2$ describe the "spin-up" state, while the eigenvector $w^{(-1/2)} = \begin{pmatrix} 0 \\ 1 \end{pmatrix}$ with the negative eigenvalue $s = -1/2$ represent the "spin-down" state. In our further discussion, we will explore such electron beams for which the polarization states are chosen to be these spin states.

Another possibility for the choice of the spinor w is the so-called *helicity* states that appear as an eigenstate of the operator $(\boldsymbol{p}\cdot\boldsymbol{\sigma})\,/\,(2p)$ with eigenvalues $\Lambda = \pm 1/2$ [68]. For the sake of completeness, we conclude this subsection with a discussion of the third possible way to describe the Dirac bi-spinor. Whilst both the polarization and the helicity are properties of the spinor w, the *chirality* is a property of the bi-spinor (1.2). These states are the eigeinstates of the γ_5 matrix (see the next subsection) with eigenvalues ± 1. The helicity and chirality are important quantum numbers, especially, in high energy physics, where the fermions can be approximately considered massless, as, for instance, the neutrino [69].

1.1.2 Algebra of Dirac matrices

In our further calculations, we will use some rules for γ matrices, independent of their particular representation. In this subsection, we shortly introduce the general properties of Dirac matrices that form the so-called Dirac algebra. First of all, these matrices satisfy the anticommutation relation

$$\gamma^\mu\gamma^\nu + \gamma^\nu\gamma^\mu = 2g^{\mu\nu} , \tag{1.10}$$

where $\mu, \nu \in \{0, 1, 2, 3\}$ and $g^{\mu\nu}$ is the metric tensor of the flat Minkowski 4-space which has the form

$$g^{\mu\nu} = g_{\mu\nu} = \begin{pmatrix} 1 & 0 & 0 & 0 \\ 0 & -1 & 0 & 0 \\ 0 & 0 & -1 & 0 \\ 0 & 0 & 0 & -1 \end{pmatrix} \tag{1.11}$$

in the matrix representation. Such a choice of $g^{\mu\nu}$ corresponds to the 4-metric with a signature $(+, -, -, -)$. The metric tensor relates to each other the covariant and contravariant 4-vectors by lowering and raising the indices as follows, $x_\mu = g_{\mu\nu}x^\nu$ and $x^\mu = g^{\mu\nu}x_\nu$, where repeated indices imply summation. From Eq. (1.10), for squares of γ matrices, we can obtain

$$\left(\gamma^0\right)^2 = \mathbb{1}\,, \quad \left(\gamma^1\right)^2 = \left(\gamma^2\right)^2 = \left(\gamma^3\right)^2 = -\mathbb{1}\,, \tag{1.12}$$

where

$$\mathbb{1} = \begin{pmatrix} 1 & 0 & 0 & 0 \\ 0 & 1 & 0 & 0 \\ 0 & 0 & 1 & 0 \\ 0 & 0 & 0 & 1 \end{pmatrix} \tag{1.13}$$

is the unit (or identity) matrix.

The γ matrices satisfy also extra hermiticity conditions which are, however, restricted by anticommutation relation (1.10). Thence, we can impose [68]

$$\left(\gamma^0\right)^\dagger = \gamma^0\,, \quad (\boldsymbol{\gamma})^\dagger = -\boldsymbol{\gamma}\,, \tag{1.14}$$

where, again, "†" denotes the Hermitian conjugate of γ matrices. Taking the Hermitian conjugate of any $m \times n$ matrix

$$\mathcal{M} = \begin{pmatrix} \mathcal{M}_{11} & \mathcal{M}_{12} & \cdots & \mathcal{M}_{1n} \\ \mathcal{M}_{21} & \mathcal{M}_{22} & \cdots & \mathcal{M}_{2n} \\ \vdots & \vdots & \ddots & \vdots \\ \mathcal{M}_{m1} & \mathcal{M}_{m2} & \cdots & \mathcal{M}_{mn} \end{pmatrix}$$

means first taking its transpose by making a new, $n \times m$ matrix, i.e. exchanging the rows and columns with each other,

$$\mathcal{M}^T = \begin{pmatrix} \mathcal{M}_{11} & \mathcal{M}_{21} & \cdots & \mathcal{M}_{n1} \\ \mathcal{M}_{12} & \mathcal{M}_{22} & \cdots & \mathcal{M}_{n2} \\ \vdots & \vdots & \ddots & \vdots \\ \mathcal{M}_{1m} & \mathcal{M}_{2m} & \cdots & \mathcal{M}_{nm} \end{pmatrix}, \tag{1.15}$$

and then taking the complex conjugate (denoted by the "asterisk") of every element in already transposed matrix

$$\mathcal{M}^{\dagger} = \left(\mathcal{M}^{T}\right)^{*} = \begin{pmatrix} \mathcal{M}_{11}^{*} & \mathcal{M}_{21}^{*} & \cdots & \mathcal{M}_{n1}^{*} \\ \mathcal{M}_{12}^{*} & \mathcal{M}_{22}^{*} & \cdots & \mathcal{M}_{n2}^{*} \\ \vdots & \vdots & \ddots & \vdots \\ \mathcal{M}_{1m}^{*} & \mathcal{M}_{2m}^{*} & \cdots & \mathcal{M}_{nm}^{*} \end{pmatrix} . \tag{1.16}$$

Formally, one can also write $\mathcal{M}_{mn}^{\dagger} = \mathcal{M}_{nm}^{*}$. In addition, the hermiticity conditions (1.14) can be easily checked for the standard representation (1.4) of γ matrices.

For the completeness of the description of γ matrices, we introduce here also another 4×4 matrix γ^5 that is defined as

$$\gamma^5 \;=\; -i\gamma^0\gamma^1\gamma^2\gamma^3$$

and has the following properties:

$$\gamma^5\gamma^\mu + \gamma^\mu\gamma^5 \,=\, 0\,, \quad \left(\gamma^5\right)^2 \,=\, 1\,, \quad \left(\gamma^5\right)^\dagger \,=\, \gamma^5\,.$$

As already mentioned, this matrix plays an important role for investigation of chiral states of particles.

In relativistic quantum theory (of electrons), important expressions are used that contain scalar 4-products of γ matrices and other 4-vectors. For any two 4-vectors a^μ and b^μ, for example, one can obtain the following relations from the anticommutation relation (1.10):

$$(a\gamma)\,(b\gamma) + (b\gamma)\,(a\gamma) \,=\, 2\,(ab)\;, \quad (a\gamma)\,(a\gamma) \,=\, a^2\,. \tag{1.17}$$

Moreover, the scalar product of Dirac matrices with themselves gives $(\gamma\gamma) = \gamma^\mu\gamma_\mu = 4$, where $\gamma_\mu = g_{\mu\nu}\gamma^\nu$.

The above introduced rules for γ matrices are relevant to carry out relativistic calculations for describing the electron-field interaction. By employing the Dirac algebra, we are now ready to generalize the free-electron Dirac equation (1.3) and its solution (1.6) for electrons that couple to an external electromagnetic field.

1.2 Relativistic electrons in the presence of the electromagnetic field

In this section, we shall introduce the Dirac equation for electrons inside an external electromagnetic field. We will also obtain the well-know, exact Dirac-Volkov solutions when the external field is regarded as a plane-wave field.

1.2.1 Dirac equation for laser-driven electrons

The wave equation of an electron in a given external field can be derived in the same way as in non-relativistic theory [70]. To obtain the desired equation for a field-affected electron, let us consider an electromagnetic field with the 4-potential $A^\mu(x) = \left(A^0(x), \boldsymbol{A}(x)\right)$, where A^0

and $\boldsymbol{A}$ are the scalar and vector potentials, respectively. They define the electric and magnetic fields via the corresponding relations

$$\boldsymbol{E} = -\frac{\partial \boldsymbol{A}}{\partial t} - \boldsymbol{\nabla} A^0 , \quad \boldsymbol{B} = \boldsymbol{\nabla} \times \boldsymbol{A} , \tag{1.18}$$

where the "cross" denotes the vector product.

If we replace the 4-momentum operator $\hat{p}$ in the free Dirac equation (1.3) by the operator $\hat{p} - eA$, following the minimal coupling prescription, we will obtain a first-order equation

$$\left[\gamma \left(\hat{p} - eA\right) - m\right] \psi \;\; = \;\; 0 . \tag{1.19}$$

Here the charge e appears together with its sign, so that for electrons we have $e = -|e|$. In order to solve Eq. (1.19), however, one has to transform it into the second-order equation by applying the operator $\gamma \left(\hat{p} - eA\right) + m$

$$\left[\gamma^\mu \gamma^\nu \left(\hat{p}_\mu - eA_\mu\right)\left(\hat{p}_\nu - eA_\nu\right) - m^2\right] \psi \;\; = \;\; 0 . \tag{1.20}$$

Furthermore, we introduce the antisymmetric 4-tensor

$$\sigma^{\mu\nu} \;\; = \;\; \frac{1}{2}\left(\gamma^\mu \gamma^\nu - \gamma^\nu \gamma^\mu\right)$$

and combine it with anticommutation relation (1.10) to re-write the product $\gamma^\mu \gamma^\nu$ as

$$\gamma^\mu \gamma^\nu \;\; = \;\; g^{\mu\nu} + \sigma^{\mu\nu} .$$

The latter expression enables one to antisymmetrize the quadratic form (1.20) and to re-write it in the form [68]

$$\left[\left(\hat{p} - eA\right)^2 - m^2 - i\frac{e}{2} F_{\mu\nu} \sigma^{\mu\nu}\right] \psi \;\; = \;\; 0 , \tag{1.21}$$

which is suitable for integration. Moreover, the tensor

$$F_{\mu\nu} \;\; = \;\; \partial_\mu A_\nu - \partial_\nu A_\mu \tag{1.22}$$

is the so-called electromagnetic field tensor that is antisymmetric under the interchange $\mu \leftrightarrow \nu$, i.e. $F_{\mu\nu} = -F_{\nu\mu}$. It has six independent components which give the relevant electric $\boldsymbol{E} = (E_x, E_y, E_z)$ and magnetic $\boldsymbol{B} = (B_x, B_y, B_z)$ fields, formally shown through the matrix

$$F_{\mu\nu} \;\; = \;\; \begin{pmatrix} 0 & E_x & E_y & E_z \\ -E_x & 0 & -B_z & B_y \\ -E_y & B_z & 0 & -B_x \\ -E_z & -B_y & B_x & 0 \end{pmatrix} .$$

There are a number of advantages for using the electromagnetic field tensor. For example, one can represent the well-known Maxwell equations in the *compact* form, convenient for relativistic calculations [67, 71],

$$\partial_\mu F^{\mu\nu} \;\; = \;\; J^\nu_{\text{ext}} , \tag{1.23}$$

$$\partial^\lambda F^{\mu\nu} + \partial^\nu F^{\lambda\mu} + \partial^\mu F^{\nu\lambda} \;\; = \;\; 0 , \tag{1.24}$$

where $\lambda = \{0,1,2,3\}$ and $J^{\nu}_{\rm ext} = (\rho_{\rm ext}, \boldsymbol{J}_{\rm ext})$ is the 4-current of some *external* charges. Equation (1.23) leads to the Gauss and Ampér circuital laws:

$$\boldsymbol{\nabla}\cdot\boldsymbol{E} \;=\; \rho_{\rm ext}\,, \quad \boldsymbol{\nabla}\times\boldsymbol{B} - \frac{\partial \boldsymbol{E}}{\partial t} = \boldsymbol{J}_{\rm ext}\,.$$

While, Eq. (1.24) yields to

$$\boldsymbol{\nabla}\cdot\boldsymbol{B} \;=\; 0\,, \quad \boldsymbol{\nabla}\times\boldsymbol{E} + \frac{\partial \boldsymbol{B}}{\partial t} = 0\,,$$

the Gauss law for magnetism and the Faraday law for induction, respectively. Finally, the field tensor (1.22) enables one to directly derive the field invariants

$$F_{\mu\nu}F^{\mu\nu} \;\sim\; \boldsymbol{B}^2 - \boldsymbol{E}^2 \;=\; inv\,, \quad \epsilon^{\mu\nu\mu'\nu'}F_{\mu\nu}F_{\mu'\nu'} \;\sim\; \boldsymbol{E}\cdot\boldsymbol{B} \;=\; inv\,,$$

that remain unchanged under the Lorentz transformations [67]. Here $\epsilon^{\mu\nu\mu'\nu'} = -\epsilon_{\mu\nu\mu'\nu'}$ is the so-called Levi-Civita's antisymmetric symbol of rank-4 which is equal either to 1 or -1 according to whether $\{\mu,\nu,\mu',\nu'\}$ is an even or odd permutation of $\{0,1,2,3\}$, and zero otherwise [67].

Thus, we have generalized the free-electron equation (1.3) to the Dirac equation of the form (1.21). This second-order differential equation can be utilized in order to find analytical solutions for field-affected electrons. The only constraint that we imposed on the field is that it is a classically given one. In the next subsection, moreover, in order to construct an analytically exact solution we shall assume that this field is a *plane-wave* field and derive the Dirac-Volkov wave function.

1.2.2 Dirac-Volkov solutions for electrons in the plane-wave field

So far, we have derived the Dirac equation (1.21) that describes the motion of an electron in any arbitrary electromagnetic field which is classical (i.e. non-quantized) and satisfies the Maxwell equations (1.23)-(1.24). There are very few cases when Eq. (1.21) can be solved analytically exact [26]. One of these cases is restricted to plane-wave fields which is originally discussed by Volkov [72]. We here follow the textbook [68] and obtain the Dirac-Volkov solutions by performing Lorentz-invariant calculations. To do so, let us consider an electron that moves in the field of a plane-wave electromagnetic field with a wave 4-vector $k^{\mu} = (\omega, \boldsymbol{k})$ and the dispersion relation

$$k^2 \;=\; \omega^2 - \boldsymbol{k}^2 \;=\; 0\,. \tag{1.25}$$

For such a field, the 4-potential A^{μ} depends only on the scalar product of k^{μ} and the 4-coordinate $x^{\mu} = (t, \boldsymbol{r})$, namely $A^{\mu} = A^{\mu}(\zeta)$. Here the 4-product

$$\zeta \;\equiv\; (kx) \;=\; \omega t - \boldsymbol{k}\cdot\boldsymbol{r} \tag{1.26}$$

is a Lorentz-invariant quantity, called laser *phase*, that plays a crucial role in our further derivations.

We now assume that no external charges and currents are applied such that the field tensor (1.22) satisfies the homogeneous Maxwell equations, i.e. Eqs. (1.23)-(1.24) with $J^{\nu}_{\rm ext} = 0$. The plane-wave structure of the electromagnetic field is incporporated by the most general antisymmetric form of the field tensor [73]

$$F_{\mu\nu} \;\;=\;\; f_{\mu\nu}G(\zeta)\,, \tag{1.27}$$

where $f_{\mu\nu}$ is a constant antisymmetric tensor. Whereas, $G(\zeta)$ is an arbitrary function of ζ obeying the physical requirement that the field vanishes at infinity, i.e. $G(\pm\infty) = 0$. In the meantime, we also assume that the 4-potential obeys the Lorenz gauge [74]

$$\partial_\mu A^\mu \;=\; 0\,. \tag{1.28}$$

If we combine this gauge condition with Maxwell equations, we can derive wave equations and express their solutions in terms of the retarded (scalar and vector) potentials. This is in contrast to the Coulomb gauge, $\boldsymbol{\nabla}\cdot\boldsymbol{A} = 0$, which gives rise to an instantaneous, action-at-a-distance, scalar potential and to some complicated vector potential [75].

Given that the 4-potential is a function of only the laser phase ζ, we can reduce the Dirac equation (1.21) with partial derivatives with respect to the 4-coordinates x^μ to an equation that contains only total derivatives with respect to the same ζ-variable. To do so, we transform the partial derivative $\partial_\mu = \partial/\partial x^\mu$ as

$$\partial_\mu \;=\; \frac{\partial\zeta}{\partial x^\mu}\frac{d}{d\zeta} \;=\; k_\mu \frac{d}{d\zeta}\,, \tag{1.29}$$

such that the field tensor (1.22), Maxwell equations (1.23)-(1.24) and the Lorenz gauge (1.28) can now be correspondingly re-written as

$$F_{\mu\nu} \;=\; k_\mu A'_\nu - k_\nu A'_\mu\,, \tag{1.30}$$

$$k_\mu f^{\mu\nu} \;=\; 0\,, \qquad k^\lambda f^{\mu\nu} + k^\nu f^{\lambda\mu} + k^\mu f^{\nu\lambda} \;=\; 0\,, \tag{1.31}$$

$$k_\mu A^{\mu\prime} \;=\; kA' \;=\; 0\,. \tag{1.32}$$

Here "prime" means derivation with respect to the laser phase ζ.

Let us now obtain a simpler form for the Lorenz gauge (1.32), quite important for our further analyses. By comparing Eqs. (1.27) and (1.30), one can express the antisymmetric tensor in the form (see also Ref. [76])

$$f_{\mu\nu} \;=\; k_\mu a_\nu - k_\nu a_\mu\,, \tag{1.33}$$

where a_μ is some constant 4-vector. We can therefore re-write the field tensor as $F_{\mu\nu} = k_\mu a_\nu G - k_\nu a_\mu G$, combine it with Eq. (1.30) and find $A'_\mu = a_\mu G$. This allows us (i) to represent the 4-potential in terms of the integral

$$A_\mu(\zeta) \;=\; a_\mu \int_0^\zeta \mathrm{d}\tilde{\zeta} G(\tilde{\zeta})$$

and (ii) to re-write the gauge condition (1.32) as

$$ka \;=\; 0\,.$$

The latter two expressions directly lead to the following form of the Lorenz gauge

$$kA \;=\; 0\,. \tag{1.34}$$

We should note, moreover, that the Maxwell equations are automatically fulfilled if we insert the tensor (1.33) in Eqs. (1.31) and take into account the dispersion law (1.25) along with the gauge condition $ka = 0$.

To simplify the Dirac equation (1.21) for plane-wave fields, we now expand the square $(\hat{p} - eA)^2$ and consider that $\partial_\mu (A^\mu \psi) = A^\mu \partial_\mu \psi$ due to the Lorenz gauge (1.28). The resulting equation is

$$\left[-\partial^2 - 2ie\,(A\partial) + e^2 A^2 - m^2 - ie\,(\gamma k)\left(\gamma A'\right)\right]\psi \;=\; 0\,, \tag{1.35}$$

where $\partial^2 = \partial_\mu \partial^\mu = \partial_t^2 - \boldsymbol{\nabla}^2$ is the 4-dimensional Laplace operator, also called D'Alembert operator. The form of Eq. (1.35) enables one to factorize the wave function ψ and represent it as a product of the "free motion of the electron" and the "influence of the laser on such a motion". Thus, we can use the Ansatz

$$\psi \;=\; e^{-ipx} F\left(\zeta\right) \tag{1.36}$$

to seek a solution of Eq. (1.35). Here the exponential e^{-ipx} describes the free motion of electrons and $F\left(\zeta\right)$ is some smoothly changing function that arises due to the presence of the external field. In other words, the field modifies both the phase and the constant amplitude of the initially free electron (see the upcoming Eq. (1.38) for contribution of the field into the electron phase).

If we insert the Ansatz (1.36) into the Dirac equation (1.35) and utilize Eqs. (1.25) and (1.29) (to show that $\partial^2 F = k^2 F'' = 0$ and $\partial^\mu F = k^\mu F'$), we will obtain a homogeneous first-order differential equation for $F\left(\zeta\right)$

$$2i\,(kp)\,F' + \left[-2e\,(pA) + e^2 A^2 - ie\,(\gamma k)\left(\gamma A'\right)\right] F \;=\; 0\,. \tag{1.37}$$

We should remind the reader that this equation has been obtained from Eq. (1.19) under the only assumption about the plane-wave nature of the external field. We are now ready to integrate the Dirac equation for field-affected electrons. In fact, we can represent the formal integral of the equation (1.37) as

$$F \;=\; \frac{u_p}{\sqrt{2\mathcal{E}_0}} \exp\left[-i\mathcal{F} + i\mathcal{G} + \frac{e\,(\gamma k)\,(\gamma A)}{2\,(kp)}\right].$$

Here the constant bi-spinor u_p is chosen to coincide with the free-particle bi-spinor (1.7) in order to ensure that we recover the field-free solutions when we remove the field. The terms

$$\mathcal{F} \equiv \int_0^\zeta \mathrm{d}\tilde{\zeta}\, \frac{e(pA(\tilde{\zeta}))}{(kp)}\,, \quad \mathcal{G} \equiv \int_0^\zeta \mathrm{d}\tilde{\zeta}\, \frac{e^2 A^2(\tilde{\zeta})}{2\,(kp)} \tag{1.38}$$

describe the field-affected phase of the electron, thus, giving rise to the *quasimomentum* and *quasienergy* of such an electron. Furthermore, in order to simplify the latter exponential we notice that all the powers of $(\gamma k)\,(\gamma A)$ beyond the first order are zero. Indeed, if we employ the properties (1.17) of Dirac matrices and take into account the dispersion relation (1.25) and the Lorenz gauge (1.34) we obtain

$$(\gamma k)\,(\gamma A)\,(\gamma k)\,(\gamma A) \;=\; -\,(\gamma k)\,(\gamma k)\,(\gamma A)\,(\gamma A) + 2\,(kA)\,(\gamma k)\,(\gamma A) \;=\; -k^2 A^2 \;=\; 0\,.$$

Thence, the exponential can be (exactly) replaced by a simpler form

$$\exp \frac{e\,(\gamma k)\,(\gamma A)}{2\,(kp)} \;=\; 1 + \frac{e}{2\,(kp)}\,(\gamma k)\,(\gamma A)\,.$$

Finally, the solution (1.36) of the Dirac equation (1.35) for electron(s) inside the plane-wave field takes the well-known Dirac-Volkov form [68]

$$\boxed{\psi_p(x) \;=\; \left[1+\frac{e}{2(kp)}(\gamma k)(\gamma A)\right]\frac{u_p}{\sqrt{2\mathcal{E}}}\,e^{iS}\,.} \tag{1.39}$$

Here the exponential $S=-(px)-\mathcal{F}+\mathcal{G}$ is proportional to the classical action of an electron within a plane-wave electromagnetic field [67]. When we switch off the field, i.e. $A=\mathcal{F}=\mathcal{G}=0$, we recover the free-electron solution (1.6), as one would expect. Moreover, the infinitely slow application of the field does not alter the orthonormalization of Dirac-Volkov solutions [68]

$$\int \psi^{\dagger}_{p'}\psi_p \mathrm{d}^3x \;=\; (2\pi)^2\,\delta\left(\boldsymbol{p}'-\boldsymbol{p}\right)\,,$$

a form that also holds for field-free electrons.

Derivation of the exact, Dirac-Volkov solution for the interaction of plane-wave electrons with a plane-wave field is the first main results of this chapter. To already give a hint, we shall use the solution (1.39) in order to construct Bessel-type solutions of the Dirac equation (1.21) or (1.35). We will realize this by superimposing the Dirac-Volkov wave functions over well-defined amplitudes representing the characteristic momentum distribution of Bessel beams.

Let us now consider a particular case of electron-field interaction when the electron "collides head-on" with a linearly polarized laser beam meaning that the two beams counter-propagate with respect to each other. We choose the z-axis directed along the electron propagation direction, while the y-axis shows the polarization direction of the field. In virtue of this assumption, 4-momenta of the electron and the field can be expressed as $p^\mu=\left(\mathcal{E},0,0,p_{||}\right)$ and $k^\mu=(\omega,0,0,-k)$, respectively. Moreover, the 4-potential $A^\mu=(0,0,A(\zeta),0)$. For this particular scenario, the Dirac-Volkov solution (1.39) can be simplified to

$$\psi_p(x) \;=\; \left[1+\frac{e}{2(kp)}(\gamma k)(\gamma A)\right]\frac{u_{p_{||}}}{\sqrt{2\mathcal{E}}}\,\exp\left[i\left(p_{||}z-\mathcal{E}t\right)+i\int_0^{\zeta}d\tilde{\zeta}\,\frac{e^2A^2(\tilde{\zeta})}{2(kp)}\right]\,. \tag{1.40}$$

Here the constant bi-spinor

$$u_{p_{||}} \;=\; \begin{pmatrix}\sqrt{\mathcal{E}+m}\,w\\ \sqrt{\mathcal{E}-m}\,\sigma_z w\end{pmatrix}\,, \tag{1.41}$$

and the 4-products take the form

$$(\gamma k)\;=\;\gamma^0\omega+\gamma^3 k\,,\quad (\gamma A)\;=\;-\gamma^2 A\,,\quad (kp)\;=\;\omega\mathcal{E}+kp_{||}\,. \tag{1.42}$$

In our forthcoming study, we shall use Eq. (1.40) to compare it with our generalized solutions for laser-driven electron vortex beams, representing the same geometry of the head-on collision.

1.2.3 4-current of the Dirac-Volkov electron

The Dirac-Volkov wave function can be employed in order to construct measurable quantities for field-affected electrons, such as the electron 4-current in the presence of the field

$$j^\mu \;=\; (\rho,\boldsymbol{j}) \;=\; \bar{\psi}_p\gamma^\mu\psi_p\,. \tag{1.43}$$

Here $\rho = \bar{\psi}_p \gamma^0 \psi = \psi_p^\dagger \psi$ and $\boldsymbol{j} = \bar{\psi}_p \boldsymbol{\gamma} \psi_p$ are the probability density and the three-dimensional current of laser-driven electrons, respectively. To calculate these quantities we first have to define the Dirac conjugate of the wave function (1.39). For this purpose, we note that the hermiticity conditions (1.14) yield

$$[(\gamma k)(\gamma A)]^\dagger = (\gamma A)^\dagger (\gamma k)^\dagger = \gamma^0 (\gamma A)(\gamma k)\gamma^0 . \tag{1.44}$$

If we combine this expression with the anticommutation relation (1.10) we can represent the Dirac conjugate wave function in the form

$$\bar{\psi}_p(x) = \frac{\bar{u}_p}{\sqrt{2\mathcal{E}}} \left[1 + \frac{e}{2(kp)}(\gamma A)(\gamma k)\right] e^{-iS} , \tag{1.45}$$

where

$$\bar{u}_p = u_p^\dagger \gamma^0 = \left(\sqrt{\mathcal{E}+m}\, w^\dagger, -\sqrt{\mathcal{E}-m}\, w^\dagger \frac{(\boldsymbol{p}\cdot\boldsymbol{\sigma})}{p}\right)$$

is a 1×4 bi-spinor, the Dirac conjugate of the free electron bi-spinor (1.7).

To evaluate the 4-current we substitute Eqs. (1.39) and (1.45) in Eq. (1.43) and make use of relations (1.17) and the Lorenz gauge (1.34), resulting in

$$\left[1 + \frac{e}{2(kp)}(\gamma A)(\gamma k)\right] \gamma^\mu \left[1 + \frac{e}{2(kp)}(\gamma k)(\gamma A)\right] = \gamma^\mu - eA^\mu \frac{(\gamma k)}{(kp)} + k^\mu \left[\frac{e(\gamma A)}{(kp)} - \frac{e^2 A^2 (\gamma k)}{2(kp)^2}\right] .$$

Furthermore, for quantum-mechanical averages of γ matrices and of their 4-products with k^μ and A^μ, we obtain

$$\bar{u}_p \gamma^\mu u_p = 2p^\mu , \quad \bar{u}_p (\gamma k) u_p = 2(kp) , \quad \bar{u}_p (\gamma A) u_p = 2(pA) .$$

Inserting last four expressions into Eq. (1.43), we will arrive to a final form of the 4-current of laser-driven plane-wave electrons

$$\boxed{j^\mu = \frac{1}{\mathcal{E}} \left\{ p^\mu - eA^\mu + k^\mu \left[\frac{e(pA)}{(kp)} - \frac{e^2 A^2}{2(kp)}\right]\right\} .} \tag{1.46}$$

Equation (1.46) is the second main result of this chapter and will also be generalized for laser-driven twisted electron beams. In addition, non of components of the 4-current depends on the polarization states of electron, i.e. neither spin nor helicity states are involved here, in contrast to the wave function (1.39). Nevertheless, to already give a hint, we stress here that the analogous 4-current of field-affected electron Bessel beams depends on the polarization states of electron. This is due to the new fundamental degree of freedom – the electron OAM – that couples to the spin of electron and gives rise to the so-called intrinsic spin-orbit interaction.

For the head-on scenario, represented by the wave function (1.40), the components of the 4-current take the simpler form

$$\rho = 1 - \frac{\omega e^2 A^2}{2(kp)\mathcal{E}} , \tag{1.47}$$

$$j^{(x)} = 0 , \tag{1.48}$$

$$j^{(y)} = -\frac{eA}{\mathcal{E}} , \tag{1.49}$$

$$j^{(z)} = \frac{1}{\mathcal{E}} \left[p_z + \frac{k e^2 A^2}{2(kp)}\right] , \tag{1.50}$$

where, to remind the reader, the z-axis is chosen along the propagation direction of electrons, and the y-axis is aligned along the field polarization. Again, as we explicitly recognize, the spin of electron is not enrolled in the formulae (1.47)-(1.50). However, the twist of electron would split such a spin-degeneracy of the 4-current, as we discuss quite in details in the next chapter.

1.3 Summary

In this chapter, we have studied the relativistic quantum theory of electrons that interact with a given electromagnetic field. We have described the dynamics of both field-free and field-affected plane-wave electrons by finding analytically exact solutions to the Dirac equation. Particularly, we have obtained the known Dirac-Volkov solutions that characterize the coupling of electrons with a plane electromagnetic field. Furthermore, we have calculated the 4-current of Dirac-Volkov electrons to reveal the influence of the radiation field onto the electron dynamics. We have shown that the components of the 4-current are degenerated with respect to the polarization states of the electron, despite the fact that the Dirac-Volkov wave function depends on spin. In the next chapter, we shall employ these wave functions in order to construct exact Bessel-type solutions of the Dirac equation for twisted electrons inside the plane-wave field. For this purpose, we will make use of the superposition principle of relativistic quantum theory and superimpose the Dirac-Volkov solutions with well-defined monoenergetic spectrum of Bessel beams. In contrast to scalar Bessel beams in free-space, as discussed in Introduction, we naturally expect essential changes in properties of laser-driven vector Bessel beams due to both the relativistic nature of electron dynamics and the presence of the laser field. The next chapter is completely devoted to such an analysis, where we discuss very recent developments of the theory of electron vortex beams, part of which has been originally done by us.

Chapter 2

Interaction of relativistic electron vortex beams with a laser light

> The research worker, in his efforts to express the fundamental laws of Nature in mathematical form, should strive mainly for mathematical beauty.
>
> P.A.M. Dirac

In this chapter, we shall derive Bessel-type solutions of the Dirac equation for electrons both in the absence and presence of an external plane-wave electromagnetic field. These solutions will enable us to describe the dynamics of the field-free and laser-driven electron vortex beams both in paraxial and non-paraxial domains. We will further show that apart from the spin degree of freedom such beams carry non-zero OAM along their direction of propagation. We shall explicitly demonstrate how the presence of the SAM and OAM leads to the intrinsic SOI inside the EVB and how this SOI is modified within the laser field. Moreover, we will construct measurable quantities, namely the components of the 4-current, to illustrate the influence of both the electron and laser parameters upon the intensity and current distributions of EVBs. We shall pay a specific attention to the non-paraxial and relativistic regimes of electron propagation where these observables experience a fine spin-slitting. Although our theory enables one to consider plane-wave fields of any shape, we shall carry out our computations especially for few-cycle laser pulses.

2.1 Electron vortex beams in free space

In this section, we recover the results of the original work by Bliokh and coworkers for field-free EVBs [45] in order to provide an appropriate introduction to our advanced studies of laser-driven EVBs.

2.1.1 Bessel-type solutions of the free-electron Dirac equation

We consider a free electron beam which moves along a direction that is chosen to be the z-axis. We examine such a propagation of electrons with their well-defined spin z-component in the rest frame. In order to construct exact Bessel-type solutions that represent the angular momentum eigenstates of a free Dirac electron, we start from the free-electron equation (1.3) with solutions expressed via the orthonormalized states (1.6)-(1.7). We recall the recipe for production of Bessel beams (see Introduction) and write the field-free EVB state as

$$\psi_{\ell s}(x) \;=\; \int \tilde{\psi}_\ell(\boldsymbol{p})\; \psi_p(x)\, p_\perp \mathrm{d}p_\perp \mathrm{d}\phi\,. \tag{2.1}$$

Here the Bessel spectrum $\tilde{\psi}_\ell$ is defined via Eq. (1), ψ_p is the free-electron wave function, Eq. (1.6), and the indices ℓ and s correspondingly indicate the presence of non-zero OAM and SAM for field-free EVBs, as we show below.

To evaluate the integral (2.1), we substitute here Eq. (1.6) and assume that the polarization amplitudes (1.7) are the same for all the plane-waves. First, we carry out the integral with respect to $p_\perp$ and obtain

$$\psi_{\ell s}(\boldsymbol{r},t) \;=\; e^{i\Phi}\int_0^{2\pi} \mathrm{d}\phi\, \frac{e^{i\ell\phi}}{2\pi i^\ell}\, \frac{u_{p_0}}{\sqrt{2\mathcal{E}_0}}\, e^{i\xi\cos(\phi-\varphi)}\,, \tag{2.2}$$

where the index "0" means that the energy as well as the longitudinal and transverse components of the electron momentum are taken at the monoenergetic cone [cf. Fig. 1a]. Moreover, $\xi = p_{\perp 0} r$ describes the width of the beam and

$$\Phi(z,t) \;=\; p_{||0} z - \mathcal{E}_0 t \tag{2.3}$$

is both z- and t-dependent phase that demonstrates the *non-spreading* propagation of EVBs along the z-axis, similar to the same behavior of scalar Bessel beams of electrons.

To perform the integration (2.2) with respect to ϕ, we express the constant bi-spinor u_{p_0} via the cylindrical coordinates in momentum space as

$$u_{p_0} \;=\; \begin{pmatrix} \sqrt{\mathcal{E}_0+m}\, w^{(s)} \\ \sqrt{\mathcal{E}_0-m}\, \dfrac{p_{||0}}{p_0}\sigma_z w^{(s)} \end{pmatrix} + \begin{pmatrix} 0 \\ 0 \\ \sqrt{\mathcal{E}_0-m}\, \dfrac{p_{\perp 0}}{p_0} \begin{pmatrix} 0 & e^{-i\phi} \\ e^{i\phi} & 0 \end{pmatrix} w^{(s)} \end{pmatrix}. \tag{2.4}$$

Here the spin states of electron are chosen to be the eigenstates $w^{(s)} = (\alpha,\beta)^T$ of the σ_z operator with eigenvalues $s = \pm 1/2$ [cf. Eq. 1.9], in contrast to Ref. [77] where the basis states of polarization for EVBs are chosen to be the helicity eigenstates of $\boldsymbol{\sigma}\cdot\boldsymbol{p}/(2p)$. Our particular choice of the basis states for the spin is natural for massive particles [45, 50].

Let us now insert Eq. (2.4) into the integral (2.2) and obtain

$$\begin{aligned}\psi_{\ell s}(\boldsymbol{r},t) &= \frac{e^{i\Phi}}{\sqrt{2}}\left[\begin{pmatrix}\sqrt{1+\dfrac{m}{\mathcal{E}_0}}\begin{pmatrix}\alpha\\ \beta\end{pmatrix}\\ \sqrt{1-\dfrac{m}{\mathcal{E}_0}}\cos\theta_0\begin{pmatrix}\alpha\\ -\beta\end{pmatrix}\end{pmatrix}\int_0^{2\pi}\mathrm{d}\phi\,\frac{e^{i\ell\phi}}{2\pi i^{\ell}}\,e^{i\xi\cos(\phi-\varphi)}\right.\\ &+\begin{pmatrix}0\\0\\0\\ \alpha\sqrt{1-\dfrac{m}{\mathcal{E}_0}}\sin\theta_0\end{pmatrix}\int_0^{2\pi}\mathrm{d}\phi\,\frac{ie^{i(\ell+1)\phi}}{2\pi i^{\ell+1}}\,e^{i\xi\cos(\phi-\varphi)}\\ &\left.+\begin{pmatrix}0\\0\\ \beta\sqrt{1-\dfrac{m}{\mathcal{E}_0}}\sin\theta_0\\0\end{pmatrix}\int_0^{2\pi}\mathrm{d}\phi\,\frac{-ie^{i(\ell-1)\phi}}{2\pi i^{\ell-1}}\,e^{i\xi\cos(\phi-\varphi)}\right]. \end{aligned}\tag{2.5}$$

If we utilize the integral representation (10) of Bessel functions we will arrive to the final form of the wave function of a field-free EVB

$$\boxed{\psi_{\ell s}(\boldsymbol{r},t) = \frac{e^{i\Phi}}{\sqrt{2}}\left[\mathcal{A}_1 e^{i\ell\varphi}J_{\ell}(\xi)+\mathcal{A}_2 e^{i(\ell+1)\varphi}J_{\ell+1}(\xi)+\mathcal{A}_3 e^{i(\ell-1)\varphi}J_{\ell-1}(\xi)\right],}\tag{2.6}$$

where the following (constant) bi-spinors are introduced for notational convenience:

$$\mathcal{A}_1 \equiv \begin{pmatrix}\sqrt{1+\dfrac{m}{\mathcal{E}_0}}\begin{pmatrix}\alpha\\ \beta\end{pmatrix}\\ \sqrt{1-\dfrac{m}{\mathcal{E}_0}}\cos\theta_0\begin{pmatrix}\alpha\\ -\beta\end{pmatrix}\end{pmatrix},\quad \mathcal{A}_2 \equiv \begin{pmatrix}0\\0\\0\\ i\alpha\sqrt{\Delta}\end{pmatrix},\quad \mathcal{A}_3 \equiv -\begin{pmatrix}0\\0\\ i\beta\sqrt{\Delta}\\0\end{pmatrix}.\tag{2.7}$$

Moreover, the parameter

$$\boxed{\Delta = \left(1-\frac{m}{\mathcal{E}_0}\right)\sin^2\theta_0 < 1}\tag{2.8}$$

determines the strength of coupling between the orbital and spin degrees of freedom in the relativistic EVB. It is called *intrinsic spin-orbit interaction* parameter, that vanishes in the paraxial ($\theta_0 \to 0$) and/or in the non-relativistic ($p_0 \to 0$) limits, as $\Delta \approx \theta_0^2 p_0/m$ [45]. The intrinsic SOI arises only for *vector* Bessel beams, when the spin degree of freedom is taken into account, and naturally vanishes for scalar Bessel beams.

The exact wave function (2.6) is the first main result of this chapter. It describes relativistic electron Bessel beams in free space, i.e. the electron counterpart of optical (vector) Bessel beams [50]. The first term in square brackets represents a scalar Bessel beam of the order of ℓ:

$$\psi_{\ell s}^{\text{scalar}}(\boldsymbol{r},t) = \frac{1}{\sqrt{2}}\mathcal{A}_1 e^{i(\Phi+\ell\varphi)}J_{\ell}(\xi),\tag{2.9}$$

whereas, the second and third terms, proportional to $\sqrt{\Delta}$, characterize the polarization-dependent Bessel beam of the order of $\ell + 2s$. Such terms represent the intrinsic SOI and give rise to both the spin- and orbital-angular-momentum-dependent dynamics of relativistic EVBs, as we discuss in the next subsection.

We can find an "integral of motion" to demonstrate the conservation of the (z-component) of the total angular momentum $\ell + s$ that acts as a "good" quantum number for relativistic field-free EVBs. To this end, we first define the TAM operator projected onto the z-axis as a sum of z-components of the canonical OAM (the same as Eq. (14))

$$\hat{\mathcal{L}}_z \;=\; -i\frac{\partial}{\partial\varphi} \tag{2.10}$$

and the SAM operators [68]

$$\hat{\Sigma}_z \;=\; \frac{1}{2}\,\mathrm{diag}\,(\boldsymbol{\sigma},\boldsymbol{\sigma})_z \;=\; \frac{1}{2}\begin{pmatrix}\sigma_z & 0\\ 0 & \sigma_z\end{pmatrix}, \tag{2.11}$$

i.e.

$$\hat{\mathcal{T}}_z \;=\; \hat{\mathcal{L}}_z + \hat{\Sigma}_z\,. \tag{2.12}$$

We are now ready to show that the free EVB wave function (2.6) is the eigenmode of the operator $\hat{\mathcal{T}}_z$. To do so, we act with operators (2.10) and (2.11) on Eq. (2.6) and obtain

$$\begin{aligned}
\hat{\mathcal{L}}_z\psi_{\ell s} &= \frac{e^{i\Phi}}{\sqrt{2}}\left[\mathcal{A}_1\ell e^{i\ell\varphi}J_\ell\left(\xi\right) + \mathcal{A}_2\left(\ell+1\right)e^{i(\ell+1)\varphi}J_{\ell+1}\left(\xi\right) + \mathcal{A}_3\left(\ell-1\right)e^{i(\ell-1)\varphi}J_{\ell-1}\left(\xi\right)\right],\\
\hat{\Sigma}_z\psi_{\ell s} &= \frac{e^{i\Phi}}{\sqrt{2}}\left[\mathcal{A}_1 s e^{i\ell\varphi}J_\ell\left(\xi\right) - \frac{1}{2}\mathcal{A}_2 e^{i(\ell+1)\varphi}J_{\ell+1}\left(\xi\right) + \frac{1}{2}\mathcal{A}_3 e^{i(\ell-1)\varphi}J_{\ell-1}\left(\xi\right)\right],
\end{aligned} \tag{2.13}$$

where the following expressions are taken into account:

$$\hat{\Sigma}_z\mathcal{A}_1 \;=\; s\mathcal{A}_1\,, \quad \hat{\Sigma}_z\mathcal{A}_2 \;=\; -\frac{1}{2}\mathcal{A}_2\,, \quad \hat{\Sigma}_z\mathcal{A}_3 \;=\; \frac{1}{2}\mathcal{A}_3\,.$$

If we add Eqs. (2.13) we find the desired relation

$$\boxed{\hat{\mathcal{T}}_z\psi_{\ell s} \;=\; (\ell+s)\,\psi_{\ell s}\,,} \tag{2.14}$$

which exhibits the conservation of the z-component of the TAM for relativistic non-paraxial EVBs. In contrast, in paraxial regime, i.e. when $\Delta \to 0$, one can readily notice that the scalar Bessem beams (2.9) are the eigenmodes of both OAM and SAM operators at the same time:

$$\boxed{\hat{\mathcal{L}}_z\psi_{\ell s}^{\mathrm{scalar}} \;=\; \ell\psi_{\ell s}^{\mathrm{scalar}}\,, \quad \hat{\Sigma}_z\psi_{\ell s}^{\mathrm{scalar}} \;=\; s\psi_{\ell s}^{\mathrm{scalar}}\,.} \tag{2.15}$$

This scenario is quite similar to the simultaneous conservation of both OAM and SAM of Laguerre-Gauss (optical) modes in the paraxial regime proposed already by Allen and coworkers [3]. Moreover, Eqs. (2.14) and (2.15) exactly coincide with similar predictions for optical Bessel beams in non-paraxial and paraxial domains, respectively [50].

Until now, we have obtained exact, Bessel-type solutions of the free-electron Dirac equation. These solutions can be used in order to calculate measurable quantities for free EVBs, such as the probability density and the components of the three-dimensional electronic current. In order to demonstrate how the intrinsic SOI affects these quantities, in the next subsection, we construct the relativistic 4-current of field-free EVBs.

2.1.2 4-current of field-free EVBs

To determine observables from the wave function (2.6), we here calculate the 4-current of the field-free EVB and show how the intrinsic SOI manifests itself in both SAM- and OAM-dependent distributions of the electronic probability density and current. These quantities are correspondingly defined as scalar and vector components of the 4-dimensional current [cf. Eq. (1.43)]

$$j^{\mu}_{\ell s} \;=\; (\rho_{\ell s}\,,\boldsymbol{j}_{\ell s}) \;=\; \left(\bar{\psi}_{\ell s}\gamma^{0}\psi_{\ell s}\,,\bar{\psi}_{\ell s}\boldsymbol{\gamma}\psi_{\ell s}\right) \;=\; \left(\psi^{\dagger}_{\ell s}\psi_{\ell s}\,,\psi^{\dagger}_{\ell s}\gamma^{0}\boldsymbol{\gamma}\psi_{\ell s}\right). \tag{2.16}$$

Here $\bar{\psi}_{\ell s}$ is the Dirac conjugate of the wave function (2.6) and can be written as

$$\bar{\psi}_{\ell s}\,(\boldsymbol{r},t) \;\;=\;\; \frac{e^{-i\Phi}}{\sqrt{2}}\left[\bar{\mathcal{A}}_{1}e^{-i\ell\varphi}J_{\ell}\,(\xi)+\bar{\mathcal{A}}_{2}e^{-i(\ell+1)\varphi}J_{\ell+1}\,(\xi)+\bar{\mathcal{A}}_{3}e^{-i(\ell-1)\varphi}J_{\ell-1}\,(\xi)\right], \tag{2.17}$$

with the conjugated constant 1×4 bi-spinors (compare with Eqs. (2.7))

$$\bar{\mathcal{A}}_{1} \;=\; \mathcal{A}^{\dagger}_{1}\gamma^{0} \;=\; \left(\sqrt{1+\frac{m}{\mathcal{E}_{0}}}\,(\alpha\,,\;\;\beta)\;\,,\;\;\sqrt{1-\frac{m}{\mathcal{E}_{0}}}\cos\theta_{0}\,(-\alpha\,,\;\;\beta)\right),$$

$$\bar{\mathcal{A}}_{2} \;=\; \mathcal{A}^{\dagger}_{2}\gamma^{0} \;=\; \left(0\,,\;\;0\,,\;\;0\,,\;\;i\alpha\sqrt{\Delta}\right),\quad \bar{\mathcal{A}}_{3} \;=\; \mathcal{A}^{\dagger}_{3}\gamma^{0} \;=\; -\left(0\,,\;\;0\,,\;\;i\beta\sqrt{\Delta}\,,\;\;0\right).$$

We can further multiply the above expressions by γ matrices and bi-spinors (2.7) to evaluate products of the form $\bar{\mathcal{A}}_{i}\gamma^{\mu}\mathcal{A}_{i}$ $(i=\{1,2,3\})$, values of which are shown in tables. While calculating these products, we take into account that $\alpha\beta=0$ and $\alpha^{2}+\beta^{2}=1$ since the spin-up and spin-down states "exclude" each other.

	$\gamma^{0}\mathcal{A}_{1}$	$\gamma^{0}\mathcal{A}_{2}$	$\gamma^{0}\mathcal{A}_{3}$	$\gamma^{1}\mathcal{A}_{1}$	$\gamma^{1}\mathcal{A}_{2}$	$\gamma^{1}\mathcal{A}_{3}$
$\bar{\mathcal{A}}_{1}$	$\left(\alpha^{2}+\beta^{2}\right)(2-\Delta)$	0	0	0	$i\alpha^{2}\dfrac{p_{\perp 0}}{\mathcal{E}_{0}}$	$-i\beta^{2}\dfrac{p_{\perp 0}}{\mathcal{E}_{0}}$
$\bar{\mathcal{A}}_{2}$	0	$\alpha^{2}\Delta$	0	$-i\alpha^{2}\dfrac{p_{\perp 0}}{\mathcal{E}_{0}}$	0	0
$\bar{\mathcal{A}}_{3}$	0	0	$\beta^{2}\Delta$	$i\beta^{2}\dfrac{p_{\perp 0}}{\mathcal{E}_{0}}$	0	0

Table 2.1: Products $\bar{\mathcal{A}}_{i}\gamma^{0}\mathcal{A}_{i}$ and $\bar{\mathcal{A}}_{i}\gamma^{1}\mathcal{A}_{i}$, where $i=\{1,2,3\}$.

	$\gamma^{2}\mathcal{A}_{1}$	$\gamma^{2}\mathcal{A}_{2}$	$\gamma^{2}\mathcal{A}_{3}$	$\gamma^{3}\mathcal{A}_{1}$	$\gamma^{3}\mathcal{A}_{2}$	$\gamma^{3}\mathcal{A}_{3}$
$\bar{\mathcal{A}}_{1}$	0	$\alpha^{2}\dfrac{p_{\perp 0}}{\mathcal{E}_{0}}$	$\beta^{2}\dfrac{p_{\perp 0}}{\mathcal{E}_{0}}$	$\left(\alpha^{2}+\beta^{2}\right)\dfrac{2p_{\|\|0}}{\mathcal{E}_{0}}$	0	0
$\bar{\mathcal{A}}_{2}$	$\alpha^{2}\dfrac{p_{\perp 0}}{\mathcal{E}_{0}}$	0	0	0	0	0
$\bar{\mathcal{A}}_{3}$	$\beta^{2}\dfrac{p_{\perp 0}}{\mathcal{E}_{0}}$	0	0	0	0	0

Table 2.2: Products $\bar{\mathcal{A}}_{i}\gamma^{2}\mathcal{A}_{i}$ and $\bar{\mathcal{A}}_{i}\gamma^{3}\mathcal{A}_{i}$, where $i=\{1,2,3\}$.

Thus, after readily performed calculations we obtain the components of the 4-current of the relativistic field-free EVB

$$\boxed{\rho_{\ell s}(\xi) \;=\; \left(1-\frac{\Delta}{2}\right) J_\ell^2(\xi) + \frac{\Delta}{2} J_{\ell+2s}^2(\xi)\;,} \tag{2.18}$$

$$j_{\ell s}^{(x)}(\xi,\varphi) \;=\; -\frac{p_{\perp 0}}{\mathcal{E}_0}\sin\varphi\, J_\ell(\xi)\, J_{\ell+2s}(\xi)\;, \tag{2.19}$$

$$j_{\ell s}^{(y)}(\xi,\varphi) \;=\; \frac{p_{\perp 0}}{\mathcal{E}_0}\cos\varphi\, J_\ell(\xi)\, J_{\ell+2s}(\xi)\;, \tag{2.20}$$

$$j_\ell^{(z)}(\xi) \;=\; \frac{p_{\|0}}{\mathcal{E}_0} J_\ell^2(\xi)\;. \tag{2.21}$$

We can immediately recognize that both x- and y-components of the current depend on the azimuthal angle φ and the dimensionless transverse coordinate ξ, in contrast to the probability density $\rho_{\ell s}$ and the z-component of the current, $j_\ell^{(z)}$. If we employ, however, the cylindrical symmetry of the EVB propagation and re-write the three-dimensional current in cylindrical coordinates, $\boldsymbol{j}_{\ell s} = \left(j_\ell^{(r)}, j_\ell^{(\varphi)}, j_\ell^{(z)}\right)$, we can show that the *azimuthal* current $j_\ell^{(\varphi)}$ becomes only ξ-dependent. Whereas, the *radial* current $j_\ell^{(r)}$ vanishes due to the non-diffracting propagation of the (field-free) electron Bessel beam, in agreement with the same type of propagation of optical Bessel beams [54]. To show these features, let us make use of standard relations between components of a vector in Cartesian and polar coordinates

$$\begin{aligned} j^{(r)} &= j^{(x)}\cos\varphi + j^{(y)}\sin\varphi\,, \\ j^{(\varphi)} &= -j^{(x)}\sin\varphi + j^{(y)}\cos\varphi\,. \end{aligned} \tag{2.22}$$

By combining these relations with Eqs. (2.19) and (2.20), we get

$$j^{(r)} \;=\; 0\,, \tag{2.23}$$

$$j_{\ell s}^{(\varphi)}(\xi) \;=\; \frac{p_{\perp 0}}{\mathcal{E}_0} J_\ell(\xi)\, J_{\ell+2s}(\xi)\;, \tag{2.24}$$

such that the three-dimensional current of relativistic twisted electrons can be represented as a sum of the *longitudinal*

$$\boxed{\boldsymbol{j}_\ell^{\,\mathrm{long}}(\xi) \;=\; \frac{p_{\|0}}{\mathcal{E}_0} J_\ell^2(\xi)\,\boldsymbol{e}_z} \tag{2.25}$$

and *transverse*

$$\boxed{\boldsymbol{j}_{\ell s}^{\,\mathrm{tr}}(\xi) \;=\; \frac{p_{\perp 0}}{\mathcal{E}_0} J_\ell(\xi)\, J_{\ell+2s}(\xi)\,\boldsymbol{e}_\varphi} \tag{2.26}$$

components, i.e.

$$\boldsymbol{j}_{\ell s}(\xi) \;=\; \boldsymbol{j}_\ell^{\,\mathrm{long}}(\xi) + \boldsymbol{j}_{\ell s}^{\,\mathrm{tr}}(\xi)\;. \tag{2.27}$$

Here $\boldsymbol{e}_z$ and $\boldsymbol{e}_\varphi$ are the unit vectors in z- and azimuthal directions, respectively. Moreover, the ξ-dependency of both the probability density and the transverse current means that the intensity of the EVB is distributed along some concentric circles around the axis $\xi = 0$, since $j^{(r)} = 0$, as we illustrate in Figs. 2.1-2.2.

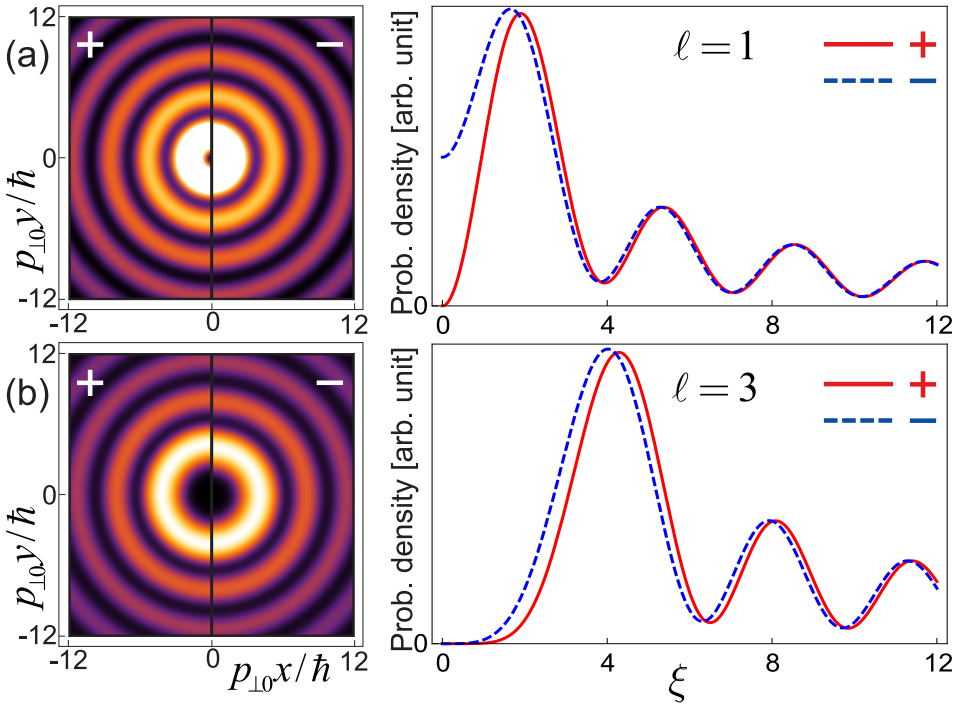

Figure 2.1: Spin-dependent distribution of the probability density of non-paraxial EVB, as depicted in Ref. [45]. The two-dimensional transverse distribution of the probability density as a function of dimensionless coordinates $p_{\perp 0}x/\hbar$ and $p_{\perp 0}y/\hbar$ represents concentric circles (left panel). The transverse distribution of the EVB intensity as a function of the dimensionless transverse coordinate ξ, indicated in arbitrary units of the same scale, obtains a Bessel-squared-type behavior (right panel). The probability density distributions are shown for the OAM $\ell = 1$ (a) and $\ell = 3$ (b). The $s = \pm 1/2$ spin states are indicated by "+" (red solid curves) and "–" (blue dashed curves), respectively. The intrinsic SOI parameter $\Delta = 0.3$, which corresponds to the electron energy 817.4 keV and the opening angle $\theta_0 = \pi/4$. In density plots, the variation of colors is the same as for Fig. 3(c) and, moreover, the beam propagates toward the reader.

Distributions of the probability density (2.18) as well as the longitudinal (2.25) and the transverse (2.26) currents are the second main result of this chapter. Equations (2.18) and (2.26) demonstrate that the transverse structure of the EVB shows *distinct* dynamics for different spin states, a new effect that is related to the existence of the electron's intrinsic OAM along its propagation direction. To emphasize once again, such an OAM for free propagating electrons itself is a new degree of freedom that couples to the SAM of electron – as it is evident from the wave function (2.6) with non-zero bi-spinors $\mathcal{A}_1$ and $\mathcal{A}_2$ – and eventually gives rise to the intrinsic spin-orbit coupling. The intrinsic SOI manifests itself in the spin-dependent observables $\rho_{\ell s}$ and $\boldsymbol{j}^{\rm tr}_{\ell s}$. This is quite in contrast to the plane-wave electrons for which the 4-current does not depend on spin [68], unless one takes into account some quantum electrodynamical effects, such as the electron's self-interaction with its (virtual) photon field [33].

In contrast to the probability density $\rho_{\ell s}$ and the transverse current $\boldsymbol{j}^{\rm tr}_{\ell s}$, Eq. (2.25) demonstrates the spin-degeneracy of the longitudinal current $\boldsymbol{j}^{\rm long}_{\ell}$. In fact, it has the same value for both $s = \pm 1/2$, though takes different values for different OAM ℓ. Such a spin-independent

behavior is characteristic for scalar Bessel beams. If we construct the 4-current from the scalar EVB (2.9), we get the only contribution both from the probability density

$$\rho_\ell^{\text{scalar}}(\xi) \;=\; J_\ell^2(\xi)\,,$$

which in this case exhibits the same dynamics for different spin states, and from the total current

$$\boldsymbol{j}_\ell^{\text{scalar}}(\xi) \;=\; \frac{p_{\|0}}{\mathcal{E}_0} J_\ell^2(\xi)\,\boldsymbol{e}_z\,,$$

defined only via the longitudinal component. This is in correlation with the fact that in the paraxial regime, i.e. when we turn from vector to scalar beams by setting $p_{\perp 0} \to 0$ (or $\theta_0 \to 0$), the azimuthal current vanishes and only the z-component of the current survives. Terms proportional to the transverse momentum $p_{\perp 0}$ and the intrinsic SOI parameter Δ will just be zero (see the above tables).

Now let us examine in more details some properties of the probability density and current of EVBs. One can easily check that the distributions of $\rho_{\ell s}$ and $|\boldsymbol{j}_{\ell s}|$ are invariant with respect to the transformation $(\ell, s) \to (-\ell, -s)$, but neither with respect to $(\ell, s) \to (\ell, -s)$ nor $(\ell, s) \to (-\ell, s)$. This invariance reflects the typical symmetry of the intrinsic SOI. Figure 2.1 shows the fine spin-dependent splitting of the probability density due to the both non-paraxial and relativistic regimes of the twisted electron beam propagation [c.f. Eq. (2.18)]. Despite the fact of the usual vortex behavior, i.e. zero intensity and undefined phase, there can be a finite probability to find an electron at $\xi = 0$ for relativistic vector Bessel beams. For example, in the case when $\ell = 1$, the last term in Eq. (2.18) leads to a radically different behavior at $\xi = 0$ and there appears an effect of a *drastic enhancement* of the probability density for the spin-down states [cf. Fig. 2.1(a)]. Whereas, the intensity of the EVB is zero for the spin-up state. In the case when, for example, $\ell = 3$ the probability density is zero for both spin states at $\xi = 0$ [cf. Fig. 2.1(b)]. It turns out, however, if we "switch on" some external influence, such as a laser light, we can "enhance" the electronic intensity at $\xi = 0$ even for $\ell = 3$ by just shifting the EVB as a whole. We discuss such a scenario quite in details in the next section.

Figure 2.2 shows the manifestation of the intrinsic SOI in the transverse current of EVBs. The SOI between the spin- and orbital-degrees of freedom leads to a fine spin dependent-splitting for the transverse (or azimuthal) current, in the same way as for the probability density $\rho_{\ell s}$. Particularly, in accordance with Eqs. (2.23), (2.24) and (2.26), Fig. 2.2 exhibits the spin-dependent distribution of the transverse current (a1,a2,b1,b2,c1,c2) and the splitting of the azimuthal current (a3,b3,c3) for different values of OAM ℓ. Figures 2.2(a1,a2,b1,b2,c1,c2) also show the absence and the presence of the "flow" of electronic current along the radial and azimuthal directions, respectively. This means that the azimuthal component of the current takes distinct values for different circles, representing different ξ, and remains constant in the azimuthal direction. Thus, the transverse current coils around only the z-axis along the concentric circles. Such a coil of the current is accompanied with the longitudinal propagation of electrons and results in the helical wavefront of the beam, characteristic for the spiraling Pointing vector of optical vortex beams [3,5]. This (oscillatory) effect disappears in the paraxial limit $p_{\perp 0} \to 0$ and is the relativistic generalization of the similar trembling motion of scalar Bessel beams of electrons (see Introduction).

There is an intriguing difference between the transverse components of the electronic current for scalar and vector Bessel beams. As we have seen before, the current of a scalar beam always rotates along the same direction in all circles for the given value of the OAM ℓ [cf. Figs. 3(e1-4)]. Whereas, the direction of the transverse current for vector beams varies depending on the radial

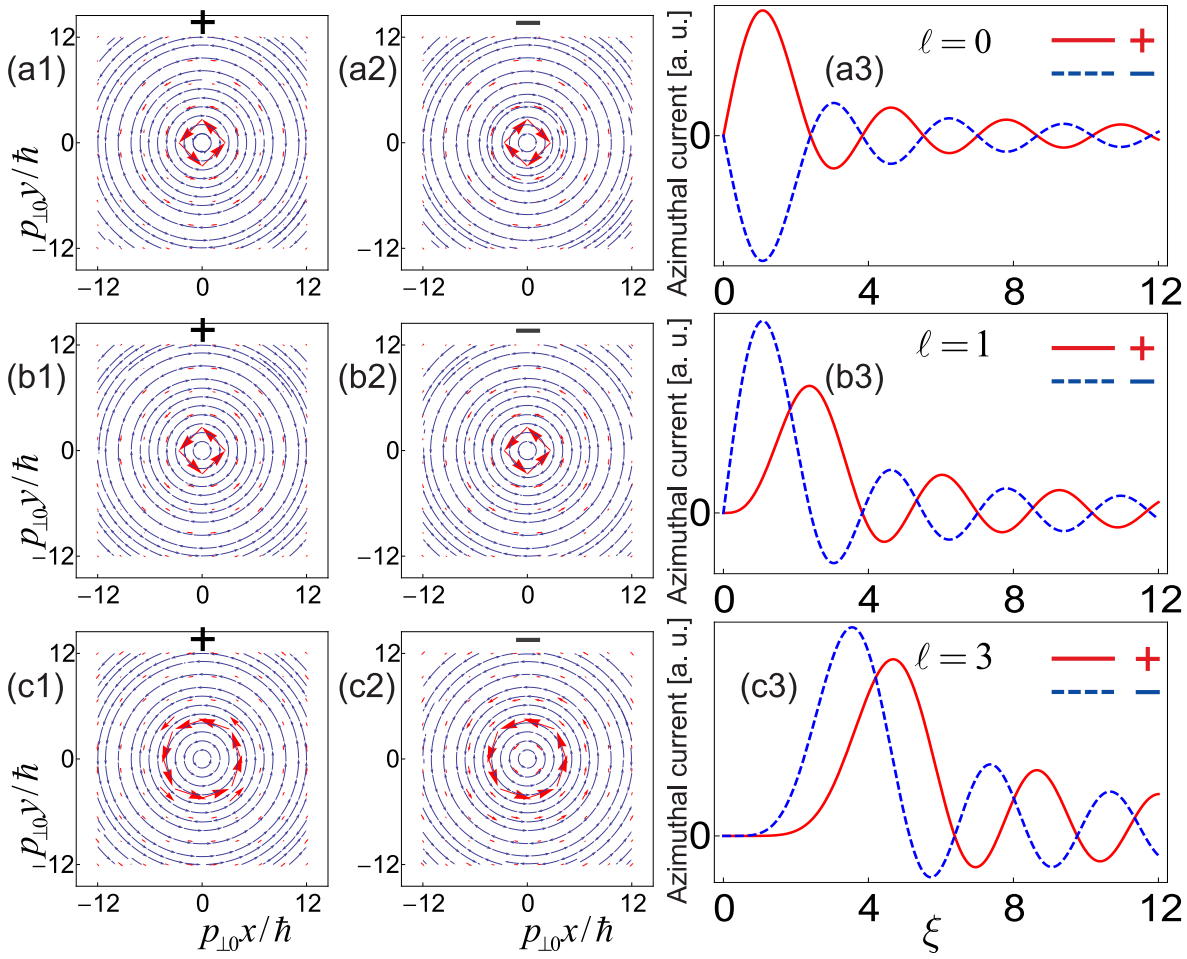

Figure 2.2: Representation of the spin-dependent transverse current $\boldsymbol{j}^{\rm tr}_{\ell s} = \left(j^{(x)}_{\ell s}, j^{(y)}_{\ell s}\right) = \left(j^{(r)}_{\ell s}, j^{(\varphi)}_{\ell s}\right)$ for OAM $\ell = 0$ (a), $\ell = 1$ (b) and $\ell = 3$ (c). Streamlines and vector plots are generated to show the vector field $\left(j^{(x)}_{\ell s}, j^{(y)}_{\ell s}\right)$ as a function of dimensionless coordinates $p_{\perp 0}x/\hbar$ and $p_{\perp 0}y/\hbar$ (the beam propagates toward the reader). Thickness of vectors increases with increasing absolute value of the transverse current $|\boldsymbol{j}^{\rm tr}_{\ell s}|$. Figures (a3), (b3) and (c3) show the distribution of the azimuthal current as a function of the dimensionless transverse coordinate ξ (in arbitrary units). The parameters of the electron beam are the same as for Fig. 2.1. Red solid ("+") and blue dashed ("–") curves indicate the spin-up and spin-down states, respectively.

coordinate ξ. This effect is also due to the intrinsic SOI and vanishes in the non-relativistic and/or paraxial regimes.

In this section, we have built the wave function of field-free EVBs (2.6) and calculated distributions of their probability density (2.18) and transverse current (2.26). We have demonstrated how the presence of the SAM and the longitudinal OAM of the electron gives rise to the intrinsic SOI that, in turn, leads to a spin-dependent dynamics of the EVB. Such analyzes have been performed for EVBs that propagate in free space. A natural question that arises out of this study is: what happens if we replace the free space with the electromagnetic radiation? In other words, how one can control and manipulate the properties of electron vortex beams by means of a laser light? To answer these questions, in the next chapter, we generalize the field-free states (2.6) to a *laser-driven* ones by superimposing the Dirac-Volkov solutions (1.39) with well-defined amplitudes corresponding to the monoenergetic distribution of electrons in Bessel beams. Such a construction would enable us to obtain yet another solution of the Dirac equation – the so-called Volkov-Bessel solution – to describe the interaction of the two feasible beams, namely the relativistic EVB and a plane-wave laser pulse. Moreover, we shall construct measurable quantities to characterize the profile and the helical wavefront of field-affected twisted electron beams in order to reveal the influence of a laser light.

2.2 Laser-driven relativistic electron vortex beams

In this section, we introduce our advanced studies of field-affected EVBs by recovering the results of our recent Letter [78] and expanding them for a more detailed examination of the "twisted electron–laser pulse" interaction.

2.2.1 Volkov-Bessel solutions of the Dirac equation

Until now, we have derived Bessel-type solutions (2.6) for the free-Dirac equation (1.3) and showed that they represent the eigenstates of the longitudinal component of the TAM operator. Based on these solutions, we have calculated the 4-current of field-free EVBs and demonstrated that it has a distinct dynamics for spin-up and spin-down states due to the intrinsic SOI. In order to see how this SOI is modified within the laser field, we here construct Bessel-type solutions of the Dirac equation (1.21) for an electron inside a given electromagnetic field. To do so, we make use of the standard procedure for constructing Bessel beams as a superposition of orthonormalized waves – which in our case will be Dirac-Volkov solutions (1.39) – over the monoenergetic momentum distribution (1). In more technical terms, again, we use the cylindrical coordinates in momentum space, $\boldsymbol{p} = (p_\perp, \phi, p_{||}) = (p\sin\theta, \phi, p\cos\theta)$, and build the *Volkov-Bessel* solutions as a superposition

$$\Psi_{\ell s}(x) \;=\; \int \tilde{\psi}_\ell(\boldsymbol{p})\; \psi_p(x)\, p_\perp \mathrm{d}p_\perp \mathrm{d}\phi\,. \tag{2.28}$$

Our aim is to generalize the wave function of the field-free EVB (2.6) to the laser-driven ones such that $\Psi_{\ell s} \to \psi_{\ell s}$ when we switch off the field. The Ansatz (2.28) allows us to realize this goal for a specifically chosen geometry of the EVB-laser coupling.

The Dirac-Volkov solution (1.39) is valid independent of the polarization of electromagnetic wave and for arbitrary relative (directions of) propagation of the electron and laser beams. To evaluate the integral (2.28), however, we here restrict ourselves to a "head-on" scenario, in which the electrons and the linearly polarized photons propagate antiparallel to each other (see Fig. 2.3). For this geometry, we choose the z-axis directed along the propagation of

the EVB which implies that the laser propagates backward along z, such that the 4-momentum of the twisted electron and the wave 4-vector of the laser take the form

$$p^\mu \,=\, (\mathcal{E}\,,\boldsymbol{p}) \,=\, \big(\mathcal{E}\,,p_\perp\cos\phi\,,p_\perp\sin\phi\,,p_{||}\big) \,=\, (\mathcal{E}\,,p\sin\theta\cos\phi\,,p\sin\theta\sin\phi\,,p\cos\theta)$$

and

$$k^\mu \,=\, (\omega,\boldsymbol{k}) \,=\, (\omega\,,0\,,0\,,-k)\ ,$$

respectively. The laser phase, therefore, will then be written as

$$\zeta \,=\, (kr) \,=\, \omega t + kz\,, \tag{2.29}$$

that depends only on the longitudinal coordinate z and time t.

To describe the given electromagnetic field we assume that no external charges are applied such that the field propagates freely. We choose, moreover, the y-axis to be the polarization axis of photons

$$A^\mu \;\;=\;\; (0\,,0\,,A\,(\zeta)\ ,0)\ ,$$

where – for the moment – we do not specify the shape of $A\,(\zeta)$. For this linearly polarized field, the exponent $\mathcal{F}$ [cf. Eq. (1.38)] contributes into the dynamics of the EVB via the $p_\perp$- and ϕ-dependent term $p_\perp A\sin\phi$, whereas, the exponent $\mathcal{G}$ remains independent of both $p_\perp$ and ϕ, since its denominator $(kp)=\omega\mathcal{E}+kp_{||}$:

$$\mathcal{F}\,\equiv\,\int_0^\zeta \mathrm{d}\tilde{\zeta}\,\frac{ep_\perp A(\tilde{\zeta})\sin\phi}{\omega\mathcal{E}+kp_{||}}\,,\quad \mathcal{G}\,\equiv\,\int_0^\zeta \mathrm{d}\tilde{\zeta}\,\frac{e^2A^2(\tilde{\zeta})}{2\,(\omega\mathcal{E}+kp_{||})}\,.$$

Furthermore, we make use of the ϕ-dependency of $\mathcal{F}$ and employ the Jacobi-Anger expansion

$$e^{if\sin\phi} \;\;=\;\; \sum_{n=-\infty}^{+\infty} J_n\,(f)\,e^{in\phi} \tag{2.30}$$

to express the exponential of the sine in the basis of its harmonics, i.e. to "decouple" the variable ϕ from the sine. This expansion enables us to reveal the so-called *intrinsic orbit-orbit* interaction (OOI) between the orbital-degree of freedom of the electron, described by ℓ, and the *OAM-components* of the plane-wave electromagnetic field, described by n (see below). Here the function f depends only on the laser phase and is originated from $\mathcal{F}$:

$$f\,(\zeta) \;\;\equiv\;\; \int_0^\zeta \mathrm{d}\tilde{\zeta}\,\frac{ep_\perp A(\tilde{\zeta})}{\omega\mathcal{E}+kp_{||}}\,. \tag{2.31}$$

We should stress here that we have a freedom to consider a large class of plane-wave lasers, such as monochromatic waves, few-cycle or chirped pulses, for which the latter integral can be calculated analytically. In our further study, however, we will put the emphasis on the ultrashort few-cycle pulses that have attracted the interest of a wide range of audience and have found numerous applications in research over the last years (see, e.g., [79–81] and references therein).

After we have characterized the polarization of the field and the geometry of the "twisted electron + laser beam" system, we are ready to carry out the integral (2.28). For this purpose,

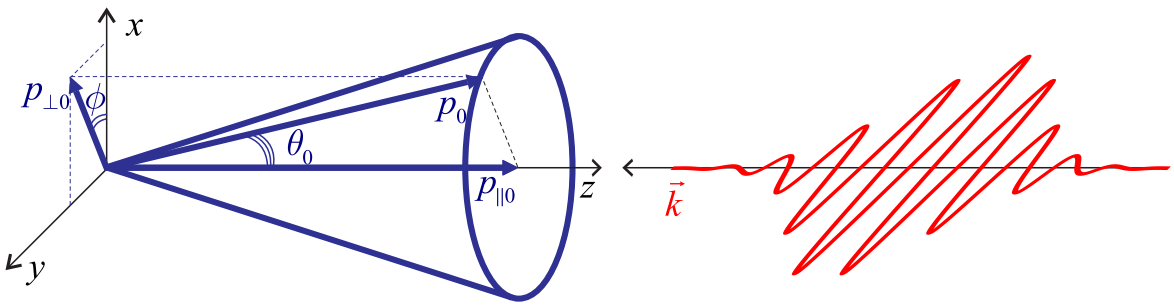

Figure 2.3: Geometry of head-on collision of relativistic EVB (with a momentum distribution indicated in blue) and linearly polarized, few-cycle laser pulse (red waveform). The z-axis is chosen parallel (anti-parallel) to the electron (laser) propagation direction, the y-axis is set to show the polarization direction of the field. Controlled by a laser field, the center of the field-affected EVB experiences a shift in comparison to the center of the field-free EVB and undergoes temporal oscillations along the field polarization direction, as shown in Figs. 2.5, 2.6, 2.8.

we again utilize the cylindrical coordinates in real (or position) space due to the cylindrical symmetry of the beam propagation, $\boldsymbol{r} = (r\,, \varphi\,, z)$. First, we integrate over $p_\perp$ and obtain

$$\begin{aligned}
\Psi_{\ell s}\left(\boldsymbol{r},t\right) &= \left[1+\frac{e}{2\left(kp_0\right)}\left(\gamma k\right)\left(\gamma A\right)\right]\frac{e^{i\left(\Phi+\mathcal{G}(p_0)\right)}}{\sqrt{2}}\sum_{n=-\infty}^{+\infty}J_n\left(f_0\right)\int_0^{2\pi}\mathrm{d}\phi\,\frac{e^{i(\ell+n)\phi}}{2\pi i^{\ell}}\,e^{i\xi\cos(\phi-\varphi)}u_{p_0} \\
&= \left[1+\frac{e}{2\left(kp_0\right)}\left(\gamma k\right)\left(\gamma A\right)\right]\frac{e^{i\left(\Phi+\mathcal{G}(p_0)\right)}}{\sqrt{2}}\sum_{n=-\infty}^{+\infty}J_n\left(f_0\right) \\
&\times \left[\mathcal{A}_1\int_0^{2\pi}\mathrm{d}\phi\,\frac{i^n e^{i(\ell+n)\phi}}{2\pi i^{\ell+n}}\,e^{i\xi\cos(\phi-\varphi)}\right. \\
&+ \left.\mathcal{A}_2\int_0^{2\pi}\mathrm{d}\phi\,\frac{i^n e^{i(\ell+n+1)\phi}}{2\pi i^{\ell+n+1}}\,e^{i\xi\cos(\phi-\varphi)}+\mathcal{A}_3\int_0^{2\pi}\mathrm{d}\phi\,\frac{i^n e^{i(\ell+n-1)\phi}}{2\pi i^{\ell+n-1}}\,e^{i\xi\cos(\phi-\varphi)}\right],
\end{aligned}$$

quite similar to the analog integration (2.5) for the field-free EVB, but with some modification arising from the presence of the external field. We further employ the integral representation of the Bessel function (10) and arrive to the following exact form of the Volkov-Bessel wave function:

$$\boxed{\Psi_{\ell s}\left(\boldsymbol{r},t\right) = \left[1+\frac{e}{2\left(kp_0\right)}\left(\gamma k\right)\left(\gamma A\right)\right]\sum_{n=-\infty}^{+\infty}i^n J_n\left(f_0\right)\psi_{\ell+n,s}\left(\boldsymbol{r},t\right)\,.} \tag{2.32}$$

Here the function $f_0 \equiv f\left(p_0\right)$ is taken for those values of momentum and energy that represent the monoenergetic cone (1). As for the field-free EVB, the dimensionless transverse coordinate $\xi = p_{\perp 0} r$ effectively defines the width of the laser-driven EVB. Moreover, the states

$$\begin{aligned}
\psi_{\ell+n,s}\left(\boldsymbol{r},t\right) &= \frac{e^{i\tilde{\Phi}}}{\sqrt{2}}\left[\mathcal{A}_1 e^{i(\ell+n)\varphi}J_{\ell+n}\left(\xi\right)\right. \\
&+ \left.\mathcal{A}_2 e^{i(\ell+n+1)\varphi}J_{\ell+n+1}\left(\xi\right)+\mathcal{A}_3 e^{i(\ell+n-1)\varphi}J_{\ell+n-1}\left(\xi\right)\right],
\end{aligned} \tag{2.33}$$

with constant bi-spinors (2.7), look like the Bessel-type solution (2.6) of the free Dirac equation, but with some modified phase (compare to Eq. (2.3))

$$\tilde{\Phi}\left(z,t\right) \equiv p_{||0}z - \mathcal{E}_0 t + \mathcal{G}\left(p_0\right) = \Phi\left(z,t\right) + \mathcal{G}\left(p_0\right)$$

and modified OAM $\ell + n$, where ℓ is the OAM of the (initially) field-free EVB [45]. This modified OAM arises naturally due to the *coupling* between the phase factors $e^{in\phi}$ (from the Jacobi-Anger expansion) and $e^{i\ell\phi}$ (from the Bessel spectrum). In other words, the change of the OAM is due to the intrinsic OOI between the OAM of the electron and the OAM-components of the field. Such an orbit-orbit coupling enables one to interpret n as an *additional* OAM due to the laser. Let us also note that the wave function (2.32) represents a superposition of infinitely many modes $J_{\ell+n}$ and $J_{\ell+n\pm1}$ (for a given ℓ), similar to the expression of plane-waves as an infinite sum of spherical harmonics.

Apart from the OOI, the presence of both the non-zero SAM and OAM of the electron gives rise to the intrinsic SOI in the laser-driven EVB, in a similar way as for field-free EVBs. Equation (2.33) shows that the coupling between the spin and angular degrees of freedom is described via the modes $J_{\ell+n\pm1}$ which appear with the coefficients $\mathcal{A}_2$ and $\mathcal{A}_3$ [cf. Eq. (2.7)] that, in turn, are proportional to the square root of the intrinsic SOI-parameter, $\sqrt{\Delta}$. To remind the reader, again, the coefficients $\mathcal{A}_2$ and $\mathcal{A}_3$ remain finite in both the non-paraxial ($\theta_0 \neq 0$) and relativistic ($p_0 \neq 0$) regimes. Whereas, in paraxial ($\theta_0 \to 0$) and/or in non-relativistic ($p_0 \to 0$) limits the SOI parameter vanishes and, therefore, only the "scalar" mode $J_{\ell+n}$ contributes in the Volkov-Bessel states (2.32)-(2.33). Indeed, the corresponding approximated wave function in the paraxial domain takes the form

$$\Psi_{\ell s}^{\text{scalar}}\left(\boldsymbol{r},t\right) = \left[1 + \frac{e}{2\left(kp_0\right)}\left(\gamma k\right)\left(\gamma A\right)\right] \sum_{n=-\infty}^{+\infty} i^n J_n\left(f_0\right) \frac{1}{\sqrt{2}} \mathcal{A}_1 e^{i\left(\tilde{\Phi}+(\ell+n)\varphi\right)} J_{\ell+n}\left(\xi\right) , \quad (2.34)$$

which is the generalization of the scalar, field-free wave function (2.9). In nowadays experiments [cf., e.g., Ref. [39]], the EVBs are produced only within the paraxial regime. Therefore, our scalar wave function (2.34) is of particular interest to understand the outcome of experiments.

The exact Volkov-Bessel solution (2.32) of the Dirac equation (1.21) is the second main results of this chapter. It describes the motion of relativistic electron vortex beams that are driven by a linearly polarized plane-wave laser field with the vector potential $A\left(\zeta\right)$ of an *arbitrary* shape. Our newly obtained solution generalizes, on one hand, the recently obtained field-free relativistic electron vortex beams [cf. Eq. (2.6) and Ref. [45]], on the other hand, the Dirac-Volkov solution (1.39) for the laser-driven plane-wave electrons (see also Ref. [68]). We can easily demonstrate how to recover these known results if we consider appropriate limiting cases. First, let us switch off the laser field by setting $A = 0$, which gives rise to the vanishing function f_0, $f_0 = 0$ [cf. Eq. (2.31)]. Therefore, Bessel functions in the Volkov-Bessel solution (2.32) can be replaced by their particular values

$$J_n\left(f_0 = 0\right) = \begin{cases} 1\,, & \text{for} \quad n = 0 \\ 0\,, & \text{for} \quad n \neq 0 \end{cases} , \quad (2.35)$$

such that the only non-zero contribution comes from the summand with the index $n = 0$. This can be interpreted as "switching off the OOI" or "switching off the field". Equations (2.32) and (2.35) eventually lead to the wave function of the field-free EVB (2.6), as one would expect. Second, let us now keep the field on and switch off the "twistedness" of the electron by considering its plane-wave limit, i.e. by setting the opening angle $\theta_0 = 0$, transverse momentum

$p_{\perp 0} = 0$ and the longitudinal OAM $\ell = 0$. For these vales, the intrinsic SOI-parameter $\Delta = 0$ and the Bessel functions in Eqs. (2.32)-(2.33) take the form

$$J_{\ell+n}(\xi = 0) \;=\; \begin{cases} 1\,, & \text{for} \quad n = 0\,,\, \ell = 0 \\ 0\,, & \text{for} \quad n \neq 0\,,\, \ell = 0 \end{cases} . \tag{2.36}$$

We can, therefore, formally write

$$\Psi_{\ell s}(\boldsymbol{r}, t) \quad \xrightarrow[\text{twisted wave}\to\text{plane-wave}]{} \quad \left[1 + \frac{e}{2\,(kp_0)}\,(\gamma k)\,(\gamma A)\right] \frac{\mathcal{A}_1}{\sqrt{2}} e^{i\tilde{\Phi}}\,,$$

that exactly coincides with the Dirac-Volkov solution (1.40) if we notice that $\mathcal{A}_1 = u_{p_{||}0}/\sqrt{\mathcal{E}_0}$ (compare Eqs. (1.41) and (2.7) for $\theta_0 = 0$).

After we have constructed the Volkov-Bessel solutions and discussed their limiting cases, we are now ready to employ them in order to calculate the 4-current of laser-driven relativistic EVBs. We shall study how the intensity and the current distribution of the twisted electron change within an external laser field in both non-paraxial and paraxial regimes.

2.2.2 4-current of field-affected EVBs

The Volkov-Bessel solutions (2.32) can be employed to calculate various different observables related to the EVB-laser interaction. For instance, we can analyze the 4-current of the laser-driven EVB by using Eqs. (2.32)-(2.33) to better understand how a linearly polarized laser field affects an EVB with a given energy in both non-paraxial ($\Delta < 1$) and paraxial ($\Delta \to 0$) regimes. For this, we have to evaluate all the components of the 4-current

$$\mathcal{J}^{\mu}_{\ell s} \;=\; (\Xi_{\ell s}\,, \boldsymbol{\mathcal{J}}_{\ell s}) \;=\; \bar{\Psi}_{\ell s} \gamma^{\mu} \Psi_{\ell s}\,, \tag{2.37}$$

where $\Xi_{\ell s}$ and $\boldsymbol{\mathcal{J}}_{\ell s}$ are the probability density and the three-dimensional current of the laser-driven EVB, respectively. The presence of the electromagnetic field does not violate the (general) cylindrical symmetry of the EVB propagation. Therefore, we shall make use of the cylindrical coordinates and express the current $\boldsymbol{\mathcal{J}}_{\ell s}$ as a sum of the longitudinal and transverse components

$$\boldsymbol{\mathcal{J}}_{\ell s} \;=\; \boldsymbol{\mathcal{J}}^{\text{long}}_{\ell s} + \boldsymbol{\mathcal{J}}^{\text{tr}}_{\ell s}\,, \tag{2.38}$$

in analogy with field-free EVBs (2.27). Moreover, we expect that the Volkov-Bessel 4-current (2.37) experiences a spin-splitting due to the intrinsic SOI, however, with some *dynamic* modification due to the laser field.

To calculate the 4-current (2.37), we write the Dirac conjugate of the wave function (2.32) in the form

$$\bar{\Psi}_{\ell s}(\boldsymbol{r}, t) \;=\; \sum_{n=-\infty}^{+\infty} i^{-n} J_n(f_0)\, \bar{\psi}_{\ell+n,s}(\boldsymbol{r}, t) \left[1 + \frac{e}{2\,(kp_0)}\,(\gamma A)\,(\gamma k)\right], \tag{2.39}$$

where

$$\begin{aligned} \bar{\psi}_{\ell+n,s}(\boldsymbol{r}, t) \;&=\; \frac{e^{-i\tilde{\Phi}}}{\sqrt{2}} \Big[\bar{\mathcal{A}}_1 e^{-i(\ell+n)\varphi} J_{\ell+n}(\xi) \\ &+\; \bar{\mathcal{A}}_2 e^{-i(\ell+n+1)\varphi} J_{\ell+n+1}(\xi) + \bar{\mathcal{A}}_3 e^{-i(\ell+n-1)\varphi} J_{\ell+n-1}(\xi)\Big] \end{aligned} \tag{2.40}$$

is the Dirac conjugate of the modified (field-free) EVB (2.33). In order to proceed analytically, we make use of the summation rule

$$\begin{aligned}\sum_{n,n'=-\infty}^{+\infty}\mathcal{C}_{n,n'}e^{i\Omega(n'-n)} &= \frac{1}{2}\left(\sum_{n,n'=-\infty}^{+\infty}\mathcal{C}_{n,n'}e^{i\Omega(n'-n)}+\sum_{n,n'=-\infty}^{+\infty}\mathcal{C}_{n',n}e^{i\Omega(n-n')}\right)\\ &= \sum_{n,n'=-\infty}^{+\infty}\mathcal{C}_{n,n'}\cos\left(\Omega\left(n-n'\right)\right), \end{aligned} \tag{2.41}$$

valid for an arbitrary Ω and coefficients $\mathcal{C}_{n,n'}$ with the only constraint that they are symmetric under the interchange $n \leftrightarrow n'$, i.e. $\mathcal{C}_{n,n'} = \mathcal{C}_{n',n}$. By substituting the wave functions (2.32)-(2.33) and their conjugates (2.39)-(2.40) into Eq. (2.37) and utilizing the rule (2.41), we obtain the following exact components of the 4-current:

$$\begin{aligned}\Xi_{\ell s}(\boldsymbol{r},t) &= \mathcal{J}^{0}_{\ell s}(\boldsymbol{r},t) = \sum_{n,n'=-\infty}^{+\infty}J_n(f_0)\,J_{n'}(f_0)\\ &\times \left\{\cos\left[\left(n'-n\right)\left(\frac{\pi}{2}+\varphi\right)\right]\cdot\left[\left(1-\frac{\delta^2}{2}\right)\varrho_{\ell snn'}(\xi)-\frac{\delta^2 p_{||0}}{2\mathcal{E}_0}J_{\ell+n}(\xi)\,J_{\ell+n'}(\xi)\right]\right.\\ &+ \left.\frac{\delta p_{\perp 0}}{\mathcal{E}_0}\cos\left[2s\left(n'-n\right)\left(\frac{\pi}{2}+\varphi\right)+\varphi\right]\cdot J_{\ell+n}(\xi)\,J_{\ell+n'+2s}(\xi)\right\}. \end{aligned} \tag{2.42}$$

$$\begin{aligned}\mathcal{J}^{(x)}_{\ell s}(\boldsymbol{r},t) &= -\frac{p_{\perp 0}}{\mathcal{E}_0}\sum_{n,n'=-\infty}^{+\infty}J_n(f_0)\,J_{n'}(f_0)\\ &\times \sin\left[2s\left(n'-n\right)\left(\frac{\pi}{2}+\varphi\right)+\varphi\right]\cdot J_{\ell+n}(\xi)\,J_{\ell+n'+2s}(\xi), \end{aligned} \tag{2.43}$$

$$\begin{aligned}\mathcal{J}^{(y)}_{\ell s}(\boldsymbol{r},t) &= \sum_{n,n'=-\infty}^{+\infty}J_n(f_0)\,J_{n'}(f_0)\\ &\times \left\{\frac{p_{\perp 0}}{\mathcal{E}_0}\cos\left[2s\left(n'-n\right)\left(\frac{\pi}{2}+\varphi\right)+\varphi\right]\cdot J_{\ell+n}(\xi)\,J_{\ell+n'+2s}(\xi)\right.\\ &- \left.\delta\cos\left[\left(n'-n\right)\left(\frac{\pi}{2}+\varphi\right)\right]\cdot\left[\varrho_{\ell snn'}(\xi)+\frac{p_{||0}}{\mathcal{E}_0}J_{\ell+n}(\xi)\,J_{\ell+n'}(\xi)\right]\right\}, \end{aligned} \tag{2.44}$$

$$\begin{aligned}\mathcal{J}^{(z)}_{\ell s}(\boldsymbol{r},t) &= \sum_{n,n'=-\infty}^{+\infty}J_n(f_0)\,J_{n'}(f_0)\\ &\times \left\{\cos\left[\left(n'-n\right)\left(\frac{\pi}{2}+\varphi\right)\right]\cdot\left[\frac{p_{||0}}{\mathcal{E}_0}\left(1+\frac{\delta^2}{2}\right)J_{\ell+n}(\xi)\,J_{\ell+n'}(\xi)+\frac{\delta^2}{2}\varrho_{\ell snn'}(\xi)\right]\right.\\ &- \left.\frac{\delta p_{\perp 0}}{\mathcal{E}_0}\cos\left[2s\left(n'-n\right)\left(\frac{\pi}{2}+\varphi\right)+\varphi\right]\cdot J_{\ell+n}(\xi)\,J_{\ell+n'+2s}(\xi)\right\}. \end{aligned} \tag{2.45}$$

Here

$$\delta \equiv \frac{\omega e A}{(k p_0)} \tag{2.46}$$

is a dimensionless parameter which shows how strong or weak the laser is. Moreover,

$$\varrho_{\ell s n n'}(\xi) \equiv \left(1-\frac{\Delta}{2}\right) J_{\ell+n}(\xi) J_{\ell+n'}(\xi) + \frac{\Delta}{2} J_{\ell+n+2s}(\xi) J_{\ell+n'+2s}(\xi) \tag{2.47}$$

looks like the probability density of the field-free EVB (2.18), again with modified OAMs $\ell+n$ and $\ell+n'$. It coincides exactly with the intensity of the EVB in free space if $n = n' = 0$. Equations (2.42)-(2.45) are the fourth main result of this chapter. They enable us to reveal the influence of the electromagnetic field on the EVB dynamics and, therefore, to show how the beam can be controlled and manipulated by the laser.

We can now calculate the components of the transverse current $\boldsymbol{\mathcal{J}}^{\mathrm{tr}}_{\ell s} = \left(\mathcal{J}^{(x)}_{\ell s}, \mathcal{J}^{(y)}_{\ell s}\right)$ to construct also the radial $\mathcal{J}^{(r)}_{\ell s}$ and the azimuthal $\mathcal{J}^{(\varphi)}_{\ell s}$ currents. To this end, we use similar relations (2.22) between the Cartesian and polar coordinates of the two-dimensional vector $\boldsymbol{\mathcal{J}}^{\mathrm{tr}}_{\ell s}$ and obtain

$$\begin{aligned}
\mathcal{J}^{(r)}_{\ell s}(\boldsymbol{r},t) &= \sum_{n,n'=-\infty}^{+\infty} J_n(f_0) J_{n'}(f_0) \\
&\times \left\{ -\frac{p_{\perp 0}}{\mathcal{E}_0} \sin\left[2s\left(n'-n\right)\left(\frac{\pi}{2}+\varphi\right)\right] J_{\ell+n}(\xi) J_{\ell+n'+2s}(\xi) \right. \\
&- \left. \delta \sin\varphi \cos\left[\left(n'-n\right)\left(\frac{\pi}{2}+\varphi\right)\right] \cdot \left[\varrho_{\ell s n n'}(\xi) + \frac{p_{||0}}{\mathcal{E}_0} J_{\ell+n}(\xi) J_{\ell+n'}(\xi)\right] \right\},
\end{aligned} \tag{2.48}$$

$$\begin{aligned}
\mathcal{J}^{(\varphi)}_{\ell s}(\boldsymbol{r},t) &= \sum_{n,n'=-\infty}^{+\infty} J_n(f_0) J_{n'}(f_0) \\
&\times \left\{ \frac{p_{\perp 0}}{\mathcal{E}_0} \cos\left[2s\left(n'-n\right)\left(\frac{\pi}{2}+\varphi\right)\right] \cdot J_{\ell+n}(\xi) J_{\ell+n'+2s}(\xi) \right. \\
&- \left. \delta \cos\varphi \cos\left[\left(n'-n\right)\left(\frac{\pi}{2}+\varphi\right)\right] \cdot \left[\varrho_{\ell s n n'}(\xi) + \frac{p_{||0}}{\mathcal{E}_0} J_{\ell+n}(\xi) J_{\ell+n'}(\xi)\right] \right\}.
\end{aligned} \tag{2.49}$$

Equations (2.42), (2.45), (2.48), (2.49) show that apart from the dimensionless transverse coordinate ξ, the probability density and the cylindrical components of the three-dimensional current depend on the longitudinal coordinate z, time t [cf. the expression for f_0] and the azimuthal angle φ, quite in contrast to the corresponding quantities of the field-free EVB [cf. Eqs. (2.18),(2.21), (2.23), (2.24)]. The φ-dependency is due to the (polarization of the) laser field and can be regarded as an influence of the Lorentz force upon the EVB. Whereas, both the z- and t-dependencies arise from the laser phase ζ [cf. Eq. (2.29)]. The longitudinal coordinate z defines the transverse plane where the EVB-laser interaction takes place at time t. We should emphasize here that the EVB is delocalized both in the z-direction and in time, while the laser beam, being delocalized in the xy-plane, can have a *finite* wave-packet spread both along z and in time, as depicted in Fig. 2.3. The extension of such a wave packet becomes infinitely large for a monochromatic laser beam.

We can now discuss the limiting cases of the 4-current of generalized, laser-driven EVBs and show how to recover the expressions for 4-current of both the field-free EVBs and the field-affected plane-wave electrons. To this end, first, we switch off the laser field by setting $A = 0$ and take into account the particular values of the Bessel function (2.35). This results in

$$\begin{array}{lll} \Xi_{\ell s} \quad \text{(Eq. (2.42))} & & \varrho_{\ell s 00} = \rho_{\ell s} \quad \text{(Eqs. (2.18), (2.47))} \\ \mathcal{J}^{(x)}_{\ell s} \quad \text{(Eq. (2.43))} & & j^{(x)}_{\ell s} \quad \text{(Eq. (2.19))} \\ \mathcal{J}^{(y)}_{\ell s} \quad \text{(Eq. (2.44))} & \xrightarrow[\text{switching off the field}]{} & j^{(y)}_{\ell s} \quad \text{(Eq. (2.20))} \\ \mathcal{J}^{(z)}_{\ell s} \quad \text{(Eq. (2.45))} & & j^{(z)}_{\ell} \quad \text{(Eq. (2.21))} \\ \mathcal{J}^{(r)}_{\ell s} \quad \text{(Eq. (2.48))} & & j^{(r)} \quad \text{(Eq. (2.23))} \\ \mathcal{J}^{(\varphi)}_{\ell s} \quad \text{(Eq. (2.49))} & & j^{(\varphi)}_{\ell s} \quad \text{(Eq. (2.24))}\,. \end{array}$$

We can also demonstrate that the spin-dependent 4-current of the Volkov-Bessel electron contains, as a special case, the spin-degenerated 4-current of the Dirac-Volkov electron. Indeed, if we switch off the "twistedness" of the electron beam, by setting $\ell = 0$ and $\theta_0 = 0$, and employ Eq. (2.36), we obtain

$$\begin{array}{lll} \Xi_{\ell s} & & 1 - \dfrac{\delta^2}{2}\left(1 + \dfrac{p_{||0}}{\mathcal{E}_0}\right) \\ \mathcal{J}^{(x)}_{\ell s} & & 0 \\ \mathcal{J}^{(y)}_{\ell s} & \xrightarrow[\text{twisted wave}\to\text{plane-wave}]{} & -\delta\left(1 + \dfrac{p_{||0}}{\mathcal{E}_0}\right) \\ \mathcal{J}^{(z)}_{\ell s} & & \dfrac{p_{||0}}{\mathcal{E}_0} + \dfrac{\delta^2}{2}\left(1 + \dfrac{p_{||0}}{\mathcal{E}_0}\right)\,. \end{array}$$

The expressions on the right-hand-side coincide with the known components of the 4-current of laser-driven plane-wave electrons in the head-on scenario (compare with Eqs. (1.47)-(1.50)). This becomes obvious if we take into account the definition of the parameter δ (2.46) and notice that $\varrho_{\ell s n n'} \to 1$ for $\Delta \to 0$, $p_{\perp 0} \to 0$ and $\ell \to 0$. For plane-wave electrons, moreover, the spin-dependency is naturally eliminated in the "squared" modulus of the Dirac-Volkov wave function due to the vanishing OAM ℓ. Generally, this is true only for such plane-wave electrons that do not experience a self-interaction with their virtual photon field.

In our further discussion, we are interested in describing the profile of the field-affected EVB for a relatively *weak* laser with $|\delta| \ll 1$, a condition that will be later specified in terms of numbers. We can therefore sufficiently simplify the above formulae of the probability density and current components of the EVB

$$\Xi_{\ell s}(\boldsymbol{r}, t) \approx \sum_{n,n'=-\infty}^{+\infty} J_n(f_0)\, J_{n'}(f_0) \cos\left[\left(n' - n\right)\left(\frac{\pi}{2} + \varphi\right)\right] \cdot \varrho_{\ell s n n'}(\xi)\,, \tag{2.50}$$

$$\begin{aligned} \mathcal{J}^{(y)}_{\ell s}(\boldsymbol{r}, t) &\approx \frac{p_{\perp 0}}{\mathcal{E}_0} \sum_{n,n'=-\infty}^{+\infty} J_n(f_0)\, J_{n'}(f_0) \cos\left[2s\left(n' - n\right)\left(\frac{\pi}{2} + \varphi\right) + \varphi\right] \\ &\times J_{\ell+n}(\xi)\, J_{\ell+n'+2s}(\xi)\,, \end{aligned} \tag{2.51}$$

$$\mathcal{J}_{\ell}^{(z)}(\boldsymbol{r},t) \approx \frac{p_{\|0}}{\mathcal{E}_0}\sum_{n,n'=-\infty}^{+\infty} J_n(f_0)\,J_{n'}(f_0)\cos\left[(n'-n)\left(\frac{\pi}{2}+\varphi\right)\right] \times J_{\ell+n}(\xi)\,J_{\ell+n'}(\xi)\,, \tag{2.52}$$

$$\mathcal{J}_{\ell s}^{(r)}(\boldsymbol{r},t) \approx -\frac{p_{\perp 0}}{\mathcal{E}_0}\sum_{n,n'=-\infty}^{+\infty} J_n(f_0)\,J_{n'}(f_0)\sin\left[2s\,(n'-n)\left(\frac{\pi}{2}+\varphi\right)\right] \times J_{\ell+n}(\xi)\,J_{\ell+n'+2s}(\xi)\,, \tag{2.53}$$

$$\mathcal{J}_{\ell s}^{(\varphi)}(\boldsymbol{r},t) \approx \frac{p_{\perp 0}}{\mathcal{E}_0}\sum_{n,n'=-\infty}^{+\infty} J_n(f_0)\,J_{n'}(f_0)\cos\left[2s\,(n'-n)\left(\frac{\pi}{2}+\varphi\right)\right] \times J_{\ell+n}(\xi)\,J_{\ell+n'+2s}(\xi)\,. \tag{2.54}$$

Note that the x-component of the current (2.43) does not depend on the parameter δ and, therefore, remains unchanged under $|\delta| \ll 1$. Furthermore, both the (approximated) probability density $\Xi_{\ell s}$ and the current $\boldsymbol{\mathcal{J}}_{\ell s} = \boldsymbol{\mathcal{J}}_{\ell s}^{\mathrm{tr}} + \boldsymbol{\mathcal{J}}_{\ell s}^{\mathrm{long}}$ of the laser-driven EVB possess a *mirror-reflection* symmetry with respect to the y-axis, i.e. $\Xi_{\ell s}(x) = \Xi_{\ell s}(-x)$ and $\boldsymbol{\mathcal{J}}_{\ell s}(x) = \boldsymbol{\mathcal{J}}_{\ell s}(-x)$, as schematically illustrated in Fig. 2.4. This symmetry can be interpreted classically as a manifestation of the "standard" Lorentz force $\boldsymbol{F} = e\,(\boldsymbol{E} + \boldsymbol{v}\times\boldsymbol{B})$ caused by the laser field which is applied along the y-axis. Here $\boldsymbol{v}$ is the electron velocity, the electric $\boldsymbol{E}$ and magnetic $\boldsymbol{B}$ fields are defined via Eq. (1.18) with $A^0 = 0$. To prove the mirror-reflection symmetry, that arises despite the complicated azimuthal dependence of the EVB profile, we only need to make the replacement $\varphi \to \pi - \varphi$ in Eqs. (2.50), (2.52)-(2.54) and consider the following trigonometric identities:

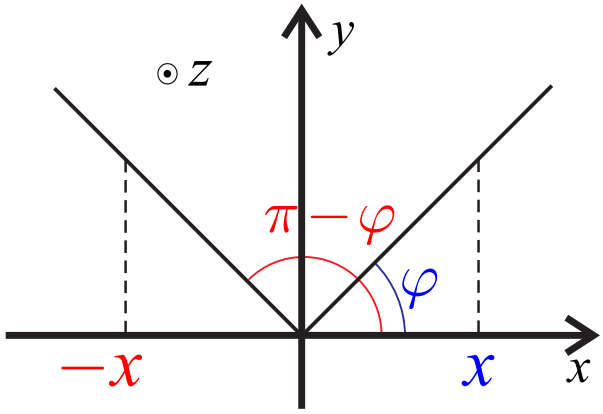

Figure 2.4: Mirror-reflection symmetry of the approximated probability density $\Xi_{\ell s}$, transverse $\boldsymbol{\mathcal{J}}_{\ell s}^{\mathrm{tr}} = \mathcal{J}_{\ell s}^{(r)}\boldsymbol{e}_r + \mathcal{J}_{\ell s}^{(\varphi)}\boldsymbol{e}_\varphi$ and longitudinal $\boldsymbol{\mathcal{J}}_{\ell s}^{\mathrm{long}} = \mathcal{J}_{\ell s}^{(z)}\boldsymbol{e}_z$ currents.

$$\cos\left[(n'-n)\left(\frac{\pi}{2}+\pi-\varphi\right)\right] = \cos\left[(n'-n)\left(2\pi-\frac{3\pi}{2}+\varphi\right)\right] = \cos\left[(n'-n)\left(\frac{\pi}{2}+\varphi\right)\right],$$

$$\sum_{n,n'=-\infty}^{+\infty} g_{n,n'}\sin\left[2s\,(n'-n)\left(\frac{\pi}{2}+\pi-\varphi\right)\right] = -\sum_{n,n'=-\infty}^{+\infty} g_{n,n'}\sin\left[2s\,(n'-n)\left(\frac{\pi}{2}+\varphi\right)\right] =$$

$$-\sum_{n,n'=-\infty}^{+\infty} g_{n',n}\sin\left[2s\,(n-n')\left(\frac{\pi}{2}+\varphi\right)\right] = \sum_{n,n'=-\infty}^{+\infty} g_{n,n'}\sin\left[2s\,(n'-n)\left(\frac{\pi}{2}+\varphi\right)\right].$$

Here the function $g_{n,n'}$ combines all the terms in Eq. (2.53) that do not depend on the azimuthal angle φ. Moreover, since the indices n and n' run from $-\infty$ to $+\infty$, the function $g_{n',n}$ can

be replaced by $g_{n,n'}$ under the summation sign. In the following, we will explicitly exhibit the mirror-reflection symmetry of the EVB profile with regard to the y-axis when we depict the electron intensity distribution in the transverse plane perpendicular to the EVB propagation axis. In addition, a similar symmetric azimuthal dependence appears also in the profile of laser-driven twisted atoms [82, 83], as we discuss in the second part of this thesis.

The 4-current components (2.50)-(2.54) can be constructed also from the Volkov-Bessel states (2.32)-(2.33) if we approximate them via

$$\Psi_{\ell s}(\boldsymbol{r},t) \approx \sum_{n=-\infty}^{+\infty} \tilde{\Psi}_{\ell+n,s}(\boldsymbol{r},t) , \tag{2.55}$$

where we introduce the wave function

$$\tilde{\Psi}_{\ell+n,s}(\boldsymbol{r},t) \equiv i^n J_n(f_0)\,\psi_{\ell+n,s} ,$$

with $\psi_{\ell+n,s}$ defined by Eq. (2.33). If we now utilize this approximated form of $\Psi_{\ell s}$ we can find an "integral of motion" for laser-driven EVBs which also explains our motivation to consider the weak-field regime [1]. Indeed, we can easily demonstrate that the components $\tilde{\Psi}_{\ell+n}$ of the decomposition (2.55) are the eigenstates of the longitudinal "total" angular momentum operator $\hat{\mathcal{T}}_z$ [cf. Eq. (2.12)] with

$$\hat{\mathcal{L}}_z = -i\partial/\partial\varphi$$

and

$$\hat{\Sigma}_z = \frac{1}{2}\,\mathrm{diag}\,(\sigma_z,\sigma_z)$$

representing the longitudinal OAM and SAM operators of the electron, respectively. The corresponding eigenvalues of the TAM operator will then be $\ell+n+s$, i.e. the sum of the electron and the laser OAMs and the electron SAM along the z-axis. Thus, we can write

$$\hat{\mathcal{T}}_z\tilde{\Psi}_{\ell+n,s} = (\ell+n+s)\,\tilde{\Psi}_{\ell+n,s} ,$$

derivation of which is very similar to the analogous calculations for field-free EVBs (see Eqs. (2.12)-(2.14)). In the paraxial regime, moreover, we shall use the scalar Volkov-Bessel state (2.34) and express it in the following approximated form

$$\Psi^{\mathrm{scalar}}_{\ell s}(\boldsymbol{r},t) \approx \sum_{n=-\infty}^{+\infty} \tilde{\Psi}^{\mathrm{scalar}}_{\ell+n,s}(\boldsymbol{r},t) , \tag{2.56}$$

with the decomposition components

$$\tilde{\Psi}^{\mathrm{scalar}}_{\ell+n,s}(\boldsymbol{r},t) \equiv i^n J_n(f_0)\,e^{i\mathcal{G}(p_0)}\psi^{\mathrm{scalar}}_{\ell+n,s}(\boldsymbol{r},t) .$$

Here the wave function $\psi^{\mathrm{scalar}}_{\ell+n,s}$ looks like the wave function of the field-free scalar EVB (2.9), but with the modified OAM $\ell+n$. One can readily verify that the components $\tilde{\Psi}^{\mathrm{scalar}}_{\ell+n,s}$ are simultaneously the eigenstates of the OAM and SAM operators

$$\hat{\mathcal{L}}_z\tilde{\Psi}^{\mathrm{scalar}}_{\ell+n,s} = (\ell+n)\,\tilde{\Psi}^{\mathrm{scalar}}_{\ell+n,s} , \quad \hat{\Sigma}_z\tilde{\Psi}^{\mathrm{scalar}}_{\ell+n,s} = s\tilde{\Psi}^{\mathrm{scalar}}_{\ell+n,s} , \tag{2.57}$$

[1] Examination of the strong-field regime deserves a specific attention as it would require a more complicated "integral of motion".

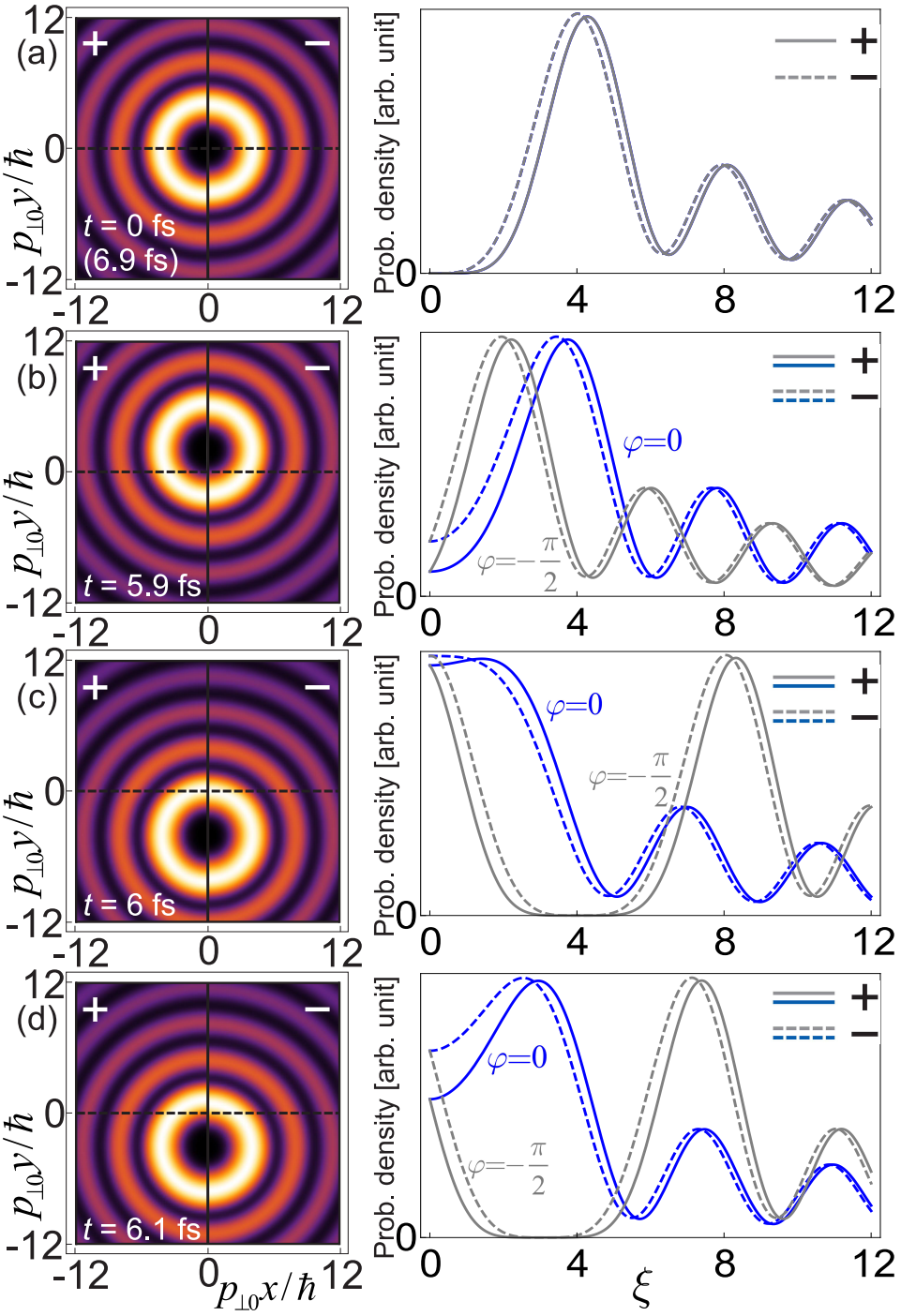

Figure 2.5: Spin-, time- and azimuthal-angle-dependent distributions of the probability density of laser-driven non-paraxial EVB (in arbitrary units of the same scale). The $s = \pm 1/2$ spin states are indicated by "+" (solid curves) and "–" (dashed curves), respectively. At $t = 0$ fs and $t = 6.9$ fs the profile corresponds to the field-free propagation of EVB. The parameters of the laser pulse and the EVB are given in the text. The variation of colors at the snapshots is the same as for Fig. 3(c).

again, similar to those for the field-free EVB (2.15). Finally, when we switch off the laser field, from Eqs. (2.56) and (2.57), we get (2.14) and (2.15) for non-paraxial and paraxial regimes, respectively.

We are now ready to investigate the *spatiotemporal* characteristics of the EVB profile. So far, we kept the form of the vector 4-potential A^μ general that appears in the argument f_0 of the Bessel function in Eqs. (2.50)-(2.54) (see also Eq. (2.31)). We shall, however, specify the shape of the applied laser field in order to carry out numerical simulations. To this end, as already mentioned above, we examine a few-cycle Gaussian pulse [cf. Fig. 2.3]

$$A \;=\; \mathscr{A}_0 e^{-\zeta^2/a^2}\cos\zeta\,,$$

where $\mathscr{A}_0$ is a constant amplitude of the potential and a is a dimensionless *waist* size of the laser beam. For this specific waveform, f_0 can be integrated exactly

$$f \;=\; \frac{ep_{\perp 0}\mathscr{A}_0 a\sqrt{\pi}}{4\,(kp_0)}e^{-a^2/4}\left[\mathrm{erf}\left(i\frac{a}{2}+\frac{\zeta}{a}\right)+\mathrm{erf}\left(i\frac{a}{2}-\frac{\zeta}{a}\right)\right],$$

where

$$\mathrm{erf}\,(\mathcal{Z}) \;=\; \frac{2}{\sqrt{\pi}}\int_0^{\mathcal{Z}} e^{-\tau^2}\mathrm{d}\tau$$

is the so-called Gauss error function [64]. Furthermore, for the sake of definiteness and also to fulfill the condition $|\delta| \ll 1$, we consider a laser pulse with the electric field amplitude $E = 10^8$ V/cm, central angular frequency $\omega = 10^{16}$ Hz and the waist size $a = 9$, corresponding to the pulse duration $\tau \approx 5.5$ fs, number of cycles $N \approx 5$ and the intensity $I \approx 1.3\cdot 10^{13}$ W/cm^2 [cf., e.g., Ref. [84]]. We also consider an EVB in the non-paraxial regime with the OAM $\ell = 3$, the opening angle $\theta_0 = \pi/4$ and the kinetic energy 817.4 keV corresponding to the intrinsic SOI parameter $\Delta = 0.3$, as discussed in [45] (see also the caption of Fig. 2.1). For these values, $|\delta| \lesssim 10^{-4}$ and, therefore, we can replace in very good approximation expressions (2.42), (2.45), (2.48), (2.49) by the simpler form (2.50), (2.52), (2.53), (2.54), respectively. Moreover, the terms with the laser OAM greater than $n = n' = 7$ no longer contribute in Eqs. (2.42)-(2.50).

After we have chosen the parameters of the "EVB + laser" system we return to the "head-on" scenario, in which the free EVB propagates along the positive direction of z and collides with the laser pulse, localized both in z and in time t [cf. Fig. 2.3]. For this collision, we choose the initial condition such that the laser pulse is switched on at $t = 0$ in the transverse xy-plane at $z_0 = -1100$ nm. This means that at $t \leq 0$, the EVB is described by means of the field-free state (2.6) [cf. Figs. 2.5(a), 2.6(a1-a3), 2.7(a)]. When the laser is switched on the EVB evolves within the electromagnetic field and propagates through the peak of the laser pulse at $t \approx 3$ fs. After the pulse passes the plane z_0, the EVB still remains affected within the next ~ 1.4 femtoseconds. This period, in principle, is enough in order to reveal the influence of the field on the dynamics of the EVB profile. Figures 2.5, 2.6 and 2.7 display both the spin- and azimuthal-dependent distributions of the probability density, the transverse and the azimuthal currents of the laser-driven EVB, respectively. The snapshot of these quantities are depicted as a function of the dimensionless transverse coordinate ξ for selected time intervals. The dependence on the spin can be clearly seen in all figures due to the non-paraxiality of the relativistic EVB propagation, i.e. as a result of the intrinsic SOI in EVB both in the presence and absence of the laser (compare dashed and solid lines as well as the left and right density plots and streamlines). The dependence of the probability density and the transverse

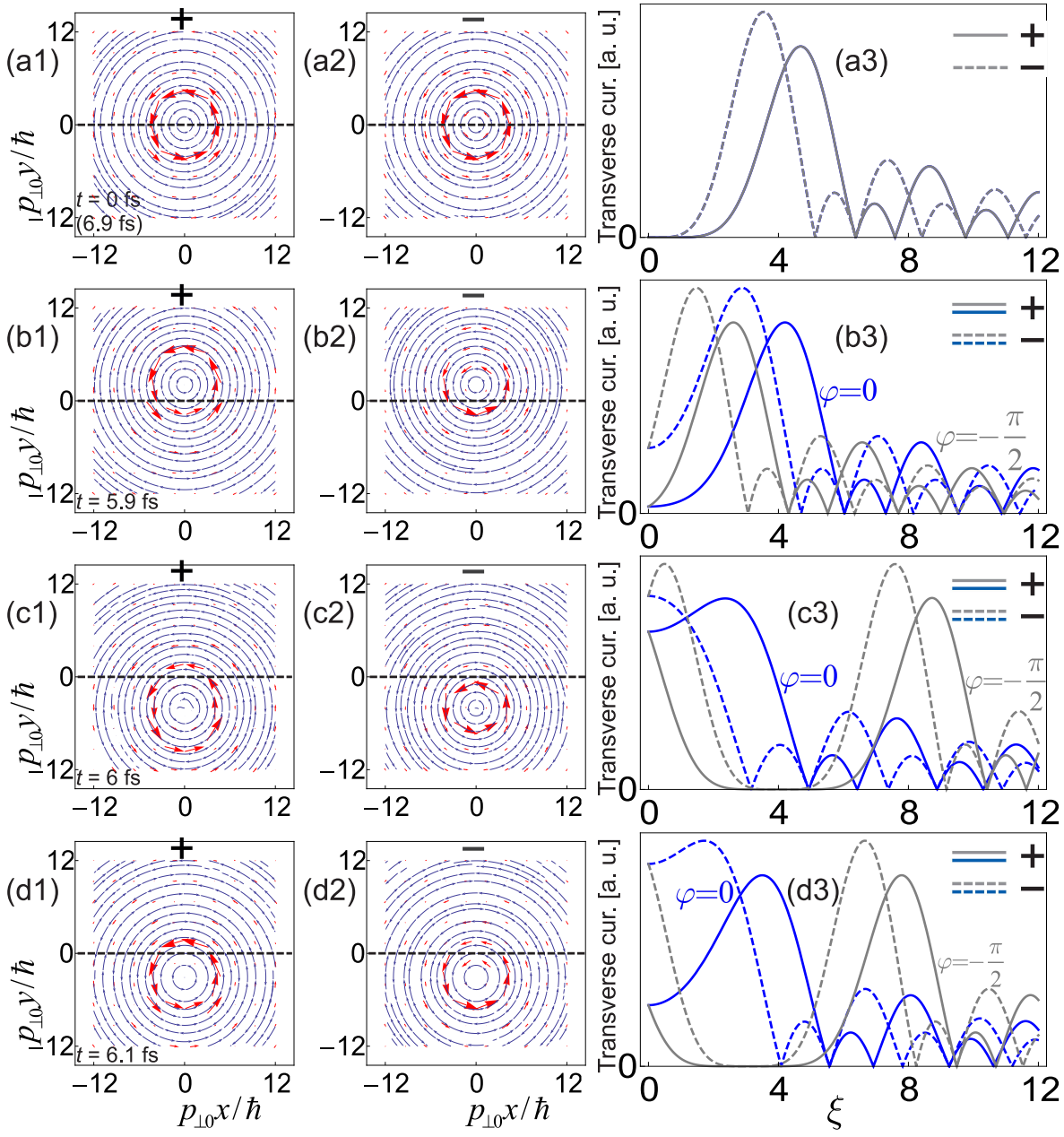

Figure 2.6: Representation of the spin-, time- and the azimuthal-angle-dependent transverse current of laser-driven non-paraxial EVB, $\boldsymbol{\mathcal{J}}^{\rm tr}_{\ell s} = \left(\mathcal{J}^{(x)}_{\ell s}, \mathcal{J}^{(y)}_{\ell s}\right) = \left(\mathcal{J}^{(r)}_{\ell s}, \mathcal{J}^{(\varphi)}_{\ell s}\right)$. Streamlines and vector plots are generated to show the vector field $\left(\mathcal{J}^{(x)}_{\ell s}, \mathcal{J}^{(y)}_{\ell s}\right)$ as a function of dimensionless coordinates $p_{\perp 0}x/\hbar$ and $p_{\perp 0}y/\hbar$ (the beam propagates toward the reader). Thickness of vectors increases within increasing absolute value of the transverse current $|\boldsymbol{\mathcal{J}}^{\rm tr}_{\ell s}|$. Figures (a3), (b3), (c3) and (d3) show the distribution of $|\boldsymbol{\mathcal{J}}^{\rm tr}_{\ell s}|$ as a function of the dimensionless transverse coordinate ξ (in arbitrary units of the same scale). The $s \pm 1/2$ spin states are indicated by "+" (solid curves) and "−" (dashed curves), respectively. Moreover, the parameters of electron and laser beams are the same as for Fig. 2.5 and are given in the text.

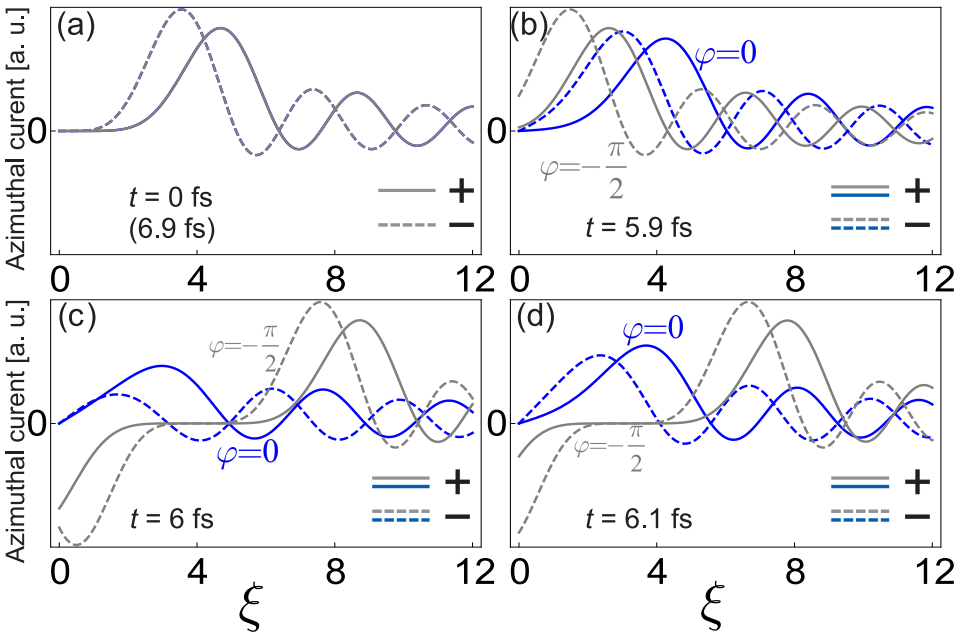

Figure 2.7: Spin-, time- and azimuthal-angle-dependent distributions of the azimuthal current of laser-driven non-paraxial EVB (in arbitrary units of the same scale). Solid and dashed curves indicate the spin-up and spin-down states, respectively

(azimuthal) current on the azimuthal angle manifests itself in the profile of the EVB due to the electron-laser coupling [cf. Figs. 2.5(b-d), 2.6(b-d), 2.7(b-d) and Eqs. (2.50), (2.53), (2.54)]. This φ-dependency is incorporated via the *shift* of the center of the EVB with respect to the center of the (initially) field-free EVB both along the positive (Figs. 2.5(b), 2.6(b1,b2)) and negative (Figs. 2.5(c,d), 2.6(c1,c2,d1,d2)) directions of the y-axis. Overall, Figs. 2.5(b-d) and 2.6(b1,b2,c1,c2,d1,d2) show that the cylindrical symmetry of the probability density and the transverse current remains the same also in the presence of the laser field, as we expected. Only the "center" of this symmetry is shifted along the direction of the field polarizaton (y-axis), due to the "standard" Lorentz force. For $t = 6$ fs, the numerical estimate of this shift gives ~ 0.009 nm which is the 19.9% of the beam width $\hbar\xi_0/p_{\perp 0}$. Here we have taken $\xi_0 = 20$ for which the distribution of the electronic probability density and the transverse current is effectively zero. Moreover, such a shift causes a non-zero probability for finding an electron at the center ($\xi = 0$) of the initially field-free beam [cf. Figs. 2.5(c,d), 2.6(c,d), 2.7(c,d)]. Finally, at $t = 6.9$ fs the EVB evolves back to the field-free EVB and, therefore, obtains the same distribution of the probability density, transverse and azimuthal currents as for $t = 0$ fs [Fig. 2.5(a), 2.6(a), 2.7(a)].

Until now, we have discussed only how the laser pulse affects the dynamics of the relativistic EVB in the non-paraxial regime. Since the first EVBs [36, 39, 40, 85] have been constructed for electrons with energies $\sim 200 - 300$ keV and opening angles $\theta_0 \leq 20$ mrad, which are within the paraxial regime, we find desirable also to discuss the influence of the laser field onto the EVB dynamics for these – nowadays available – experimental parameters. This would motivate the experimentalists to consider the EVB-laser interaction and to reveal the influence of the laser light upon many various parameters of the twisted electron beam. In particular, we again examine the "head-on" scenario for the propagation of electrons and the

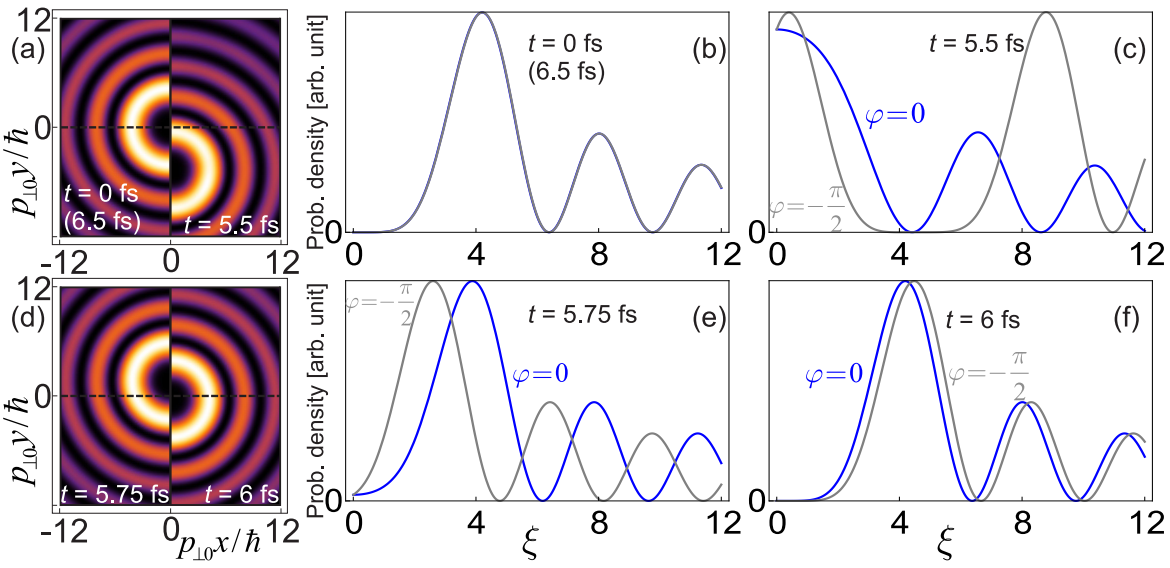

Figure 2.8: Time- and azimuthal-angle-dependent distribution of the probability density of laser-driven paraxial EVB (in arbitrary units of the same scale). At $t = 0$ fs and $t = 6.5$ fs the profile corresponds to the free motion of EVB. The variation of colors in snapshots is the same as for Fig. 3(c) and the parameters of the "EVB + laser" system are given in the text.

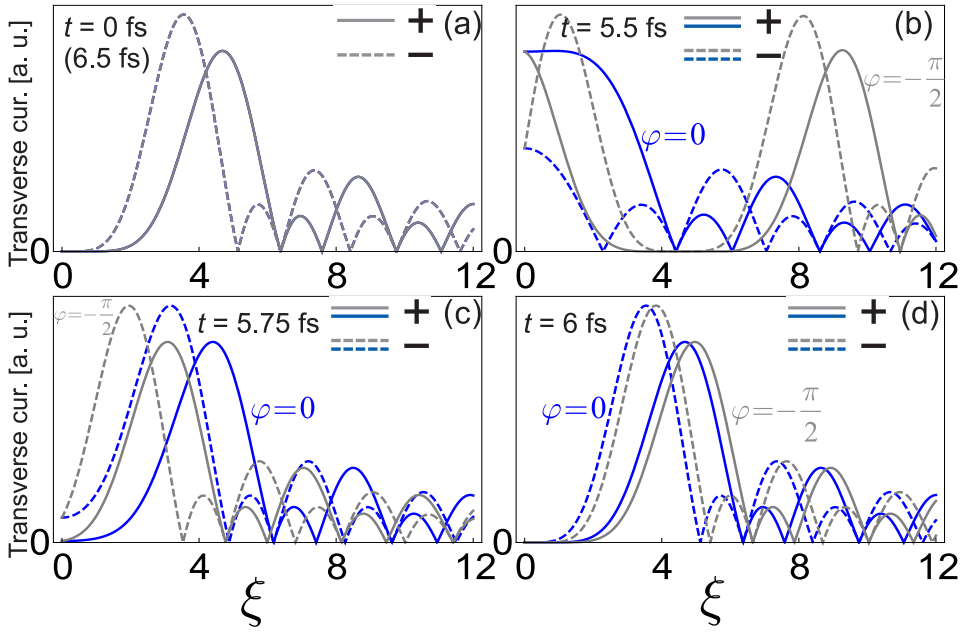

Figure 2.9: Spin-, time- and azimuthal-angle-dependent distributions of modulus of the transverse current of laser-driven paraxial EVB (in arbitrary units of the same scale). Solid and dashed curves indicate the spin-up and spin-down states, respectively. Parameters of both the electron and laser beams are the same as for Fig. 2.8 and are given in the text.

laser beam. If we consider an EVB with the OAM $\ell = 3$, opening angle $\theta_0 = 20$ mrad and the kinetic energy 300 keV, corresponding to the SOI parameter $\Delta = 0.0015$, and the few-cycle laser pulse with the same parameters as taken before, the probability density of the EVB is no longer spin-dependent, as shown in Fig. 2.8 and in contrast to the non-paraxial regime. However, the presence of the field gives rise to a *shift* of the center of EVB with respect to the center of the initially free paraxial beam (compare the density plots in Figs. 2.8a and 2.8d). For $t = 5.5$ fs, this shift is ~ 0.02 nm which is the 20% of the *full width at half maximum diameter* of the EVB [86], thus making it accessible for measurement. Additional analyzes of the current of laser-driven paraxial EVBs, $\boldsymbol{\mathcal{J}}_{\ell s}$, show that it has a similar spin-independent behavior, as the probability density. The dominant contribution in the paraxial domain comes from the longitudinal component of the current since $p_{\perp 0}/p_{||0} \ll 1$ (compare Eqs. (2.52) with Eqs. (2.53), (2.54)). However, the transverse current still exhibits a spin-dependent dynamics, as demonstrated in Fig. 2.9, that vanishes in the plane-wave limit of electron, when $p_{\perp 0} \to 0$ and $\ell \to 0$.

The relativistic EVB as a whole is spatially shifted along the (linear) polarization direction of the laser field, while the overall transverse structure of the (shifted) beam remains the same. Since the field oscillates in our case on a subfemtosecond time scale, the spatial shift of the beam center performs oscillations with a *similar* frequency. Additional computations show that these oscillations occur for all values of the (longitudinal) OAM ℓ and vanish only in the plane-wave limit $\theta_0 = 0$ and $\ell = 0$. Furthermore, the interaction with the laser pulse may lead to a pronounced probability to detect electrons at the (initially dark) center of the incident EVB (as seen at $\xi = 0$ in Figs. 2.5(c,d), 2.6(c,d), 2.7(c,d), 2.8(c) and 2.9(b)). Both the shift of the beam center and the pronounced probability on the geometrical axis of initially field-free electrons remain rather universal for both the non-paraxial and paraxial regimes, as we predict in our theory. Altogether, such a behavior of the beam can be interpreted classically: the EVB experiences the "standard" Lorentz force caused by a laser field, as already mentioned before. As a consequence of this Lorentz-like behavior, one can control and manipulate EVBs with all the experimental techniques which have been developed over the years for other kinds of (localized) electron beams.

2.3 Summary

In this chapter, we have examined quite in detail vector Bessel beams of relativistic electrons – electron vortex beams – that were constructed recently both in the absence [45] and presence [78] of an electromagnetic field. We have shown that the field-free EVBs carry a well-defined TAM along their propagation direction which represents the sum of the longitudinal SAM and OAM of the electrons. These two degrees of freedom couple to each other and give rise to the intrinsic SOI inside the EVB. We have calculated the components of the 4-current of field-free EVBs and demonstrated the fine spin-dependent splitting of distributions of electronic probability density and transverse current due to the intrinsic SOI. Furthermore, we have examined a head-on collision of two feasible beams, namely the relativistic EVB and the few-cycle laser pulse, to show how the intrinsic SOI is modified inside the field. To do so, we have generalized the free EVB states (2.6) [cf. [45]] to the laser-driven Volkov-Bessel states (2.32) [cf. [78]] by utilizing the Dirac-Volkov solution (1.39). Apart from the intrinsic SOI, our solutions exhibit the intrinsic OOI between the electron OAM and OAM-components of the plane-wave laser. Both the SOI and (the infinite summation of) the OOI contribute in the spin- and laser-dependent distribution of the 4-current of field-affected EVBs. By calculating

the components of this 4-current, we have shown the shift of the center of the laser-driven EVB, with respect to the center of the initially field-free EVB. We have analyzed this shift both in the non-paraxial and paraxial regimes, and we have seen that it can give rise to a finite probability to detect an electron at the center of the initially free EVB. Such a pronounced probability and the shift are unavoidably accompanied with an azimuthal dependence of the electron intensity and can be important observables that manifest themselves in the interaction of the twisted electrons with laser pulses. We believe that recent advances in electron microscopy [43, 87–90] will enable one to observe the above introduced effect by employing, for instance, the so-called pump-probe experiments.

Part II

Angular momentum representation of laser-driven two-level atoms

In an effort to extend the study of electron vortex beams to another type of matter vortex beams, in the second part of the thesis, we create a theoretical construct of Bessel beams of *two-level* atoms that are *driven* by a laser light. To demonstrate this construction, we divide the current part into two chapters.

In chapter 3, we describe the semi-classical coupling of a neutral two-level atom with a laser field in a general case when the atom is not at rest but possesses a momentum which forms an arbitrary angle with respect to the wave vector of the field. In section 3.1, we describe the Hamiltonian of this "atom + field" system. Particularly, in subsection 3.1.1, we first define the atomic *external* and *internal* variables to describe the quantum dynamics of electron(s) inside the atom and the semi-classical motion of the atomic center-of-mass, respectively. Next, in subection 3.1.2, we introduce the atom-field Hamiltonian in the *long wave approximation* (LWA) where we assume that the wavelength of the laser field is much larger than atomic sizes. In subsection 3.1.3, we also define the electric field which depends both on space- and time-coordinates and resonantly drives the two-level atom. For such an atom, in section 3.2, we make an Ansatz for the wave function of the "atom + field" system and factorize it to separate the dependence upon the external and internal coordinates in the LWA. In order to describe probability amplitudes of laser-driven two-level atoms, in the last section of chapter 3, we find solutions to the space- and time-dependent Schrödinger equation. To do so, we employ the same mathematical method as it is done for the Dirac equation to describe the dynamics of laser-driven electrons.

In chapter 4, we construct Bessel beams of laser-driven two-level atoms. For this purpose, we superimpose the wave function of plane-wave atoms, obtained in the previous chapter, with well-defined amplitudes corresponding to the typical monoenergetic distribution of atoms in Bessel beams. Particularly, we define the wave function of such atomic beams in the so-called collinear- (subsection 4.1.1) and crossed-beam scenarios (subsection 4.1.2) where the atomic and laser beams correspondingly propagate parallel or perpendicular to each other. Furthermore, we show that Bessel beams of atoms carry non-zero OAM along their direction of propagation. This longitudinal OAM represents a new, fundamental degree of freedom for atom beams, in analogy with electron and optical vortex beams. Finally, in section 4.2, we spatially and temporally characterize the atomic Bessel beams and discuss the influence of the resonantly driving laser light on the beam profile.

We conclude each chapter with a summary. Moreover, notations for physical quantities *do not* coincide with those of the first part of the thesis.

Chapter 3

Semi-classical coupling of two-level atoms to a laser field

> A great deal of my work is just playing with equations and seeing what they give.
>
> P.A.M. Dirac

The coherent interaction of a two-level atom with a radiation field has been explored since the early days of quantum optics [91–94]. Nowadays, this *atomic coherence* is known as an effective tool for achieving control about (atomic and molecular) samples [95–97] and it can be utilized to examine various effects with atomic beams, such as generation of entanglement [98], investigation of the optical force [99,100] or exhibition of vortices [101–103] in beams. In order to examine how this coherent control can be exploited also for tuning and guiding *atomic Bessel beams*, in the following, we shall describe the coherent coupling of a moving atom to a laser field that depends both on spatial and temporal coordinates. To do so, in this chapter we solve the Schrödinger equation for laser-driven two-level atoms by applying the method known from the Dirac theory of the electron-field interaction. Such a solution enables one to enroll the directions of linear momenta of both atom and laser beams in the space-time-dependent wave function that adequately describes the "atom + laser" system. In addition, we here also assume that the external field of the laser is a classically "given" one, i.e. the number of particles is conserved and no quantization of the field is considered. Moreover, we shall work in the single-particle approximation meaning that the atoms inside the beam do not couple with each other, thus, enabling us to use the terms "atom" and "atom beam" equivalently.

To describe the interaction of a two-level atom with a classical radiation field and to start our derivations, let us first characterize the field and the interaction Hamiltonian between the atom and this field. We hereby assume that the atom has the (rest) mass m, a dipole moment $\boldsymbol{d}$, and that it moves as a whole with constant momentum $\boldsymbol{p}$ along some *given* direction.

3.1 Hamiltonian of the "atom + laser" system

Here we review and comment upon a few basic concepts regarding atom-laser interaction that is useful for our further discussion.

3.1.1 External and internal atomic variables

For the atom, a clear distinction must be made between the external, that characterize the motion of the center-of-mass of the atom, and the internal variables, that describe the internal dynamics of the atom in its rest frame. The separation of these two types of variables is well known for one-electron atoms, such as hydrogen and alkali metal atoms. Let $\boldsymbol{r}_e$ and $\boldsymbol{r}_N$ be the positions of the electron and the nucleus, with mass m_e and m_N, and linear momenta $\boldsymbol{p}_e$ and $\boldsymbol{p}_N$, respectively. We introduce new, *relative* or *internal* variables (see, e.g., [94])

$$\begin{cases} \tilde{\boldsymbol{r}} = \boldsymbol{r}_e - \boldsymbol{r}_N \,, \\ \tilde{\boldsymbol{p}} = \dfrac{\tilde{m}}{m_e}\boldsymbol{p}_e - \dfrac{\tilde{m}}{m_N}\boldsymbol{p}_N \,, \end{cases} \tag{3.1}$$

with $\tilde{\boldsymbol{r}}$ and $\tilde{\boldsymbol{p}}$ being the electron's relative coordinate and momentum with regard the nucleus. We also introduce *center-of-mass* or *external* variables

$$\begin{cases} \boldsymbol{r} = \dfrac{m_e\boldsymbol{r}_e + m_N\boldsymbol{r}_N}{m} \,, \\ \boldsymbol{p} = \boldsymbol{p}_e + \boldsymbol{p}_N \,, \end{cases} \tag{3.2}$$

where $\boldsymbol{r}$ and $\boldsymbol{p}$ are the atom center-of-mass coordinate and momentum, respectively. Moreover, $m = m_e + m_N$ is the total mass of the atom and $\tilde{m} = m_e m_N/m$ is the so-called reduced mass.

The Hamiltonian of the two particles interacting by a potential V, that depends only on the distance between them, has the form

$$H_{\text{atom}} = \frac{\hat{\boldsymbol{p}}_e^2}{2m_e} + \frac{\hat{\boldsymbol{p}}_N^2}{2m_N} + V\left(|\hat{\boldsymbol{r}}_e - \hat{\boldsymbol{r}}_N|\right) \,,$$

where "hat" means operators of the corresponding variables. In the coordinate representation, i.e. when $\hat{\boldsymbol{p}}_e = -i\hbar\boldsymbol{\nabla}_e = -i\hbar\partial/\partial\boldsymbol{r}_e$ and $\hat{\boldsymbol{p}}_N = -i\hbar\boldsymbol{\nabla}_N = -i\hbar\partial/\partial\boldsymbol{r}_N$, the Hamiltonian reads

$$H_{\text{atom}} = \frac{\hat{\boldsymbol{p}}_e^2}{2m_e} + \frac{\hat{\boldsymbol{p}}_N^2}{2m_N} + V\left(|\boldsymbol{r}_e - \boldsymbol{r}_N|\right) \,. \tag{3.3}$$

We can further simplify this Hamiltonian by employing the relative (3.1) and center-of-mass (3.2) coordinates. The outcome is the following

$$H_{\text{atom}} = \frac{\hat{\boldsymbol{p}}^2}{2m} + \frac{\hat{\tilde{\boldsymbol{p}}}^2}{2\tilde{m}} + V\left(|\tilde{\boldsymbol{r}}|\right) \,, \tag{3.4}$$

where the relative and center-of-mass momentum operators are expressed via $\hat{\boldsymbol{p}} = -i\hbar\boldsymbol{\nabla} = -i\hbar\partial/\partial\boldsymbol{r}$ and $\hat{\tilde{\boldsymbol{p}}}_e = -i\hbar\tilde{\boldsymbol{\nabla}} = -i\hbar\partial/\partial\tilde{\boldsymbol{r}}$, respectively. We can clearly see that the coordinates in Hamiltonian (3.4) are now separated, in contrast to the form (3.3). Such a separation is very important in order to find analytical solutions to the corresponding Schrödinger equation by factorizing the wave function, as we do below. Although we here consider one-electron atoms, the separation of coordinates can be extended also to many-electron atoms if interactions

depend only on the relative positions of particles [104]. In addition, the new variables, Eqs. (3.1) and (3.2), obey the same commutation relations as $\boldsymbol{r}_e$ and $\boldsymbol{r}_N$, i.e.

$$\left[\tilde{r}_i, \hat{\tilde{p}}_j\right] = i\hbar\delta_{ij}\,, \quad [r_i, \hat{p}_j] = i\hbar\delta_{ij}\,, \quad \{i,j\} = \{1,2,3\}\,,$$

where

$$\delta_{ij} = \begin{cases} 1, & i = j \\ 0, & i \neq j \end{cases}$$

is the Kronecker symbol.

The Hamiltonian (3.4) describes a two-particle system without an external field. In the next subsection, we "switch on" the laser field and examine how this Hamiltonian is modified in the presence of an external field.

3.1.2 Atom-field interaction Hamiltonian in the long wave approximation

So far, we have discussed the Hamiltonian of the one-electron atom without external influences. From now on, we are interested in the dynamics of such an atom within the laser field with the scalar U and vector potentials $\boldsymbol{A}$. To modify the Hamiltonian (3.3), we follow the minimal coupling prescription and replace the operators $\hat{\boldsymbol{p}}_e$ and $\hat{\boldsymbol{p}}_N$ with $\hat{\boldsymbol{p}}_e - q_e\boldsymbol{A}$ and $\hat{\boldsymbol{p}}_N - q_N\boldsymbol{A}$, respectively (see also the subsection 1.2.1). Here q_e and q_N are the electron and nucleus charges, respectively, which for the neutral (one-electron) atom are nothing but $q_N = -q_e = |e|$.

In the semi-classical theory, the quantum dynamics of the atom is driven by the external field but this "motion" does *not* re-act back upon the field as this would require a quantization of the electromagnetic field [91]. Therefore, the Hamiltonian of the "atom + laser" system does not contain a term that describes only the field such that the Hamiltonian of an atom in the classical field takes the form

$$\begin{aligned} H_{\text{atom+laser}} &= \frac{1}{2m_e}\left(\boldsymbol{p}_e - q_e\boldsymbol{A}\left(\boldsymbol{r}_e, t\right)\right)^2 + \frac{1}{2m_N}\left(\boldsymbol{p}_N - q_N\boldsymbol{A}\left(\boldsymbol{r}_N, t\right)\right)^2 \\ &+ e\,U\left(\boldsymbol{r}_e, t\right) + e\,U\left(\boldsymbol{r}_N, t\right) + V\left(|\boldsymbol{r}_e - \boldsymbol{r}_N|\right)\,. \end{aligned} \tag{3.5}$$

Formally, we can write

$$H_{\text{atom+laser}} = H_{\text{atom}} + H_{\text{int}}\,,$$

where H_{atom} is given by Eq. (3.3) and the *interaction* Hamiltonian reads

$$H_{\text{int}} = -\frac{q_e}{m_e}\boldsymbol{A}\left(\boldsymbol{r}_e, t\right)\hat{\boldsymbol{p}}_e - \frac{q_N}{m_N}\boldsymbol{A}\left(\boldsymbol{r}_N, t\right)\hat{\boldsymbol{p}}_N + \frac{q_e^2\boldsymbol{A}^2\left(\boldsymbol{r}_e, t\right)}{2m_e} + \frac{q_N^2\boldsymbol{A}^2\left(\boldsymbol{r}_N, t\right)}{2m_N}$$

in the Coulomb gauge ($\boldsymbol{\nabla}_e \cdot \boldsymbol{A}\left(\boldsymbol{r}_e\right) = 0$, $\boldsymbol{\nabla}_N \cdot \boldsymbol{A}\left(\boldsymbol{r}_N\right) = 0$) and for a free propagating field, i.e. in the absence of external charges ($U = 0$). If we consider also single photon transitions, moreover, last terms quadratic in $\boldsymbol{A}$ can be ignored [94]. Thus, for the neutral one-electron atom, that couples to a classical electromagnetic field, the interaction Hamiltonian reads

$$H_{\text{int}} = |e|\left(\frac{\boldsymbol{A}\left(\boldsymbol{r}_e, t\right)\hat{\boldsymbol{p}}_e}{m_e} - \frac{\boldsymbol{A}\left(\boldsymbol{r}_N, t\right)\hat{\boldsymbol{p}}_N}{m_N}\right)\,,$$

a form which can be further simplified if we restrict ourselves to the optical frequencies of the electromagnetic wave.

In our further examination, we are interested in such a regime where the wavelength of the field is very large compared to the size of the atom. Such an approximation is well-justified especially for optical range of frequencies. In this *long wave approximation* (LWA), called also *dipole approximation*, we may neglect the variation of the field over distances of the order of atomic sizes and replace the vector potential at $\boldsymbol{r}_j = \{\boldsymbol{r}_e\,, \boldsymbol{r}_N\}$ with its value taken at the center-off-mass position $\boldsymbol{r}$

$$\boldsymbol{A}\,(\boldsymbol{r}_j) \;=\; \boldsymbol{A}\,(\boldsymbol{r} + \boldsymbol{r}_j - \boldsymbol{r}) \;\approx\; \boldsymbol{A}\,(\boldsymbol{r})\;. \tag{3.6}$$

Thence, the interaction Hamiltonian can be re-written as

$$H_{\rm int} \;\approx\; |e|\,\boldsymbol{A}\,(\boldsymbol{r},t)\left(\frac{\hat{\boldsymbol{p}}_e}{m_e} - \frac{\hat{\boldsymbol{p}}_N}{m_N}\right) \;=\; \frac{|e|}{\tilde{m}}\boldsymbol{A}\,(\boldsymbol{r},t)\cdot\hat{\tilde{\boldsymbol{p}}}\,, \tag{3.7}$$

where the vector potential is a function of the center-of-mass position of the atom. In LWA, one can perform a unitary transformation on the atom-field Hamiltonian to re-write $H_{\rm int}$ in a more familiar form [105, 106]

$$H_{\rm int} \;\;=\;\; -\boldsymbol{d}\cdot\boldsymbol{E}\,(\boldsymbol{r},t)\;, \tag{3.8}$$

which describes the interaction of the electric dipole moment $\boldsymbol{d} = -\,|e|\,\tilde{\boldsymbol{r}}$ of the atom (being an internal operator) with the electric field $\boldsymbol{E}\,(\boldsymbol{r},t)$ (being an external classical field taken at the center-of-mass position of the atom). As we learn below, the interaction Hamiltonian in its form (3.8) and the unperturbed atomic Hamiltonian in its form (3.3) would enable us to factorize the wave function of the "atom + laser" system. Before we proceed with our calculations, in the next subsection, we shall characterize the classically given electromagnetic field, by considering a linearly polarized monochromatic plane-wave field.

3.1.3 Characterization of the classical field

We consider the classical electric field of laser beam as a monochromatic plane-wave

$$\boldsymbol{E} \;\;=\;\; \boldsymbol{\varepsilon}\,e^{i(\boldsymbol{k}\cdot\boldsymbol{r}-\omega t)}\,, \tag{3.9}$$

with a constant electric-field amplitude $\boldsymbol{\varepsilon}$, angular frequency ω and wave vector $\boldsymbol{k} \equiv k\,\boldsymbol{n}$, which satisfies Maxwell's equations, and where the unit vector $\boldsymbol{n}$ defines the propagation direction of the wave [67, 107]. While, in general, $\boldsymbol{E}$ and $\boldsymbol{\varepsilon}$ are both complex-valued vectors in Eq. (3.9), the physically relevant *electric* field is given by the real part, $\Re(\boldsymbol{E})$, and is for transverse waves always perpendicular to its propagation, i.e. $\boldsymbol{n}\cdot\boldsymbol{\varepsilon} = 0$. For our further discussion, moreover, it is useful to introduce a set of real and mutually orthogonal unit vectors $(\boldsymbol{\epsilon}_1\,, \boldsymbol{\epsilon}_2\,, \boldsymbol{n})$, and to re-write the field amplitude in terms of these vectors as

$$\boldsymbol{\varepsilon} \;\;=\;\; \boldsymbol{\epsilon}_1\,\varepsilon_0 \;+\; \boldsymbol{\epsilon}_2\,\varepsilon_0'\,,$$

with the two (in general complex) constants ε_0 and ε_0'.

Most generally, the laser field amplitude $\boldsymbol{\varepsilon}$ in Eq. (3.9) describes an *elliptically* polarized plane wave; as a special case, this definition includes *linearly* polarized waves if the complex constants ε_0 and ε_0' fulfill proper relations. We choose $\varepsilon_0' = 0$ which corresponds to a linearly polarized field in $\boldsymbol{\epsilon}_1$ direction

$$\boldsymbol{E}\,(\boldsymbol{r},t) \;\;=\;\; \boldsymbol{\epsilon}_1\,\varepsilon_0\,e^{i(\boldsymbol{k}\cdot\boldsymbol{r}-\omega t)}$$

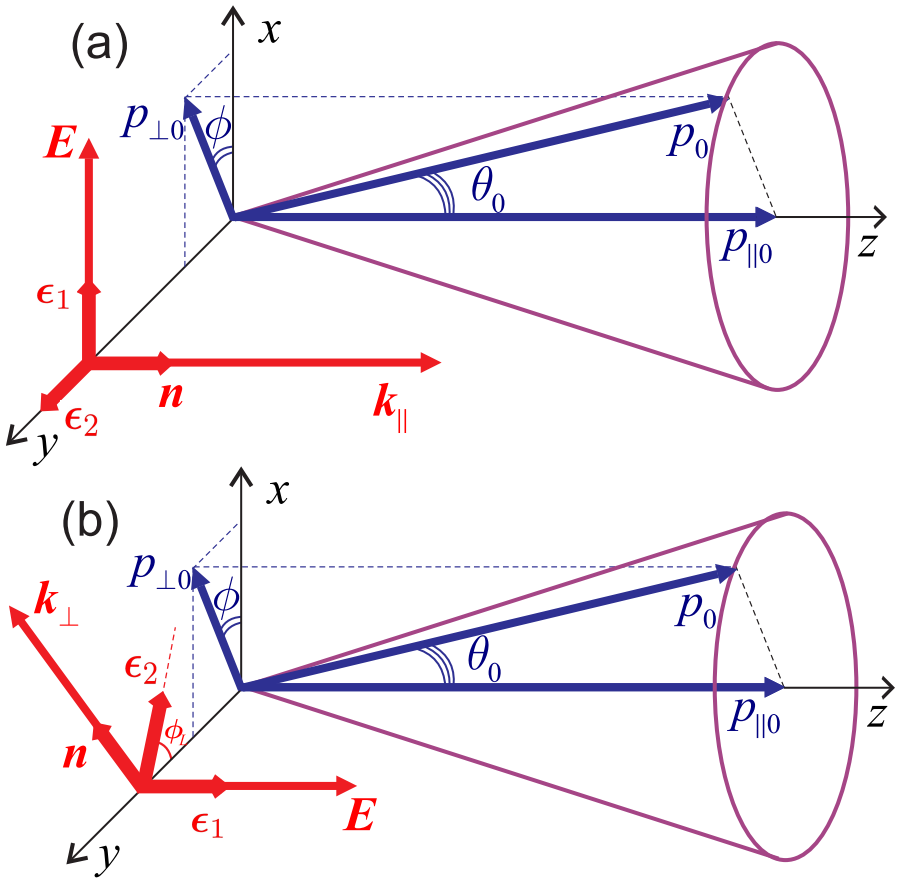

Figure 3.1: Collinear-beam (a) and crossed-beam (b) scenarios for the interposition of linearly polarized plane-wave laser and atomic Bessel beams. Red sketches indicate directions of the field polarization and the wave vector. Blue sketches indicate the momentum distribution of the atomic Bessel beam. A twisted two-level atom driven by the laser field is a superposition of the orthonormalized waves (3.39) (a) or (3.41) (b) with a fixed conical momentum spread $p_0 = const$, polar angle θ_0 and the azimuthal phase factor $e^{i\ell\phi}$.

with the (real) amplitude ε_0. Therefore, for this wave the relevant electric field is given by

$$\boldsymbol{E} \;=\; \boldsymbol{\epsilon}_1 \varepsilon_0 \cos\zeta = \boldsymbol{\varepsilon} \cos\zeta\,, \tag{3.10}$$

where $\zeta \equiv \boldsymbol{k}\cdot\boldsymbol{r} - \omega t$ is the *phase* of the plane-wave laser independent of its particular polarization properties. We here should remind the reader that the field is evaluated at the center-of-mass position $\boldsymbol{r} \equiv (x, y, z)$ of the atom.

The field and the atom propagation directions, in principle, can be chosen arbitrarily which will form the geometry of the "atom + laser" system. To describe the linearly polarized laser field we specify this geometry already in this subsection. We examine two scenarios that depend on the interposition of propagation directions of laser and atomic beams. These are the so-called *collinear-* and *crossed-beam* scenarios for which the laser and the atomic beams correspondingly propagate parallel or perpendicular to each other [cf. Figure 3.1]. We choose the z-axis along the propagation direction of the atomic beam. In collinear-beam scenario, moreover, we chose the x- and z-axes directed along the polarization $\boldsymbol{\epsilon}_1$ and laser

beam propagation, respectively. In contrast to this, in crossed-beam scenario, we restrict ourselves with the polarization along z-axis and consider propagation in xy-plane, where the x-axis is declined from the laser propagation direction under ϕ_L angle.

With the distinction of these collinear- and crossed-beam scenarios the laser field (3.10) and the phase ζ obtain the form

$$\boldsymbol{E}^{(||)} = \left(\varepsilon \cos\zeta^{(||)}, 0, 0\right), \quad \zeta^{(||)} = k_{||} z - \omega t\,, \tag{3.11}$$

$$\boldsymbol{E}^{(\perp)} = \left(0, 0, \varepsilon \cos\zeta^{(\perp)}\right), \quad \zeta^{(\perp)} = k_{\perp} r \cos\left(\phi_L - \varphi\right) - \omega t\,, \tag{3.12}$$

respectively, with a transverse coordinate $r = \sqrt{x^2 + y^2}$ of the atomic center-of-mass.

In the following, we assume that the field resonantly excites only one level of the atom such that the atom can be considered as a two-level system within a good approximation. We also define the Hamiltonian of such a system and determine the atomic states that are driven by the laser field (3.11) or (3.12).

3.2 Solution of the Schrödinger equation in the center-of-mass frame of the atom

In this section, we consider a beam of two-level atoms that interact with a monochromatic plane-wave laser, polarized linearly. For such atoms, we take into account that the de' Broglie wavelength of the atom is much smaller than the laser wavelength in order to utilize the so-called *eikonal* approximation. This will allow us to reduce both the space- and time-dependent Schrödinger equation for probability amplitudes of atomic levels to a system of coupled, first-order linear differential equations. We assume, moreover, that the laser field resonantly drives the atoms in order to employ the *rotating wave* approximation and to construct exact analytical solutions for such "atom + laser" systems.

3.2.1 Schrödinger equation in the center-of-mass frame of the atom

We consider a beam of neutral one-electron atoms in the single-particle approach, i.e., inside the beam, we neglect the interaction of atoms with each other. For such atom(s), we re-write the atomic Hamiltonian (3.3) in the form

$$H_{\text{atom}} = \frac{\hat{\boldsymbol{p}}^2}{2m} + H_0\,, \tag{3.13}$$

where $\frac{\hat{p}^2}{2m}$ denotes the kinetic energy (operator) as associated with the center-of-mass motion, whereas

$$H_0 \equiv \frac{\hat{\tilde{\boldsymbol{p}}}^2}{2\tilde{m}} + V\left(|\tilde{\boldsymbol{r}}|\right)$$

refers to the internal "motion" of the atom and describes the quantum dynamics of the electron in the field of a positively charged "core". If we consider a hydrogen atom, for instance, the interaction potential V is nothing else but the Coulomb potential

$$V_{\text{Coulomb}}\left(|\tilde{\boldsymbol{r}}|\right) = -\frac{e^2}{|\tilde{\boldsymbol{r}}|} = -\frac{e^2}{\tilde{r}}\,.$$

Such a potential leads to an analytically exact solution of the corresponding Schrödinger equation for the Hamiltonian H_0 [c.f., e.g., [93,108]]. In contrast to hydrogen atom, the Schrödinger equation for alkali-metal atoms can be solved only numerically or by approximated methods [cf., e.g., [93]].

Next, we "switch on" the external monochromatic electromagnetic field and assume that the field frequency is nearly in resonance with the atomic transition frequency between two, *upper* and *lower* levels. This means that the atom can be described as a two-level system within a good approximation. Therefore, the internal dynamics of such a two-level atom can be characterized via the Hamiltonian

$$H_0 \;=\; E_a \left|a\right\rangle \left\langle a\right| + E_b \left|b\right\rangle \left\langle b\right| \,, \tag{3.14}$$

where the two state vectors $|a\rangle$ and $|b\rangle$ denote the upper and lower levels of the atom and are supposed to be eigenstates of the Hamiltonian H_0:

$$\begin{aligned} H_0 \left|a\right\rangle &= E_a \left|a\right\rangle \,, \\ H_0 \left|b\right\rangle &= E_b \left|b\right\rangle \,. \end{aligned}$$

Here E_a and E_b are the energies of upper and lower states, respectively.

Thus, for two-level atoms, that are driven by a monochromatic field, the "atom + field" Hamiltonian (3.5) takes the form

$$H_{\text{atom+laser}} \;=\; \frac{\hat{\boldsymbol{p}}^2}{2m} + E_a \left|a\right\rangle \left\langle a\right| + E_b \left|b\right\rangle \left\langle b\right| + H_{\text{int}} \,, \tag{3.15}$$

where the H_{int} is given via Eq. (3.8) to characterize (as usual) the minimal coupling between atom and field in the LWA. Making use of the completeness relation

$$\left|a\right\rangle \left\langle a\right| + \left|b\right\rangle \left\langle b\right| \;=\; 1$$

for a two-level system, the interaction Hamiltonian of the atom with a *linearly* polarized wave can be written in the form

$$H_{int}^{(\shortparallel)} \;=\; -\hbar\Omega_{R_x}\Big(e^{i\phi_{d_x}} \left|b\right\rangle \left\langle a\right| + e^{-i\phi_{d_x}} \left|a\right\rangle \left\langle b\right|\Big)\cos\zeta^{(\shortparallel)}, \tag{3.16}$$

$$H_{int}^{(\perp)} \;=\; -\hbar\Omega_{R_z}\Big(e^{i\phi_{d_z}} \left|b\right\rangle \left\langle a\right| + e^{-i\phi_{d_z}} \left|a\right\rangle \left\langle b\right|\Big)\cos\zeta^{(\perp)} \tag{3.17}$$

for collinear- and crossed-beam scenarios, respectively. In accordance to these scenarios, here

$$\Omega_{R_x} \;=\; \frac{\left|e\left\langle b\right|\tilde{x}\left|a\right\rangle\right|\varepsilon_0}{\hbar}\,, \quad \Omega_{R_z} \;=\; \frac{\left|e\left\langle b\right|\tilde{z}\left|a\right\rangle\right|\varepsilon_0}{\hbar}$$

denote the Rabi frequencies that describe the coupling strength of the atom either with the x- (3.11) or z-polarized (3.12) field, respectively. With this distinction for the Rabi frequencies, the exponentials ϕ_{d_x} and ϕ_{d_z} denote the phases of the dipole matrix elements $e\left\langle b\right|u\left|a\right\rangle = \left|e\left\langle b\right|u\left|a\right\rangle\right| e^{i\phi_{d_u}}$ where $u = \tilde{x}, \tilde{z}$. Here both $\tilde{x}$ and $\tilde{z}$ refer to the internal variables, Eq. (3.1), of the atom and are the electron's relative coordinates with regard to the nucleus. The Rabi frequencies, moreover, arise naturally as non-diagonal matrix elements of the atom dipole moment if we express the interaction Hamiltonian in the $\{\left|a\right\rangle, \left|b\right\rangle\}$ basis. This, in turn,

makes the interaction Hamiltonian dependent on atomic states $|a\rangle$, $|b\rangle$ and the center-of-mass coordinate of the atom [1].

For such an effective factorization of the interaction Hamiltonian, and as described in many texts before [91–93], the two-level atom undergoes Rabi oscillations between its lower and upper states with frequency Ω_{R_x} or Ω_{R_z}, quite analogue to a spin-1/2 system in an oscillating magnetic field [109]. In contrast to the standard derivation (see, for example, Ref. [91]), however, the interaction Hamiltonian (3.16)-(3.17) now also depends on the phase $\zeta^{(||)}$ and $\zeta^{(\perp)}$ of the radiation field to account for the time- *and* space-dependency of the atom-laser interaction. In addition, some time ago an approximate technique, i.e. expansion of the exponent (1.6) in the interaction Hamiltonian, has been applied to the helium and hydrogen atoms in order to examine their coupling to an intense laser field [110].

To explore the time evolution of the atom, let us search for solutions of the time-dependent Schrödinger equation

$$H_{\text{atom+field}}\,\psi \;=\; i\hbar\frac{\partial\psi}{\partial t}\,. \tag{3.18}$$

If we utilize the (effective) factorization of the interaction Hamiltonian (3.16)-(3.17) we can use the Ansatz

$$\psi\left(\boldsymbol{r},t\right) \;=\; e^{\frac{i}{\hbar}(\boldsymbol{p}\cdot\boldsymbol{r}-\mathcal{E}t)}\left(\psi_a(\zeta)\;|a\rangle+\psi_b(\zeta)\;|b\rangle\right)\,, \tag{3.19}$$

as a solution of the Schrödinger equation. Here $\zeta\equiv\zeta^{(||)}$, $\zeta^{(\perp)}$ is the laser phase for collinear- or crossed-beam scenarios, respectively. The constant (non-relativistic) momentum $\boldsymbol{p}\equiv m\boldsymbol{v}$ of the center-of-mass of atom hereby gives rise to the space-dependent "translation factor" $e^{\frac{i}{\hbar}\boldsymbol{p}\boldsymbol{r}}$ to account for its overall motion with energy $\mathcal{E}$ within the given coordinates. This factorization of the wave function is very similar to that of laser-driven electrons (compare with Eq. (1.36)). In other words, the propagation of the two-level atom inside the field is represented as a "plane-wave" motion $e^{\frac{i}{\hbar}(\boldsymbol{p}\cdot\boldsymbol{r}-\mathcal{E}t)}$ with a modified (non-constant) amplitude $\psi_a(\zeta)\;|a\rangle+\psi_b(\zeta)\;|b\rangle$. In addition, a similar Ansatz has been employed in [111] in order to investigate Stark splitting of a three-level atom, by applying Fourier-transform of the space-dependent wave function.

In the next subsection, we solve the Schrödinger equation (3.18) by applying the following, physically relevant assumptions. We prepare the atom initially in the upper state and then employ the typical, eikonal and rotating wave approximations, for which the atom rest energy is much larger than the photon energy (EA) that, in turn, is resonant to the atomic transition energy (RWA). For light two-level atoms, both the EA and RWA are valid with high accuracy [91].

3.2.2 Solutions to the Schrödinger equation

To determine the probability amplitudes ψ_a and ψ_b for the atomic states $|a\rangle$ and $|b\rangle$, we take into account that the overall dynamics of the (plane-wave) atom-laser system remains the same for the collinear- and crossed-beam scenarios (compare Eqs. (3.16)-(3.17)), though they imply different coupling strengths and phases in the interaction Hamiltonian. For these similar Hamiltonians, in our further calculations we will adopt generic notations Ω_R, ϕ_d and ζ in order to replace the Rabi frequencies Ω_{R_x}, Ω_{R_z}, the dipole matrix element exponentials ϕ_{d_x},

[1] Hereinafter, for notational convenience we drop the "tilde" of the indices x and y at the Rabi frequencies and the exponentials of the dipole matrix elements. This will not cause a confusion since already at this step the dependence on the electron's relative coordinate is eliminated in the interaction Hamiltonian (3.16)-(3.17).

ϕ_{d_z} and the laser phases $\zeta_{||}$, $\zeta_{\perp}$, respectively. The replacement of these laser phases is justified since the solution which we construct contains terms with scalar products of the form $\boldsymbol{k}\cdot\boldsymbol{r}$ and $\boldsymbol{p}\cdot\boldsymbol{r}$ [cf. Eq. (3.19)] that, in turn, remains unchanged in any system of reference.

In order to describe the dynamics of laser-driven two-level atoms we take into account the fact that the laser phase ζ contains both, the time- and space-variables. This enables one to express the corresponding partial derivatives by the total derivative with respect to this phase

$$\frac{\partial}{\partial \boldsymbol{r}} = \boldsymbol{k}\frac{d}{d\zeta}\,, \quad \frac{\partial}{\partial t} = -\omega\frac{d}{d\zeta}\,, \quad \Delta \equiv \frac{\partial^2}{\partial \boldsymbol{r}^2} = \boldsymbol{k}^2\frac{d^2}{d\zeta^2}$$

(compare with the relativistic analogue, Eq. (1.29)). Based on this mathematical trick we can re-write the (space- and time-dependent) Schrödinger equation as an ordinary differential equation of only one variable, in a similar way as the Dirac equation has been examined earlier by Volkov [68] (see also section (1.2.2)) and by Skobelev [112, 113] who found solutions for the relativistic motion of electrons and neutrons, respectively. Such a method is for the first time applied for describing the motion of two-level atoms inside the radiation field in Refs. [82, 83]. Thus, by making use of this technique and substituting the Ansatz (3.19) into the time-dependent Schrödinger equation (3.18), we obtain the following two coupled equations

$$\boxed{\begin{aligned} \frac{\hbar^2k^2}{2m}\psi_a'' + i\hbar\,(\boldsymbol{v}\cdot\boldsymbol{k}-\omega)\,\psi_a' - E_a\psi_a + \hbar\Omega_R\,e^{-i\phi_d}\cos\zeta\,\psi_b &= 0\,,\\ \frac{\hbar^2k^2}{2m}\psi_b'' + i\hbar\,(\boldsymbol{v}\cdot\boldsymbol{k}-\omega)\,\psi_b' - E_b\psi_b + \hbar\Omega_R\,e^{i\phi_d}\cos\zeta\,\psi_a &= 0\,. \end{aligned}}$$

Here the prime denotes derivation with regard to the phase ζ and $\boldsymbol{v} = \boldsymbol{p}/m$ is the center-of-mass velocity of the atom that moves with the non-relativistic energy $\mathcal{E} = p^2/(2m)$. Similar techniques have been applied more recently also to the Mott scattering of an electron in the presence of intense single-mode laser fields [114], both within the relativistic and non-relativistic regimes. For non-relativistic electrons and neutrons, moreover, such an approach was taken in Refs. [115] and [116, 117], respectively.

Owing to the large mass m of the atom, whose rest energy mc^2 is much larger than the photon energy $\hbar\omega$, we typically have $\hbar^2k^2/(2m\hbar\omega) \leq 10^{-10}$ even for ultraviolet frequencies and can hence make use of the EA [67]. In this approximation, we will drop the first terms in the last system of equations and rewrite them in the form

$$\psi_a' + i\alpha\psi_a = i\Omega\,e^{-i\phi_d}\,\cos\zeta\,\psi_b, \tag{3.20}$$

$$\psi_b' + i\beta\psi_b = i\Omega\,e^{i\phi_d}\,\cos\zeta\,\psi_a, \tag{3.21}$$

by introducing the following notations

$$\alpha \equiv \frac{E_a}{\hbar\,(\boldsymbol{v}\boldsymbol{k}-\omega)}\,, \quad \beta \equiv \frac{E_b}{\hbar\,(\boldsymbol{v}\boldsymbol{k}-\omega)}\,, \quad \Omega \equiv \frac{\Omega_R}{\boldsymbol{v}\boldsymbol{k}-\omega}\,. \tag{3.22}$$

The denominator $\boldsymbol{v}\cdot\boldsymbol{k}-\omega$ hereby illustrates the Doppler shifted radiation frequency as seen by the moving atom [67].

Eqs. (3.20) and (3.21) describe the evolution of the probability amplitudes in EA. To find solutions for these two first-order equations, we may use the Ansatz

$$\psi_a = A(\zeta)\,e^{-i\alpha\zeta}, \tag{3.23}$$

$$\psi_b = B(\zeta)\,e^{-i\beta\zeta} \tag{3.24}$$

to bring them into the simpler form

$$A' = i\Omega\, e^{-i\phi_d}\, \cos\zeta\, e^{i(\alpha-\beta)\zeta}\, B, \tag{3.25}$$
$$B' = i\Omega\, e^{i\phi_d}\, \cos\zeta\, e^{-i(\alpha-\beta)\zeta}\, A\,, \tag{3.26}$$

in which the second terms on the left-hand side of Eqs. (3.20) and (3.21) have been eliminated. As we will see below, this re-definition (3.23) and (3.24) of the probability amplitudes facilitates the integration of Eqs. (3.25)-(3.26). In addition, we could also *decouple* these two equations by taking the second derivative with regard to the phase ζ,

$$A'' + (-i(\alpha-\beta) + \tan\zeta)\, A' + \Omega^2 \cos^2\zeta\, A = 0 \tag{3.27}$$
$$B'' + (i(\alpha-\beta) + \tan\zeta)\, B' + \Omega^2 \cos^2\zeta\, B = 0\,, \tag{3.28}$$

and for which solutions can be obtained in terms of hypergeometric functions [64]. However, in this work we are interested in laser frequencies which are nearly resonant to atomic transition frequency. Therefore, we apply RWA to obtain solutions to Eqs. (3.27) and (3.28) in terms of elementary functions.

In our further discussion, as usual, we consider frequencies (of the radiation field) which are in resonance with (or nearly resonant) to the atomic excitation, $\hbar\omega \approx E_a - E_b$. In such a *resonance* regime, it is justified to apply the RWA [cf., e.g. [92]] for which the exact solutions can be found for Eqs. (3.25) and (3.26). If the counter-rotating terms proportional to $\exp\left[\pm i\,(\alpha-\beta-1)\,\zeta\right]$ are ignored on the right-hand side, these equations take the form

$$A' = \frac{i\Omega}{2} e^{-i\phi_d} e^{i(\alpha-\beta+1)\zeta}\, B\,, \tag{3.29}$$
$$B' = \frac{i\Omega}{2} e^{i\phi_d} e^{-i(\alpha-\beta+1)\zeta}\, A\,. \tag{3.30}$$

An exact solution for A and B is then given by

$$(\mu_1-\mu_2)\, A(\zeta) = \left[A(0)\mu_1 - \frac{i\Omega}{2} e^{-i\phi_d} B(0)\right] e^{\mu_2\zeta} - \left[A(0)\mu_2 - \frac{i\Omega}{2} e^{-i\phi_d} B(0)\right] e^{\mu_1\zeta}\,, \tag{3.31}$$
$$(\mu_1-\mu_2)\, B(\zeta) = \left[B(0)\mu_1 + \frac{i\Omega}{2} e^{i\phi_d} A(0)\right] e^{-\mu_2\zeta} - \left[B(0)\mu_2 + \frac{i\Omega}{2} e^{i\phi_d} A(0)\right] e^{-\mu_1\zeta}\,, \tag{3.32}$$

with

$$\mu_{1,2} = \frac{i}{2}\left(\alpha-\beta+1\pm\delta\right)\,, \tag{3.33}$$
$$\delta \equiv \sqrt{(\alpha-\beta+1)^2+\Omega^2}\,, \tag{3.34}$$

and where $A(0)$ and $B(0)$ refer to "initial" conditions with regard to the laser phase, $\zeta = 0$. These initial conditions are fulfilled, for instance, at the origin $\boldsymbol{r} = 0$, $t = 0$ of the space and time coordinates. Owing to the existence of the phase ζ, however, the solutions (3.31) and (3.32) are more general and can be analyzed in order to explore the time- and space-dependency of the probability amplitudes explicitly, if one wishes to take into account the wave vector of the laser field and the motion of the atom as a whole. For the atom at rest ($\boldsymbol{p} = 0$) and if we also ignore the $\boldsymbol{k}$-dependence of the laser beam, i.e. simply perform a replacement $\zeta \to -\omega t$,

the solutions (3.31) and (3.32) simplify to

$$A(t) = \left\{ A(0)\left[\cos\frac{\Lambda_2 t}{2} - i\frac{\Lambda_1}{\Lambda_2}\sin\frac{\Lambda_2 t}{2}\right] + i\frac{\Omega_R}{\Lambda_2}\, e^{-i\phi_d}\, B(0)\sin\frac{\Lambda_2 t}{2}\right\} e^{i\frac{\Lambda_1 t}{2}},$$

$$B(t) = \left\{ B(0)\left[\cos\frac{\Lambda_2 t}{2} + i\frac{\Lambda_1}{\Lambda_2}\sin\frac{\Lambda_2 t}{2}\right] + i\frac{\Omega_R}{\Lambda_2}\, e^{i\phi_d}\, B(0)\sin\frac{\Lambda_2 t}{2}\right\} e^{-i\frac{\Lambda_1 t}{2}},$$

that are in full agreement with standard texts on the two-level atom [91]. Here $\hbar\Lambda_1 = E_a - E_b - \hbar\omega$ and $\Lambda_2^2 = \Lambda_1^2 + \Omega_R^2$. Using Eqs. (3.31) and (3.32), moreover, the conservation of the overall probability of the atom, namely of being in one of the two states, $|\psi_a|^2 + |\psi_b|^2 = 1$, can be verified quite easily.

Although an oscillation of the probability amplitudes ψ_a and ψ_b can be seen already from Ansatz (3.23)-(3.24), further insights are obtained if we specify the "initial" conditions for these probability amplitudes and modulate the field in a resonance regime with the atomic transition frequencies. Therefore, two remarks are in order here before we shall further examine the solutions (3.31)-(3.32) for the amplitudes $A(\zeta)$ and $B(\zeta)$. First, the initial condition for $\zeta = 0$ should be chosen properly. If we assume the atom initially to be in the upper state, we have

$$A(0) = 1\,, \qquad B(0) = 0\,, \tag{3.35}$$

for the interaction of the atom with linearly polarized field [91]. Second, we still have some freedom in general of how to choose the physical parameters, such as the momentum $\boldsymbol{p}$ of the atom, its energies E_a, E_b of the upper and lower states, the frequency ω of the coupling field as well as the Rabi frequency Ω_R. Apart from a suitable choice of the two-level atom, these parameters are often controlled by the intensity and the propagation direction of the external field(s) acting upon the atom. For example, we may readily fulfill the *resonance* condition by assuming a field with frequency ω, so that

$$E_a - E_b = \hbar\omega_{\,\mathrm{eff}} \equiv \hbar\omega\left(1 - \frac{\boldsymbol{v}\cdot\boldsymbol{n}}{c}\right),$$

and where $\boldsymbol{n} = \boldsymbol{k}/k$ is the unit vector along the propagation direction of the field, as introduced in subsection 3.1.3. This resonance condition gives rise to the simpler relation for the reduced quantities (3.22)

$$\alpha - \beta + 1 = 0\,. \tag{3.36}$$

Thence, the fast oscillating terms have the form $\pm(\alpha - \beta - 1)$.

If we substitute the initial condition (3.35) into the solutions (3.31)-(3.32) for a linearly polarized field, the *phase*-dependent probability amplitudes read as

$$A = \frac{i\mu_2}{\delta}\, e^{\mu_1\zeta} - \frac{i\mu_1}{\delta}\, e^{\mu_2\zeta}\,,$$

$$B = \frac{\Omega}{2\delta}\, e^{i\phi_d} e^{-\mu_2\zeta} - \frac{\Omega}{2\delta} e^{i\phi_d}\, e^{-\mu_1\zeta}\,,$$

and, together with the resonance condition (3.36), take the simple form

$$A = \cos\frac{\Omega\zeta}{2}\,, \tag{3.37}$$

$$B = ie^{i\phi_d}\sin\frac{\Omega\zeta}{2}\,, \tag{3.38}$$

where we have used the relations (3.33)-(3.34). Finally, if we use the Ansatz (3.19) and Eqs. (3.23)-(3.24) and then recover the corresponding expressions of generic notations Ω_R, ϕ_d and ζ, we will arrive to the desired form of the wave function of laser-driven two-level atoms in both the collinear- and crossed-beam scenarios. The orthonormalized solution of the Schrödinger equation takes the form

$$\boxed{\psi^{(||)}(\boldsymbol{r},t) \;=\; e^{\frac{i}{\hbar}(\boldsymbol{p}\cdot\boldsymbol{r}-\mathcal{E}t)}\left(e^{-i\alpha^{(||)}\zeta^{(||)}}\cos\frac{\Omega^{(||)}\zeta^{(||)}}{2}\,|a\rangle + ie^{i\phi_{d_x}}e^{-i\beta^{(||)}\zeta^{(||)}}\sin\frac{\Omega^{(||)}\zeta^{(||)}}{2}\,|b\rangle\right)} \tag{3.39}$$

that represents the state of the laser-driven two-level atom in the collinear-beam scenario with some reduced quantities [cf. Eq. (3.22)]

$$\left\{\alpha^{(||)}\,,\,\beta^{(||)}\,,\,\Omega^{(||)}\right\} \;\equiv\; \frac{\{E_a\,,\,E_b\,,\,\Omega_{R_x}\}}{\hbar\left(kv_{||}-\omega\right)}\,. \tag{3.40}$$

Whereas, in the crossed-beam scenario, the atomic state is given by

$$\boxed{\psi^{(\perp)}(\boldsymbol{r},t) \;=\; e^{\frac{i}{\hbar}(\boldsymbol{p}\cdot\boldsymbol{r}-\mathcal{E}t)}\left(e^{-i\alpha^{(\perp)}\zeta^{(\perp)}}\cos\frac{\Omega^{(\perp)}\zeta^{(\perp)}}{2}\,|a\rangle + ie^{i\phi_{d_z}}e^{-i\beta^{(\perp)}\zeta^{(\perp)}}\sin\frac{\Omega^{(\perp)}\zeta^{(\perp)}}{2}\,|b\rangle\right)} \tag{3.41}$$

with reduced quantities

$$\hbar\left\{\alpha^{(\perp)}\,,\,\beta^{(\perp)}\,,\,\Omega^{(\perp)}\right\} \;\equiv\; \frac{\{E_a\,,\,E_b\,,\,\Omega_{R_z}\}}{kv_\perp\cos(\phi_L-\phi)-\omega}\,. \tag{3.42}$$

In Eqs. (3.39)-(3.42), $p^2 = p_{||}^2 + p_\perp^2$ is the squared total momentum of the atom with its longitudinal $p_{||}$ and transverse $p_\perp$ components and the atomic velocities $v_{||} = p_{||}/m$ and $v_\perp = p_\perp/m$, respectively. The solutions (3.39) and (3.41) represent a superposition of the upper $|a\rangle$ and lower $|b\rangle$ states with $\zeta^{(||)}$- or $\zeta^{(\perp)}$-dependent coefficients. The "translation" factor $e^{\frac{i}{\hbar}(\boldsymbol{p}\cdot\boldsymbol{r}-\mathcal{E}t)}$, as mentioned above, describes the motion of the atom as a whole with momentum vector $\boldsymbol{p}$ along some (chosen) direction and energy $\mathcal{E}$.

So far, the focus of this subsection was placed on determining solutions of the Schrödinger equation (3.18) for the linearly polarized field (3.11) or (3.12). In next chapter, we will utilize the *explicit* $\boldsymbol{r}$-dependency of (exact) solutions (3.39) and (3.41) and exploit them in order to construct a *Bessel beam* of laser-driven two-level atoms.

3.3 Summary

We have examined the resonant coupling of (the beam of) two-level atoms with a laser light. For such a system, we have represented the space- and time-dependent Schrödinger equation as an ordinary differential equation of one variable by applying the known technique for relativistic Dirac equation for laser-driven electrons. We have found analytical solutions (3.39) and (3.41) for a particular coupling of the atomic motion to the radiation field by imposing physically relevant conditions, such as the eikonal, long-wave and rotating-wave approximations. These solutions are the main result of this chapter: they generalize the known wave functions for laser-driven two-level atoms to the case when both the atomic linear momentum $\boldsymbol{p}$ and the laser

wave vector $\boldsymbol{k}$ are non-zero. In our forthcoming discussion, we shall utilize this $\boldsymbol{p}$-dependence of wave functions (3.39) and (3.41) in order to extract the monoenergetic distribution of linear momenta representing the Bessel-beam state of laser-driven two-level atoms. These states will eventually enable us to calculate the probability density of atomic Bessel beams and to characterize their (field-affected) transverse structure.

In practice, the above mentioned approximations are well justified if the frequency of the electric field is nearly resonant to the two-level excitation energy (for the RWA), the laser wavelength is larger than the atomic sizes (for the LWA) and the de' Broglie wavelength of an atom is much smaller than the wavelength of the radiation field (for the EA). Of course, these approximations might fail in other systems leading to new effects. For example, if the resonance condition is not fulfilled to a sufficient degree then the RWA fails and causes the standard Bloch shift [118] or some generalized Bloch-Siegert shift [119].

Chapter 4

Twisted two-level atoms driven by a laser light

> As time goes on, it becomes increasingly evident that the rules which the mathematician finds interesting are the same as those which Nature has chosen.
>
> P.A.M. Dirac

In this chapter, we recover and expand the results of our advanced studies [82, 83] and investigate the dynamics of Bessel beams of two-level atoms that are resonantly driven by a laser light. In order to construct such field-affected atomic Bessel beams we make use of the superposition principle of the linear quantum theory and superimpose the laser-driven plane-wave atoms, obtained in the previous chapter, with well-defined monoenergetic spectrum corresponding to Bessel beams. We shall show that these atomic beams carry a non-zero OAM defined along the direction of propagation. Furthermore, we *spatiotemporally* characterize the transverse structure of such laser-driven *twisted* beams by calculating their probability density. We explicitly show that the distribution of intensity of the atomic beam remains unchanged along the propagation direction: the beam does not spread out even though it is driven by a laser field. Finally, we exhibit how one can control and manipulate the beam profile by tuning the laser intensity.

4.1 Twisted states of laser-driven two-level atoms

In the previous subsection, we have analyzed the time- and space-dependent interaction of two-level atoms with a linearly polarized laser field and have built the states (3.39) and (3.41) which describe the spatiotemporal dynamics of laser-driven atoms. In the following, we shall utilize these states in order to construct atomic Bessel beams which carry a non-zero OAM and meanwhile do not diffract along the propagation direction.

The wave function of the laser-driven two-level atom with the projection $\ell\hbar$ of the OAM on the (atomic beam) propagation axis can be constructed as a superposition of orthonormalized

solutions (3.39) and (3.41) of the time-dependent Schrödinger equation (3.18)

$$\Psi_\ell\left(\boldsymbol{r},t\right) \;=\; \int \tilde{\psi}_\ell\left(\boldsymbol{p}\right)\,\psi\left(\boldsymbol{r},t\right)p_\perp \mathrm{d}p_\perp \mathrm{d}\phi \tag{4.1}$$

over the monoenergetic cone, Eq. (1) [cf. Fig. 3a]. This step in the construction of *twisted* atomic beams is analogue to the use of twisted electrons [45, 77, 78] (see also the previous part).

4.1.1 Collinear-beam scenario

Let us start with the collinear-beam scenario for which the integration (4.1) can be carried out easily in a similar way as for the twisted state (11) of a free (scalar) particle. Indeed, by performing the same steps, i.e. substituting the state (3.39) into Eq. (4.1) and making use of the integral representation (10) of Bessel function, we obtain a *simple* form for the twisted state of a laser-driven two-level atom

$$\boxed{\begin{aligned}\Psi_\ell^{(\shortparallel)} \;=\; & e^{\frac{i}{\hbar}(p_{\shortparallel 0}z-\mathcal{E}_0 t)}e^{i\ell\varphi}J_\ell\left(\xi\right)\left(e^{-i\alpha_0^{(\shortparallel)}\zeta^{(\shortparallel)}}\cos\frac{\Omega_0^{(\shortparallel)}\zeta^{(\shortparallel)}}{2}\;|a\rangle\right.\\ & \left.+\;ie^{i\phi_{d_x}}e^{-i\beta_0^{(\shortparallel)}\zeta^{(\shortparallel)}}\sin\frac{\Omega_0^{(\shortparallel)}\zeta^{(\shortparallel)}}{2}\;|b\rangle\right).\end{aligned}} \tag{4.2}$$

Here the dimensionless transverse coordinate $\xi = p_{\perp 0}r/\hbar$ describes the width of the beam, and the reduced quantities $\alpha_0^{(\shortparallel)}$, $\beta_0^{(\shortparallel)}$ and $\Omega_0^{(\shortparallel)}$ are taken on the cone surface $p = p_0$ [cf. Eq. (3.40) and Figure 3a].

The state (4.2) is the eigenstates of the z-component of OAM operator $\hat{\ell}_z = -i\hbar\partial/\partial\varphi$ due to the presence of the vortex phase factor $e^{i\ell\varphi}$. Hence, apart from the free propagation along the z-direction, $e^{ip_{\shortparallel 0}z/\hbar}$, and the Bessel-dependency on the (dimensionless) transverse coordinate, the twisted state $\Psi_\ell^{(\shortparallel)}$ also carries a well-defined longitudinal OAM $\ell\hbar$ quite similar to the scalar [35, 120] and spin-dependent [45] electron Bessel beams.

It is obvious that when the field is switched off, i.e. $\Omega_0^{(\shortparallel)} = \zeta^{(\shortparallel)} = 0$, the free twisted state (11) is recovered. The presence of the field causes only Rabi flopping of (already) twisted two-level atoms between the upper $|a\rangle$ and lower $|b\rangle$ states and meantime does *not* influence the Bessel-squared-shape of the beam profile. Alluding to Section 4.2, let us note that the absence of the field's impact on the beam profile is quite expected since the laser phase $\zeta^{(\shortparallel)} = k_{\shortparallel}z - \omega t$ in collinear-beam scenario contributes only in the free motion of the atomic beam along the z-axis and does not contain the radial coordinate r. This is in contrast to the laser phase $\zeta^{(\perp)}$ in the crossed-beam scenario where both r and the azimuthal angle φ are involved (compare Eqs. (3.11) and (3.12)). It is the presence of r and φ that enables one to explore an intriguing dynamics of atomic twisted states in the crossed-beam scenario as we exhibit in details in our forthcoming discussion.

4.1.2 Crossed-beam scenario

So far, we have investigated the twisted state of laser-driven atoms in the collinear-beam scenario (4.2). This state involves a *stationary* Bessel-dependency $J_\ell(\xi)$ in the profile of the beam. In contrast, the crossed-beam scenario gives rise to a time-dependent atomic beam profile. To investigate this we shall evaluate the integral (4.1) by employing the solution (3.41). This integration cannot be carried out by means of exact methods since the reduced quantities

$\alpha^{(\perp)}$, $\beta^{(\perp)}$ and $\Omega^{(\perp)}$ depend on the ϕ angle [compare Eqs. (3.40) and (3.42)]. However, if we consider a *non-relativistic regime* for the propagation of the atomic beam we can easily proceed analytically. For this purpose, we again represent the scalar product in the form $\boldsymbol{p}\cdot\boldsymbol{r} = p_\perp r\cos(\phi-\varphi) + p_{||}z$ and evaluate the integral (4.1) first with respect to transverse $p_\perp$ and longitudinal $p_{||}$ components of the linear momentum

$$\Psi_\ell^{(\perp)} = \frac{e^{\frac{i}{\hbar}(p_{||0}z-\mathcal{E}_0 t)}}{4\pi i^\ell}\int_0^{2\pi}\mathrm{d}\phi\, e^{i\ell\phi}e^{i\xi\cos(\phi-\varphi)}\sum_{n=1}^{4}e^{i\mathcal{A}_n\zeta^{(\perp)}}|\mathcal{B}_n\rangle\,, \tag{4.3}$$

where the state vectors

$$|\mathcal{B}_{1,2}\rangle \equiv |a\rangle\,, \quad |\mathcal{B}_{3,4}\rangle \equiv \pm e^{i\phi_{dz}}|b\rangle$$

refer to the upper and lower levels of the atom, respectively. For the sake of brevity, moreover, we introduce the dimensionless parameters

$$\mathcal{A}_{1,2} \equiv -\alpha_0^{(\perp)} \pm \frac{\Omega_0^{(\perp)}}{2}\,, \quad \mathcal{A}_{3,4} \equiv -\beta_0^{(\perp)} \pm \frac{\Omega_0^{(\perp)}}{2}\,, \tag{4.4}$$

which carry information about the internal structure of the atom and the strength of the atom-field coupling. These parameters are given in terms of the reduced quantities $\alpha_0^{(\perp)}$, $\beta_0^{(\perp)}$ and $\Omega_0^{(\perp)}$ and are taken at the cone surface $p = p_0$.

Now we apply our assumption about the non-relativistic regime for the propagation of atomic beam and Taylor expand $\mathcal{A}_n$ ($n = 1..4$) by keeping only the terms up to the first power in $v_{\perp 0}/c$

$$\mathcal{A}_n \approx \mathcal{C}_n\left(1+\frac{v_{\perp 0}}{c}\cos(\phi_L-\phi)\right).$$

Here

$$\mathcal{C}_{1,2} \equiv \frac{2E_a \mp \hbar\Omega_{R_z}}{2\hbar\omega}\,, \quad \mathcal{C}_{3,4} \equiv \frac{2E_b \mp \hbar\Omega_{R_z}}{2\hbar\omega}$$

are dimensionless constant energies normalized to the photon energy. This expansion enables one to re-write the wave function (4.3) in a desired form

$$\Psi_\ell^{(\perp)} = \frac{e^{\frac{i}{\hbar}(p_{||0}z-\mathcal{E}_0 t)}}{4\pi i^\ell}\sum_{n=1}^{4}e^{i\mathcal{C}_n\zeta^{(\perp)}}\int_0^{2\pi}\mathrm{d}\phi\, e^{i\ell\phi}e^{i\mathcal{X}_n\cos\phi}e^{i\mathcal{Y}_n\sin\phi}|\mathcal{B}_n\rangle \tag{4.5}$$

which is appropriate for analytical integration. Here the dimensionless *coordinates*

$$\begin{aligned}\mathcal{X}_n(\xi,\varphi,t) &\equiv \xi\cos\varphi + \mathcal{C}_n\zeta^{(\perp)}\frac{v_{\perp 0}}{c}\cos\phi_L\,,\\ \mathcal{Y}_n(\xi,\varphi,t) &\equiv \xi\sin\varphi + \mathcal{C}_n\zeta^{(\perp)}\frac{v_{\perp 0}}{c}\sin\phi_L\end{aligned} \tag{4.6}$$

contain the (time-dependent) laser phase

$$\zeta^{(\perp)} = \frac{\hbar k}{p_{\perp 0}}\xi\cos(\phi_L-\varphi)-\omega t\,, \quad k \equiv k_\perp \tag{4.7}$$

that, in turn, is independent of the integration variable ϕ.

In order to calculate the integral (4.5) we introduce a new system of "Cartesian" $\boldsymbol{R}_n \equiv (\mathcal{X}_n, \mathcal{Y}_n, \mathcal{Z})$ and "cylindrical" $\boldsymbol{R}_n \equiv (\Xi_n, \Phi_n, \mathcal{Z})$ coordinates with standard transformations

$$\mathcal{X}_n \,=\, \Xi_n \cos\Phi_n\,, \quad \mathcal{Y}_n \,=\, \Xi_n \sin\Phi_n\,, \quad \mathcal{Z} \,=\, p_{\perp 0} z/\hbar\,, \tag{4.8}$$

where $\Xi_n \,=\, \sqrt{\mathcal{X}_n^2 + \mathcal{Y}_n^2}$ is the "radial" coordinate and Φ_n is the "azimuthal" angle in the $(\mathcal{X}_n, \mathcal{Y}_n)$-plane. By inserting these new coordinates in Eq. (4.5) and making use of a simple trigonometric relation, we can exploit the integral representation of the Bessel function [cf. Eq. (10)]

$$\int_0^{2\pi} \mathrm{d}\phi\, e^{i\ell\phi} e^{i\Xi_n \cos(\phi - \Phi_n)} \;\;=\;\; 2\pi i^\ell e^{i\ell\Phi_n} J_\ell(\Xi_n)$$

and obtain the final form of the twisted state of laser-driven two-level atoms in the crossed-beam scenario

$$\boxed{\Psi_\ell^{(\perp)} \;=\; \frac{1}{2} e^{\frac{i}{\hbar}(p_{||0} z - \mathcal{E}_0 t)} \sum_{n=1}^{4} e^{i\mathcal{C}_n \zeta^{(\perp)}} e^{i\ell\Phi_n} J_\ell(\Xi_n)\, |\mathcal{B}_n\rangle\ .} \tag{4.9}$$

It is important to note that we recover the free twisted state (11) if we switch off the laser field (i.e. $\zeta^{(\perp)} \to 0$), since in this case the coordinates Ξ_n and Φ_n coincide with ξ and φ, respectively, as $(\mathcal{X}_n, \mathcal{Y}_n) \to (p_{\perp 0} x/\hbar, p_{\perp 0} y/\hbar)$ [cf. Eq. (4.6)].

Equations (4.2) and (4.9) are the first main result of this chapter. They describe the laser-driven twisted two-level atom in both the collinear- and crossed-beam scenarios, respectively. Since no restriction has been made on the longitudinal $p_{||0}$ and transverse components $p_{\perp 0}$ of the atom momentum, the states (4.2) and (4.9) apply generally for scalar Bessel beams of two-level atoms *beyond* the typical paraxial approximation for both scenarios. As we stressed in Introduction, we are not interested in the normalization of these states since it does not provide too much insight in the overall dynamics of the beam. To give a hint, however, we would like to point out that these beams, can be normalized, on one hand, by integrating their squared modulus wave function in a large, but a finite cylindrical volume, as already mentioned above and also done in [65] for twisted photons. On the other hand, we could regularize the Dirac δ-function, which arises after the integration of squared Bessel functions over the whole space, by rigorously re-defining it as a limit of regular functions (e.g. Gaussian), as also mentioned in [45] for electron Bessel beams.

In the last discussion of this section, we put the emphasis on finding an "integral of motion" that describes the propagation of the laser-driven twisted atom in the crossed-beam scenario. A similar operator description of angular momentum properties of light Bessel beams has been done in [50]. Given that the photon energy and momentum are much less than the atom rest energy and transverse momentum, respectively, i.e. $\hbar\omega/(mc^2) \ll 1$ and $\hbar k/(m v_{\perp 0}) \ll 1$, we replace (4.6) with the following approximate relations

$$\begin{aligned} \mathcal{X}_n \;&\approx\; \xi\cos\varphi - \mathcal{C}_n v_{\perp 0} k t \cos\phi_L\,, \\ \mathcal{Y}_n \;&\approx\; \xi\sin\varphi - \mathcal{C}_n v_{\perp 0} k t \sin\phi_L\,, \end{aligned} \tag{4.10}$$

that are valid with high accuracy for a wide range of frequencies, from infrared to ultraviolet regions. The wave function (4.9), therefore, can be re-written as

$$\Psi_\ell^{(\perp)} \;\approx\; \sum_{n=1}^{4} \Psi_\ell^{(n)}\,, \tag{4.11}$$

$$\Psi_\ell^{(n)} \;\equiv\; \frac{1}{2} e^{\frac{i}{\hbar}(p_{||0} z - (\mathcal{E}_0 + \mathcal{C}_n \hbar\omega) t)} e^{i\ell\Phi_n} J_\ell(\Xi_n)\, |\mathcal{B}_n\rangle\ , \tag{4.12}$$

where we have replaced the laser phase (4.7) with $\zeta^{(\perp)} \approx -\omega t$. One can immediately recognize that the exponential $e^{ip_{||0}z/\hbar}$ describes the diffraction-free propagation of the beam along the z-axis. Moreover, this free propagation occurs as a sum of four scalar Bessel modes $\Psi_\ell^{(n)}$, each of which carries a quasi-energy $\mathcal{E}_0 + \mathcal{C}_n\hbar\omega$ because the atom is dressed by the field.

The notable difference between the twisted states of laser-driven (also of free) atoms in collinear- and crossed-beam scenarios is that here the Bessel function depends on the new coordinate Ξ_n and, consequently, on time (compare Eqs. (4.2), (11) with Eqs. (4.11), (4.12)). Due to this (different) dependency, the state (4.11) is no longer the eigenstate of the *conventional* OAM operator $\hat{\ell}_z = -i\hbar\partial/\partial\varphi$, instead each of the modes (4.12) represents an eigenstate of the operator

$$\hat{\mathcal{L}}_z^{(n)} \equiv -i\hbar\frac{\partial}{\partial\Phi_n}, \tag{4.13}$$

an *OAM* operator which acts in $(\mathcal{X}_n, \mathcal{Y}_n, \mathcal{Z})$ configuration space, upon which our physical system depends. It is easy to verify that this operator has the eigenvalue $\ell\hbar$, i.e.

$$\hat{\mathcal{L}}_z^{(n)}\Psi_\ell^{(n)} = \ell\hbar\Psi_\ell^{(n)}.$$

Whereas, as mentioned in the previous subsection, the states (4.2) are the eigenstates of $\hat{\ell}_z$ with the same eigenvalue $\ell\hbar$, i.e.

$$\hat{\ell}_z\Psi_\ell^{(||)} = \ell\hbar\Psi_\ell^{(||)}.$$

In addition, as one may expect the operator (4.13) coincides with the operator $\hat{\ell}_z$ when the field is switched off, $\hat{\mathcal{L}}_z^{(n)} \to \hat{\ell}_z$ (see also Eq. (4.14)).

To get a deeper insight let us now calculate the mean value of the conventional OAM operator averaged over the modes $\Psi_\ell^{(n)}$. For this purpose, we express $\hat{\ell}_z$ in terms of coordinates (4.8) by employing the relations (4.10)

$$\begin{aligned}\hat{\ell}_z &= -i\hbar\frac{\partial}{\partial\varphi} = -i\hbar\left(\frac{\partial\Phi_n}{\partial\varphi}\frac{\partial}{\partial\Phi_n} + \frac{\partial\Xi_n}{\partial\varphi}\frac{\partial}{\partial\Xi_n}\right)\\ &= -i\hbar\left[\frac{\partial}{\partial\Phi_n} + \mathcal{C}_n v_{\perp 0}kt\frac{\cos(\Phi_n-\phi_L)}{\Xi_n}\frac{\partial}{\partial\Phi_n} + \mathcal{C}_n v_{\perp 0}kt\sin(\Phi_n-\phi_L)\frac{\partial}{\partial\Xi_n}\right]. \end{aligned}\tag{4.14}$$

Let us note that a similar operator has been derived in [77] to describe the electron with non-zero OAM and helicity in the presence of a strong laser field. Furthermore, for the quantum mechanical mean value of $\hat{\ell}_z$, when normalized to the overall intensity of the mode (4.12), we obtain

$$\boxed{\langle\hat{\ell}_z\rangle = \frac{\int \mathrm{d}\boldsymbol{R}_n \left(\Psi_\ell^{(n)}\right)^* \left(\hat{\ell}_z\Psi_\ell^{(n)}\right)}{\int \mathrm{d}\boldsymbol{R}_n \left|\Psi_\ell^{(n)}\right|^2} = \ell\hbar.} \tag{4.15}$$

Here $d\boldsymbol{R}_n = \Xi_n d\Xi_n d\Phi_n d\mathcal{Z}$ is the elementary cylindrical volume in the configuration space which is related to the elementary volume in position space via $d\boldsymbol{r} = (\hbar/p_{\perp 0})^3 d\boldsymbol{R}_n$. The last two terms of the operator (4.14) do not contribute to the integral after the integration over Φ_n. As seen, the mean values of both OAM operators coincide, $\langle\hat{\mathcal{L}}_z^{(n)}\rangle = \langle\hat{\ell}_z\rangle$. This means that, apart from the diffraction-free propagation along z-axis, the state (4.11) describes a superposition of four modes (4.12) each of which carries a non-zero OAM with respect to the same axis. This is the second main result of this chapter.

To stress, again, the time-dependent profile of the beam reveals a non-trivial dependency on the transverse coordinate ξ and the azimuthal angle φ, as seen from Eqs. (4.9) and (4.12). In the next subsection, we examine this non-triviality in details and spatiotemporally characterize Bessel beams of two-level hydrogen and selected alkali-metal atoms that are resonantly driven by the laser field without the level damping.

4.2 Spatial and temporal characterization of laser-driven atomic Bessel beams

So far we have built the twisted states (4.2) and (4.9), (4.11)-(4.12) of laser-driven two-level atoms for collinear- and crossed-beam scenarios, respectively. These states can be used in order to study the space- and time-dependent profile of atomic beams inside an electromagnetic field. In this section, therefore, we put the emphasis on the crossed-beam scenario and investigate how the radial distribution and the time evolution of the probability density of laser-driven atoms are affected by the atomic beam velocity, the nuclear charge Z and the laser intensity.

To proceed with our further discussion, we define the probability density of atoms in a twisted state with a non-zero OAM $\ell\hbar$ as

$$\rho_\ell \;=\; |\Psi_\ell|^2 \,, \tag{4.16}$$

such that $\rho = 1$ for beams (3.39) and (3.41) of *non-twisted* atoms. Depending on which of the two scenarios occurs, the probability density (4.16) acquires different forms. To show this, we substitute the wave function (4.2) into Eq. (4.16) and obtain the probability density for the collinear-beam scenario

$$\rho_\ell^{(||)} \;=\; J_\ell^2\left(\xi\right) \,, \tag{4.17}$$

as a function of only the dimensionless transverse coordinate ξ. Figures 3(b,c) show the typical "non-diffracting" distribution of the probability density, Eq. (4.17), that coincides with the beam profile of field-free twisted atoms. This coincidence is due to the transverse-coordinate-independent laser phase (3.11), as also pointed out in subsection 4.1.1.

Let us now calculate the probability density in the crossed-beam scenario. By inserting the state (4.9) into Eq. (4.16), after straightforward derivations, we obtain

$$\rho_\ell^{(\perp)} \;=\; \varrho_\ell + \Delta_\ell \,. \tag{4.18}$$

Here the space- and time-dependent term

$$\boxed{\varrho_\ell \;=\; \frac{1}{4}\sum_{n=1}^{4} J_\ell^2\left(\Xi_n\right)} \tag{4.19}$$

is responsible for the Bessel-squared-type distribution of the probability density, and the term

$$\begin{aligned}\Delta_\ell \;&=\; \frac{1}{2}\cos\!\left(\frac{\Omega_{R_z}}{\omega}\zeta_\perp + \ell(\Phi_2-\Phi_1)\right) J_\ell\left(\Xi_1\right) J_\ell\left(\Xi_2\right) \\ &-\; \frac{1}{2}\cos\!\left(\frac{\Omega_{R_z}}{\omega}\zeta_\perp + \ell(\Phi_4-\Phi_3)\right) J_\ell\left(\Xi_3\right) J_\ell\left(\Xi_4\right) ,\end{aligned} \tag{4.20}$$

is a small summand that can be neglected with high accuracy under properly tuned parameters of the "atom + laser" system, as shown below. Equation (4.19) is the third main result of

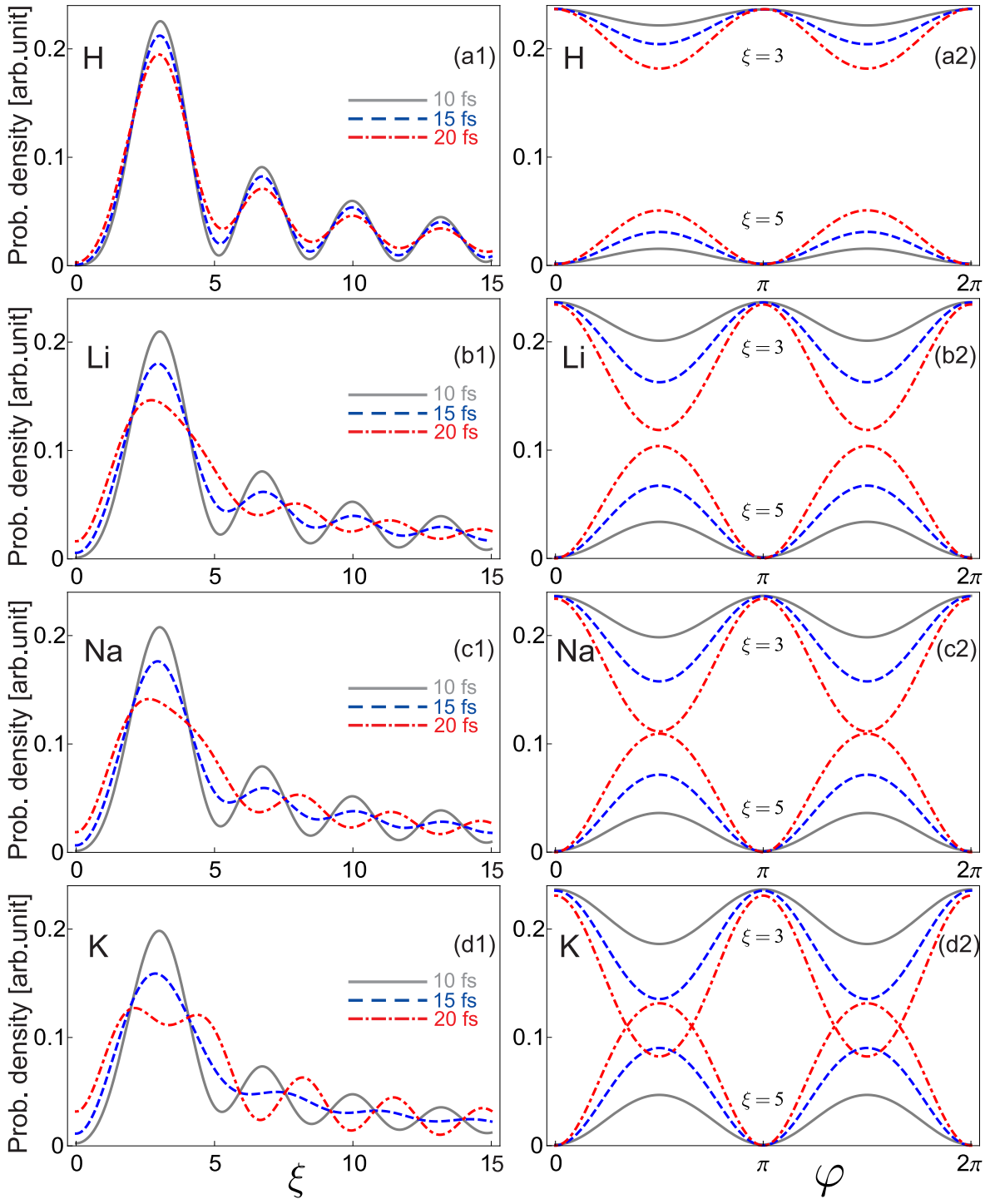

Figure 4.1: Distribution of probability density $\rho_\ell^{(\perp)}$ of laser-driven non-paraxial atomic vortex beams (in arbitrary units of the same scale) as a function of dimensionless transverse coordinate $\xi = p_{\perp 0} r/\hbar$ (left panel) and azimuthal angle φ (right panel) for $\ell = 2$, as depicted in Ref. [83]. The probability densities are shown for Bessel beams of H (a1-2) with atomic velocity $1.4 \cdot 10^6$ cm/s and of Li (b1-2), Na (c1-2), K (d1-2) with atomic velocity $0.7 \cdot 10^6$ cm/s for different propagation times 10 fs (gray solid curves), 15 fs (blue dashed curves) and 20 fs (red dot-dashed curves). The laser intensity is $I \approx 2.12 \cdot 10^{16}$ W/cm^2.

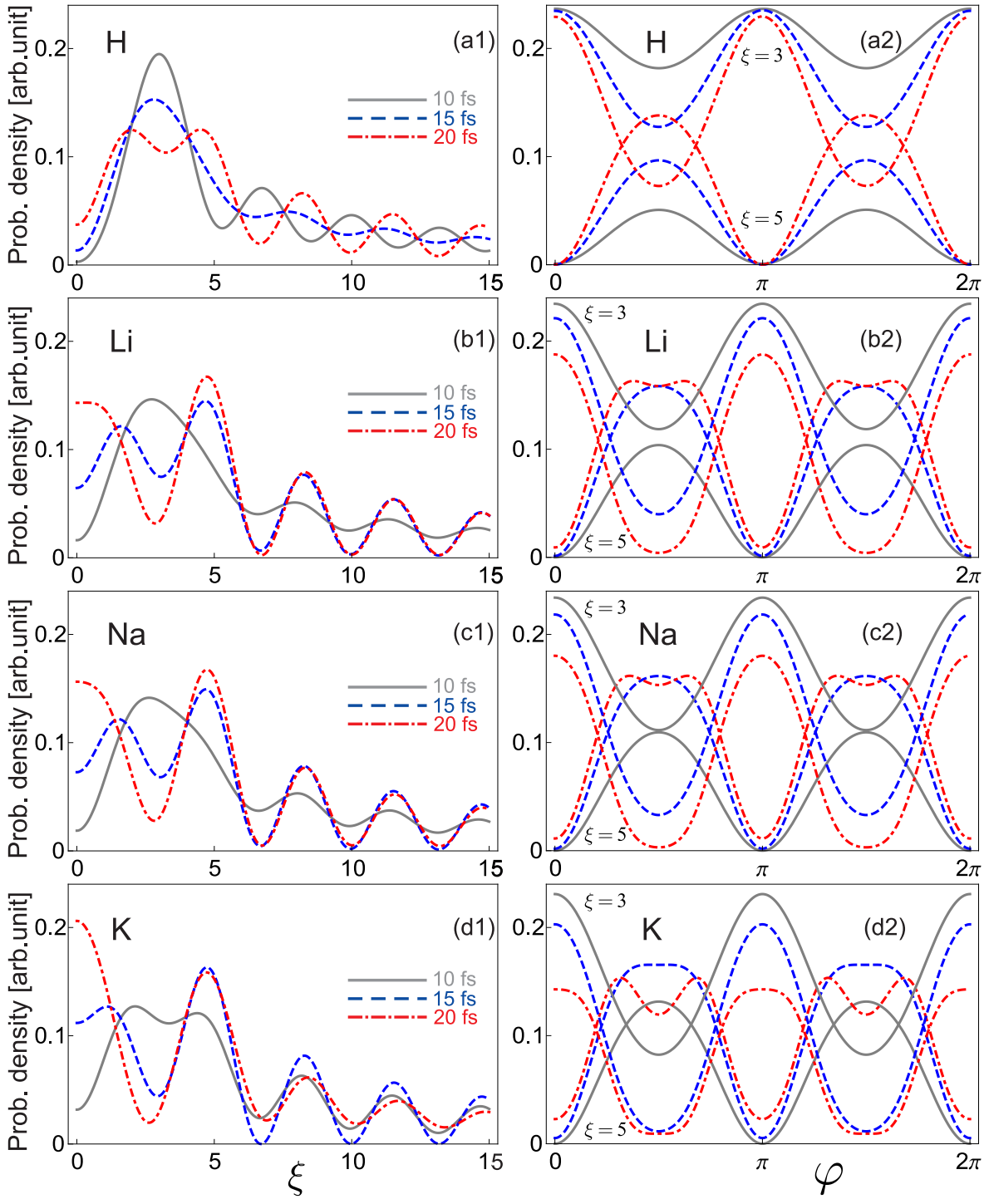

Figure 4.2: Distribution of probability density $\rho_\ell^{(\perp)}$ of laser-driven non-paraxial atomic vortex beams (in arbitrary units of the same scale) as a function of dimensionless transverse coordinate $\xi = p_{\perp 0} r/\hbar$ (left panel) and azimuthal angle φ (right panel). The atom and laser beam parameters are the same as for Fig. 4.1, apart from the laser intensity that is now doubled, i.e. $I \approx 4.24 \cdot 10^{16}$ W/cm^2.

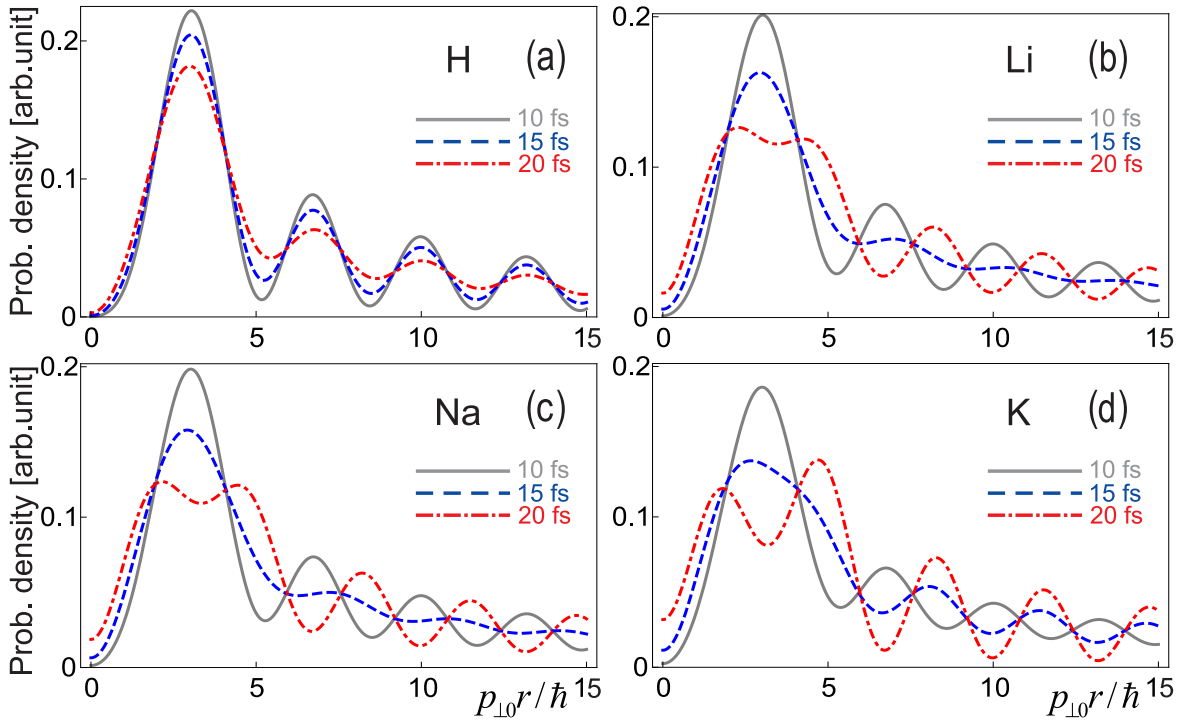

Figure 4.3: Distribution of probability density $\tilde{\varrho}_\ell^{(\perp)}$ of laser-driven non-paraxial atomic vortex beams (in arbitrary units of the same scale) as a function of the transverse coordinate $\xi = p_{\perp 0} r/\hbar$ for $\ell = 2$ and $\varphi = \phi_L$, as depicted in Ref. [82]. The parameters of the "atom + laser" system are the same as for Fig. 4.1.

this chapter; it enables one to realize the control and manipulation of atomic vortex beams via the laser field. Moreover, this formula can be sufficiently simplified along the direction that is perpendicular both to the polarization and the wave vector of the laser, i.e. when $\varphi \to \phi_L$,

$$\tilde{\varrho}_\ell^{(\perp)} \xrightarrow[\varphi - \phi_L \to 0]{} \frac{1}{4} \sum_{n=1}^{4} J_\ell^2 \left(\xi + \mathcal{C}_n \zeta_\perp \frac{v_{\perp 0}}{c} \right) .$$

In order to explore and exhibit the temporal and spatial characteristics of atomic Bessel beams let us consider, for example, two-level hydrogen, lithium, sodium and potassium, and assume that these atoms are driven on the $1s \leftrightarrow 2p$, $2s \leftrightarrow 2p$, $3s \leftrightarrow 3p$ and $4s \leftrightarrow 4p$ atomic transitions, respectively. For the sake of simplicity, however, we here also suppose that *no* decay occurs for upper levels and, thus, that no damping applies in the time-evolution of the probability amplitudes (3.37)-(3.38). For the $1s \leftrightarrow 2p$ transition, the laser and Rabi frequencies for hydrogen can be easily expressed as

$$\omega = \frac{3e^2}{8a_0\hbar}, \quad \Omega_{R_x} = \frac{2^7 a_0 e \varepsilon_0}{3^5 \hbar}, \quad \Omega_{R_z} = \sqrt{2}\Omega_{R_x} \tag{4.21}$$

by using the well-known properties of hydrogen-like ions [108]. Here a_0 is the famous Bohr radius that defines the approximate size of hydrogen atom, and is expressed via $a_0 = \hbar^2/(m_e e^2)$ in Gaussian units. For alkali-metal atoms, moreover, we make use of the known values of their spectrum [121] and dipole matrix elements [122]. Moreover, we here restrict our discussion to

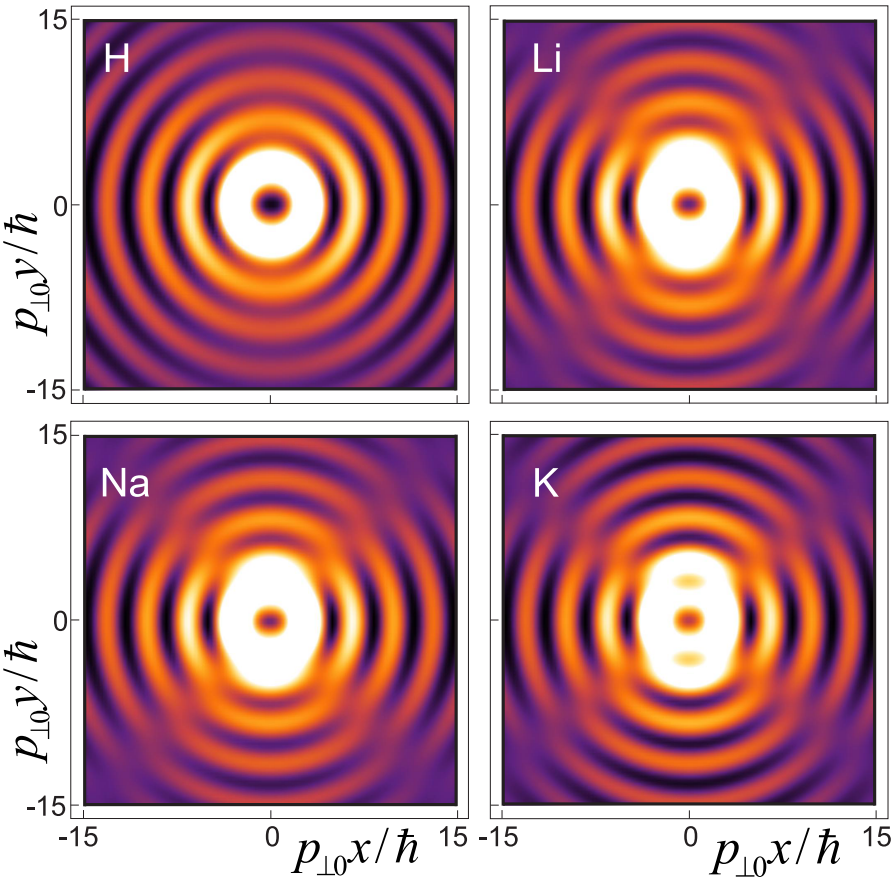

Figure 4.4: Snapshot of atomic Bessel beam profiles at $t = 20$ fs after the laser, which drives the atom, is activated [83]. The laser wave propagates along the positive direction of y-axis, the polarization vector of the field and the longitudinal linear momentum of the atomic beam point toward the reader. The Bessel beam does not change its transverse structure along the propagation axis. The parameters of the "atom + laser" system and the variation of colors are the same as in Figure 4.1 and 3(c), respectively.

low- and medium-Z atoms since the interaction Hamiltonian (3.16)-(3.17) is valid only within the LWA, i.e. when the radiation wavelength exceeds the atomic sizes.

After we have specified the type of a laser-driven two-level atom we are ready to explore both the spatial and temporal characteristics of atomic Bessel beams. When the laser field is switched off, i.e. for $t = 0$, both curves for collinear- and crossed-beam scenarios coincide. This is quite expected since in the absence of the laser radiation only a free Bessel beam propagates, as one might also expect due to the initial conditions (3.35). Once the laser is switched on, the atomic beam starts evolving in the field and changing its conventional Bessel-squared-shape. Figure 4.1 displays the probability density profile (i) at various dimensionless transverse coordinates ranging from 0 to 15 at given azimuthal angle $\varphi = \pi/3$ (left panel) as well as (ii) at various azimuthal angles ranging from 0 to 2π at given (two different values of) transverse coordinate $\xi = 3$ and $\xi = 5$ (right panel). In particular, results are shown for the nonparaxial atomic beam with transverse momentum $p_{\perp 0} = p_0/5$ and OAM $\hbar\ell = 2\hbar$ as well as for the field strength $\varepsilon = 4$ GV/cm, which corresponds to the laser intensity $I \approx 2.12 \cdot 10^{16}$

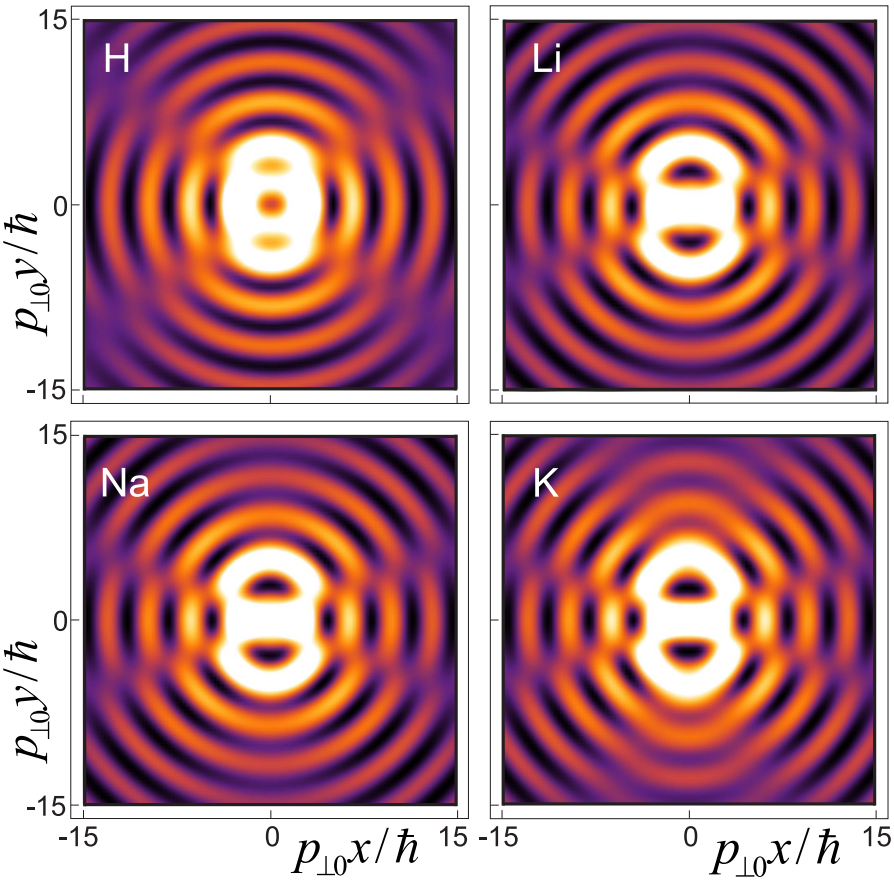

Figure 4.5: Snapshot of atomic Bessel beam profiles at $t = 20$ fs after the laser, which drives the atom, is activated. The parameters of the "atom + laser" system are the same as for Fig. 4.4, but with twice the laser intensity, $I \approx 4.24 \cdot 10^{16}$ W/cm^2.

W/cm^2, and laser propagation angle $\phi_L = \pi/2$ for three different evolution times, 10, 15 and 20 fs. Figure 4.2 displays the same distribution of the probability density but with double the laser intensity, i.e. $I \approx 4.24 \cdot 10^{16}$ W/cm^2. In addition, Fig. 4.3 shows the Bessel-squared-type profiles for the simplified $\tilde{\varrho}_\ell^{(\perp)}$ when the azimuthal dependence of the probability density is eliminated via the condition $\varphi = \phi_L$. Finally, Figs. 4.4 and 4.5 combine both the ξ- and φ-dependencies and show the *actual* profile of Bessel beams of the same atoms when they propagate 20 fs in the field.

In order to get a deeper insight about the transverse structure of atomic Bessel beams, we compare Figs. 4.1, 4.2 with density plots 4.4, 4.5. As seen in Figs. 4.1-4.3, the deviation of curves from each other increases the longer the atom propagates in the laser field. This deviation is caused by all four Bessel modes in Eq. (4.19) containing the arguments

$$\begin{aligned} \Xi_n &= \sqrt{\xi^2 + 2\xi \mathcal{C}_n \zeta^{(\perp)} \frac{v_{\perp 0}}{c} \cos(\phi_L - \varphi) + \left(\mathcal{C}_n \zeta^{(\perp)} \frac{v_{\perp 0}}{c}\right)^2} \\ &\approx \sqrt{\xi^2 - 2\xi \mathcal{C}_n v_{\perp 0} kt \cos(\phi_L - \varphi)}\,. \end{aligned} \tag{4.22}$$

The time factor $2\xi \mathcal{C}_n v_{\perp 0} kt \cos(\phi_L - \varphi)$, which involves both the transition energy and the atom-laser coupling strength, can lead to an *enhancement* of the second maximum of the

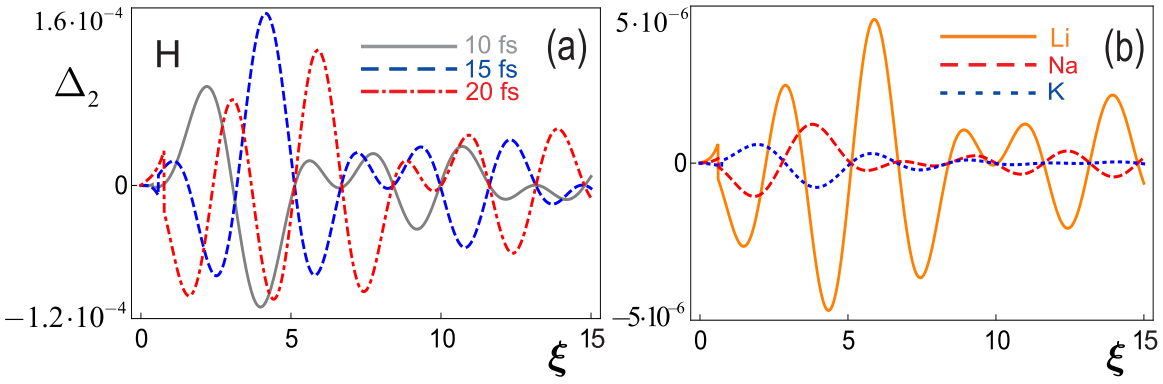

Figure 4.6: Distribution of Δ_ℓ for $\ell = 2$ as a function of dimensionless transverse coordinate $\xi = p_{\perp 0} r/\hbar$ for hydrogen with different propagation times (left panel) and for alkali-metal atoms with an evolution time 10 fs (right panel). The laser intensity is $I \approx 2.12 \cdot 10^{16}$ W/cm^2.

beam profile during its evolution in the laser field. This enhancement depends crucially on how the parameters of the "atom + laser" system are tuned. For instance, when the beam of potassium is evolved in the field within 20 fs, the first two maxima become of the same order [cf. Figure 4.1(d1)]. Such well-separated maxima can be clearly seen also (i) from Figs. 4.1(d2) and 4.2(a2-d2) in the region where the red dot-dashed curves intersect for $\xi = 3$ and $\xi = 5$ ($\varphi \sim \pi/2$) and (ii) from the white areas in the vertical direction for the potassium profile in Fig. 4.4 and for the profile of all four atoms in Fig. 4.5, especially, for the azimuthal angle $\varphi \sim \pi/2$.

Figures 4.1 and 4.2 exhibit also another intriguing feature of the beam profile in the crossed-beam scenario. This characteristic of atomic vortex beams, in fact, eventually leads to the enhancement of the second maximum of the atomic probability density. Since the term $\mathcal{C}_n v_{\perp 0} kt$ reveals different values for different atoms, this Z-dependency gives rise to a *field-induced "spread"* of the Bessel-squared-shape of the atomic probability density [cf. Figs. 4.1(b1-d1) (red dot-dashed curves) and 4.2(b1-d1) (gray solid curves)]. This behavior can be well established if we also increase the intensity of the laser beam, as shown in Fig. 4.5. However, if the beam propagates long enough inside the field, such a *broad* peak splits into two maxima (see, for example, the blue dashed and red dot-dashed curves in Figs. 4.2(b1-d1)). Both the field-induced spread and *split* of Bessel-squared-shape are rather universal and remain the same along the longitudinal coordinate z. Indeed, as both the nuclear charge and the laser intensity increase the white areas in Figs. 4.4 and 4.5 start to symmetrically spread along and against the propagation direction of the field, meanwhile keeping their shape constant along the atom propagation axis. All these non-trivial spatiotemporal characteristics are caused by the coherent interaction of atomic and laser beams and are quantitatively reflected both in the Z-dependent atomic transition energy and the atom-field interaction strength, i.e. the Rabi frequency. In addition, we note that the term Δ_ℓ does not contribute in the radial distribution of the probability density since it is effectively zero for an evolution time varying in $0, ..100$ fs and for low- and medium-Z atoms [cf. Fig. 4.6].

As, for example, in the case of optical [123, 124] and electron [124] Bessel beams, we have spatially and temporally characterized the Bessel beams of two-level atoms that are driven by the laser field. In contrast to these studies, laser-driven atomic Bessel beams, that carry

a non-zero longitudinal OAM, acquire a special type of behavior, as illustrated in Figs. 4.1-4.6, due to the coherent coupling of an atom to the laser field. To study these properties of laser-driven Bessel beams experimentally, we hope that similar methods as for the creation of electron vortex beams via nanofabricated fork-like hologram [cf. Refs. [39, 40, 43]] will be be developed for atomic systems. Moreover, for neutral atoms, that barely interact with the matter, we believe that this can be achieved by means of (i) atomic microscopes which deliver resolution of the order of few nm and (ii) laser systems which provide a resolution of the order of 10-20 fs.

4.3 Summary

The twisted states of laser-driven two-level atoms have been built and investigated, especially, in crossed-beam scenario when the laser and atomic beams are perpendicular to each other. In more detail, the interaction of a two-level atom with a linearly polarized electromagnetic field has been described by using the space- and time-dependent laser phase for solving the Schrödinger equation in a similar way as known from relativistic quantum theory of electron. Exact analytical solution to the Schrödinger equation was found within the eikonal, rotating-wave and long-wave approximations (to deal with fields nearly resonant to the two-level excitation energy and with wavelengths larger than the atomic size). Our treatment enables one to construct a twisted state of laser-driven two-level atoms with their well defined energy, transverse and longitudinal momentum components as well as the projection of the orbital angular momentum along the propagation direction. By making use of these states, detailed calculations have been performed for the distribution of the probability density of hydrogen, lithium, sodium and potassium for the $1s \leftrightarrow 2p$, $2s \leftrightarrow 2p$, $3s \leftrightarrow 3p$ and $4s \leftrightarrow 4p$ atomic transitions, respectively, *without* (level) damping. For the crossed-beam scenario, we have exhibited a non-trivial, Bessel-squared-type behavior of the beam profile that applies for both paraxial and nonparaxial regimes and depends on time. We have shown, moreover, that a possible enhancement of the second maximum of probability density may occur under a specific choice of laser and atom parameters, such as the nuclear charge, atomic velocity, the laser intensity. propagation direction and frequency that is fixed by means of the resonance condition. As we have also learnt, we are able to change the transverse distribution of the probability density of atomic vortex beams to a sufficient degree, by tuning the intensity and meanwhile keeping the propagation direction of the laser the same. Thus, we can certainly conclude that the resonantly driving laser beam acts as an apparatus which manipulates vortex beams of neutral atoms.

Outlook

Twist and shine: Controlling twisted electrons and atoms with laser light

This thesis is devoted to the theory of angular momentum representation of laser-driven matter waves. It consists of two parts. In the first part, we have developed an advanced, relativistic quantum theory for describing the interaction of *electron* vortex beams with linearly polarized laser pulses. In the second part, we have built a non-relativistic semi-classical theory to examine the resonant coupling of vortex beams of *two-level atoms* with a linearly polarized monochromatic electromagnetic wave.

Before we considered the interaction of twisted particles with laser light, we put emphasis on a special type of vortex beam, called the Bessel beam, and discussed a number of its properties in free space (or vacuum). The first (and most important) feature is that such a beam propagates with its corckscrew-like revolving wavefronts – much like "quantum" tornadoes – and possesses an orbital angular momentum along the direction of propagation, a fundamentally new degree of freedom. Another intriguing feature of Bessel beams is that they do not spread out while they propagate forward, i.e. their profile in free space remains the same at any point of the propagation axis. This means that the transverse extension of twisted wavefronts also remains constant.

To distinguish between the two types of Bessel beams, namely the scalar and vector beams, we have examined transverse distributions of their probability density and current. For vector Bessel beams, the existence of both the spin- and orbital-degrees of freedom gives rise to the intrinsic SOI. Such an interaction, in turn, causes a fine spin-dependent splitting of observables, as we have shown for the intensity distribution of relativistic EVBs. We have also demonstrated that the non-diffracting intensity profile of Bessel beams consists of concentric circles around the beam axis where the beam intensity is zero and the phase is undetermined. Despite the vortex nature of Bessel beams, however, the presence of the SOI in vector beams can lead to an enhancement of the spin-splitting of intensity at the beam center, quite in contrast to scalar beams. This fundamental difference between scalar and vector Bessel beams is due to the fact that the longitudinal OAM is well-defined only for scalar ones. Whereas, for vector Bessel beams, only the sum of longitudinal components of OAM and SAM – called TAM – represents a well-defined quantity. We have highlighted, moreover, another crucial difference between scalar and vector beams that is related to their current. The transverse current of scalar Bessel beams coils around the beam center and changes its direction depending on the sign of the OAM. In addition to this, the direction of an analogous flow of the transverse current in vector Bessel beams may vary from one circle to another.

In order to observe how the laser light can be employed for manipulating (and therefore controlling) both the electron and atom Bessel beams, we constructed an advanced theory of interaction of twisted matter waves with an electromagnetic field. To this end, we first examined the coupling of both plane-wave electrons and atoms with a plane-wave laser field. We then made use of the superposition principle of the linear quantum theory and superimposed the field-affected plane-wave electrons and atoms with well-defined amplitudes corresponding to a characteristic monoenergetic spectrum of Bessel beams. Thus, we have found new solutions for laser-driven electron and atom Bessel beams that enabled us to show the influence of a laser light upon the dynamics of twisted matter waves. In more detail, we proceeded as follows.

In chapter 1, we have studied the well-known Dirac-Volkov theory quite in details in order to describe the interaction of relativistic electrons with a plane-wave electromagnetic field. We have found the exact Dirac-Volkov wave functions that allowed us to immediately calculate the 4-current of such field-affected electrons.

In chapter 2, we have examined how twisted electrons interact with laser pulses. To this goal, we first recovered the results of Ref. [45] for field-free relativistic EVBs by finding Bessel-type solutions of the free-electron Dirac equation and calculating their 4-current. Next, we generalized these solutions to the laser-driven ones [78] and – at the meantime – showed that our new solutions contain also the Dirac-Volkov solution in the plane-wave limit for electrons [68]. Furthermore, we explicitly demonstrated that the electron OAM couples to both the SAM of electron and OAM-components of the laser field and gives rise to intrinsic spin-orbit and orbit-orbit interactions, respectively. Such (complex) interactions enabled us to illustrate that the laser light permits to control the profile of the twisted electron beam via the shift of the beam center, even in the weak-field regime. This shift can be an important observable that manifests itself in the interaction of twisted electrons with laser pulses. For example, the shift may lead to a pronounced probability to detect electrons at the (initially dark) center of the incident EVB. This phenomenon is nowadays accessible in experiments performed with paraxial EVBs.

In chapter 3, we focused on a beam of two-level atoms that are resonantly driven by a laser light. Although this fundamental problem is widely investigated in literature, we aimed to construct wave functions that explicitly contain linear momenta of both the atomic and laser beams, analogous to Dirac-Volkov wave functions for laser-driven electrons (see also chapter 1). To do so, we expressed both the space- and time-dependent Schrödinger equation as an ordinary differential equation of only one variable, the (Lorentz-invariant) laser phase, and obtained analytical solutions in physically relevant approximations, namely the LWA, EA and RWA.

The prime purpose of chapter 4 was to extend the study of field-affected electron vortex beams to atomic vortex beams which are resonantly driven by a monochromatic laser light. To the best of our knowledge, such a construction of twisted atoms have been done for the first time in our group [82, 83]. Twisted electrons and atoms are the massive twins of twisted photons: there are some similarities yet some striking differences between them. On one hand, in analogy with optical and electron vortex beams, laser-driven atomic Bessel beams carry a non-zero OAM that is defined along the direction of propagation. The non-diffracting nature of such beams also remains unchanged: their transverse structure does not vary along the beam propagation direction. On the other hand, in contrast to the profile of laser-driven EVBs, which is spatially shifted in the transverse direction and at the same time depends on the longitudinal coordinate, the profile of laser-driven atomic vortex beams experiences a field-induced broadening in the transverse direction (without being shifted) and does not depend on the longitudinal coordinate. Such a distinct behavior between electron and atom

Bessel beams is caused by the minimal coupling prescription that leads to different mechanisms of interaction of either charged or neutral particles with a laser light. This is the interaction between the atomic dipole moment and the electric field of the laser that enabled us to spatially and temporally manipulate the transverse structure of the atomic beam, by tuning the laser parameters, such as the intensity and the angular frequency. As we have shown, moreover, we are able to strongly modify the beam profile if we let the atom propagate long enough inside the (monochromatic) field. However, the time interval for such a (non-decaying) propagation should be restricted due to the finite lifetime of excited atomic level(s). Therefore, the extension of our study to this more realistic case is of a particular interest. Such a generalization would provide us a proper knowledge about the lifetime of Bessel beams of driven two-level atoms.

We would like to conclude this thesis with the following remark about future prospects of both electron and atom Bessel beams. Twisted electron beams were developed with an unique purpose to improve the magnetic mapping of materials by means of twisted electron microscopy. We believe that our results can open a new route to investigate numerous effects for these beams in external light fields for current experiments in the paraxial regime as well as for future experiments in the non-paraxial domain. It would be certainly of a broader interest to study the effective mass shift and the quantum Hall effect for relativistic twisted electrons in external fields, to also examine the interaction of both scalar and vector Bessel beams with complex systems, such as structured condensed matter, atomic clusters, etc. Our newly constructed atomic Bessel beams, in turn, can be useful for quantum communication and atomic microscopy. Since the first electron vortex beams were generated in laboratories in 2010, we are very hopeful that in the near future the atomic vortex beams can also be produced experimentally. The experimental generation of atomic vortex beams can be accomplished by employing similar production techniques already developed for both optical and electron beams with phase singularities and twisting wavefronts.

Acknowledgements

In the end of my PhD, I would like to express my sincere gratitude to people who contributed in this work, helped me during my study and supported both professionally and mentally.

First of all I wish to thank my supervisor Prof. Dr. Stephan Fritzsche for giving me the opportunity to do my PhD in the University of Heidelberg where I could accumulate a quite worthwhile experience and knowledge. I acknowledge discussions with him as well as his continuous support, encouragement and highly motivating criticism. I am grateful for the freedom I had to choose topics that I found more interesting and to develop my own ideas.

I wish to thank also Dr. Andrey Surzhykov who shared his professional experience with me in a very supportive and friendly way. I thank especially Dr. Andrea Aiello, with whom I had the opportunity to collaborate within a project at the Max Planck Institute for the Science of Light in Erlangen. The period I have spent in his group was very beneficial for me from the professional point of view. I have dramatically profited also from discussions with Dr. Jörg Evers, Dr. Rubik Petrosyan, Dr. Marco Ornigotti, Prof. Dr. Jo Verbeeck, Dr. Jörg Götte, Dr. Thomas Pfeifer, Dr. Stanislav Tashenov and Dr. Antonino Di Piazza. I would like to thank exclusively Oliver Matula for a wonderful and fruitful collaboration. His precise comments were of a special importance for my work.

Apart from these persons, I thank my examination committee members Prof. Dr. Kurt Roth and Prof. Dr. Selim Jochim for their interest in my research project. I am grateful also to my graduate schools, HGSFP and HGS-HIRe, for their genuine and beneficial support. This work could not have been fully accomplished without the support and help of my family, friends and colleagues. Particularly, I would like to express my gratitude to Vlad Hahn, Alex Kovtun, Dr. Filippo Fratini, Dr. Michael Siomau, Thorsten Jahrsetz, Dr. Sean McConnell, Dr. Denis Gonta, Hakob Avetisyan, Anna Ghazaryan, Ruben Ghazaryan, Davit Mayilyan, Chintan Shah, Dr. Pedro Amaro, Allison Pinto and, especially, to Irina Miller for their help and encouragement that played an essential role for me during these years.

Post Scriptum: Novel beams made of twisted atoms

As a postscript of the thesis, we here present the article by the science writer Sabine Louet devoted to our paper [83]. This article appeared in http://www.epj.org, as the EPJ D highlight from 01 August 2013, as well as in http://www.eurekalert.org, http://www.alphagalileo.org and http://www.sciencedaily.com.

Scientists can now theoretically construct atomic beams of a particular kind, opening the door for applications in fields like quantum communication.

Physicists have, for the first time, now built a theoretical construct of beams made of twisted atoms. These findings are about to be published in EPJ D by Armen Hayrapetyan and colleagues at Ruprecht-Karls-University Heidelberg in Germany. These so-called atomic Bessel beams can, in principle, have potential applications in quantum communication as well as in atomic and nuclear processes.

The concept for twisted atom beams stems from a similar approach with twisted photon beams, which are currently used as optical tweezers, for instance. It was later extended to twisted electron beams, which are used to improve the magnetic mapping of biological specimens and magnetic materials by means of twisted electron microscopy.

The authors focused on a beam made of twisted two-level atoms, which are driven by a laser field. They created a theoretical construct by using an equation, referred to as the non-relativistic Schrödinger equation, for atoms which are moving much slower than the speed of light. Hayrapetyan and colleagues solved this equation by taking into account the propagation directions of both the atomic and laser beams. By superimposing a multitude of plane-waves with well-defined amplitudes, they produced Bessel beams for two-level atoms that resonantly interact with the laser field.

The authors confirmed that their atomic beams fulfilled the two main characteristics of Bessel beams. First, they showed that these beams carry a non-zero orbital angular momentum, as reflected by a rotation of the beams wave front around the propagation axis in a corkscrew-like manner. Second, by taking a snapshot of the atomic beam intensity they demonstrated that these beams do not spread along the propagation axis. Moreover, they were able to control the profile of laser-driven atomic Bessel beams by tuning the parameters of both the atomic and laser beams.

Bibliography

[1] R.A. Beth, *Direct detection of the angular momentum of light*, Phys. Rev. **48**, 471 (1935).

[2] R.A. Beth, *Mechanical detection and measurement of the angular momentum of light*, Phys. Rev. **50**, 115 (1936).

[3] L. Allen, M.W. Beijersbergen, R.J.C. Spreeuw, and J.P. Woerdman, *Orbital angular momentum of light and the transformation of Laguerre-Gaussian laser modes*, Phys. Rev. A **45**, 8185 (1992).

[4] J.B. Götte, K. O'Holleran, D. Preece, F. Flossmann, S. Franke-Arnold, S.M. Barnett, and M.J. Padgett, *Light beams with fractional orbital angular momentum and their vortex structure*, Opt. Express **16**, 993 (2008).

[5] L. Allen, S.M. Barnett, and M.J. Padgett, *Optical Angular Momentum* (Institute of Physics Publishing, Bristol and Philadelphia, 2003).

[6] G. Molina-Terriza, J.P. Torres, and L. Torner, *Twisted photons*, Nature Phys. **3**, 305 (2007).

[7] J.P. Torres and L. Torner, *Twisted Photons: Applications of Light with Orbital Angular Momentum* (Wiley-VCH Verlag GmbH & Co. KGaA, Weinheim, Germany, 2011).

[8] H. He, M.E.J. Friese, N.R. Heckenberg, and H. Rubinsztein-Dunlop, *Direct observation of transfer of angular momentum to absorptive particles from a laser beam with a phase singularity*, Phys. Rev. Lett. **75**, 826 (1995).

[9] J. Arlt, K. Dholakia, J. Soneson, and E.M. Wright, *Optical dipole traps and atomic waveguides based on Bessel light beams*, Phys. Rev. A **63**, 063602 (2001).

[10] J. Arlt, V. Garcés-Cháves, W. Sibbert, and K. Dholakia, *Optical micromanipulation using a Bessel light beam*, Opt. Commun. **197**, 239 (2001).

[11] A. Mair, A. Vaziri, G. Weihs, and A. Zeilinger, *Entanglement of the orbital angular momentum states of photons*, Nature (London) **412**, 313 (2001).

[12] A. Picón, J. Mompart, J.R.Vázquez de Aldana, L. Plaja, G.F. Calvo, and L. Roso, *Photoionization with orbital angular momentum beams*, Opt. Express **18**, 3660 (2010).

[13] O. Matula, A.G. Hayrapetyan, V.G. Serbo, A. Surzhykov, and S. Fritzsche, *Atomic ionization of hydrogen-like ions by twisted photons: angular distribution of emitted electrons*, J. Phys. B: At. Mol. Opt. Phys. **46** 205002 (2013).

[14] A. Afanasev, C.E. Carlson, and A. Mukherjee, *Off-axis excitation of hydrogenlike atoms by twisted photons*, Phys. Rev. A **88**, 033841 (2013).

[15] D.G. Grier, *A revolution in optical manipulation*, Nature (London) **424**, 810 (2003).

[16] M. Padgett and R. Bowman, *Tweezers with a twist*, Nat. Photonics **5**, 343 (2011).

[17] J.W.R. Tabosa and D.V. Petrov, *Optical pumping of orbital angular momentum of light in cold cesium atoms*, Phys. Rev. Lett. **83**, 4967 (1999).

[18] V. Garcés-Cháves, D. McGloin, M.J. Padgett, W. Dultz, H. Schmitzer, and K. Dholakia, *Observation of the transfer of the local angular momentum density of a multiringed light beam to an optically trapped particle*, Phys. Rev. Lett. **91**, 093602 (2003).

[19] A. Picón, A. Benseny, J. Mompart, J.R. Vázquez de Aldana, L. Plaja, G.F. Calvo, and L. Roso, *Transferring orbital and spin angular momenta of light to atoms*, New J. Phys. **12**, 083053, (2010).

[20] M. Merano, N. Hermosa, J.P. Woerdman, and A. Aiello, *How orbital angular momentum affects beam shifts in optical reflection*, Phys. Rev. A **82**, 023817 (2010).

[21] A. Aiello, *Goos-Hänchen and Imbert-Fedorov shifts: a novel perspective*, New J. Phys. **14**, 013058 (2012).

[22] M.R. Dennis and J.B. Götte, *Topological aberration of optical vortex beams: determining dielectric interfaces by optical singularity shifts*, Phys. Rev. Lett. **109**, 183903 (2012).

[23] K.Y. Bliokh and A. Aiello, *Goos-Hänchen and Imbert-Fedorov beam shifts: an overview*, J. Opt. **15**, 014001 (2013).

[24] G. Uhlenbeck and S. Goudsmit, *Ersetzung der Hypothese vom unmechanischen Zwang durch eine Forderung bezüglich des inneren Verhaltens jedes einzelnen Elektrons*, Naturwissenschaften **13**, 953 (1925).

[25] G. Uhlenbeck and S. Goudsmit, *Spinning electrons and the structure of spectra*, Nature (London) **117**, 264 (1926).

[26] V.G. Bagrov and D.M. Gitman, *Exact Solutions of Relativistic Wave Equations* (Kluwer Academic Publ., Dordrecht, Boston, London, 1990).

[27] A. Di Piazza, C. Müller, K.Z. Hatsagortsyan, and C.H. Keitel, *Extremely high-intensity laser interactions with fundamental quantum systems*, Rev. Mod. Phys. **84**, 1177 (2012).

[28] F.H.L. Koppens C. Buizert, K.J. Tielrooij, I.T. Vink, K.C. Nowack, T. Meunier, L.P. Kouwenhoven, and L.M.K. Vandersypen, *Driven coherent oscillations of a single electron spin in a quantum dot*, Nature (London) **442**, 766 (2006).

[29] R. Hanson and D.D. Awschalom, *Coherent manipulation of single spins in semiconductors*, Nature (London) **453**, 1043 (2008).

[30] W. Gerlach and O. Stern, *Das magnetische Moment des Silberatoms*, Zeit. Phys. **9**, 353 (1922).

[31] S. Kolkowitz, Q.P. Unterreithmeier, S.D. Bennett, and M.D. Lukin, *Sensing distant nuclear spins with a single electron spin*, Phys. Rev. Lett. **109**, 137601 (2012).

[32] T.H. Taminiau, J.J.T. Wagenaar, T. van der Sar, F. Jelezko, V.V. Dobrovitski, and R. Hanson, *Detection and control of individual nuclear spins using a weakly coupled electron spin*, Phys. Rev. Lett. **109**, 137602 (2012).

[33] S. Meuren and A. Di Piazza, *Quantum electron self-interaction in a strong laser field*, Phys. Rev. Lett. **107**, 260401 (2011).

[34] S. Ahrens, H. Bauke, C.H. Keitel, and C. Müller, *Spin dynamics in the Kapitza-Dirac effect*, Phys. Rev. Lett. **109**, 043601 (2012).

[35] K.Y. Bliokh, Y.P. Bliokh, S. Savel'ev, and F. Nori, *Semiclassical dynamics of electron wave packet states with phase vortices*, Phys. Rev. Lett. **99**, 190404 (2007).

[36] M. Uchida and A. Tonomura, *Generation of electron beams carrying orbital angular momentum*, Nature (London) **464**, 737 (2010).

[37] S.N. Khonina, V.V. Kotlyar, M.V. Shinkaryev, V.A. Soifer, and G.V. Uspleniev, *The phase rotor filter*, J. Mod. Opt. **39**, 1147 (1992).

[38] M.W. Beijersbergen, R.P.C. Coerwinkel, M. Kristensen, and J.P. Woerdman, *Helical-wavefront laser beams produced with a spiral phaseplate*, Opt. Commun. **112**, 321 (1994).

[39] J. Verbeeck, H. Tian, and P. Schattschneider, *Production and application of electron vortex beams*, Nature (London) **467**, 301 (2010).

[40] B.J. McMorran, A. Agrawal, I.M. Anderson, A.A. Herzing, H.J. Lezec, J.J. McClelland, and J. Unguris, *Electron vortex beams with high quanta of orbital angular momentum*, Science **331**, 192 (2011).

[41] V.Y. Bazhenov, M.V. Vasnetsov, and M.S. Soskin, *Laser beams with screw dislocations in their wavefronts*, JETP Lett. **52**, 429 (1990).

[42] N.R. Heckenberg, R. McDuff, C.P. Smith, H. Rubinsztein-Dunlop, and M.J. Wegener, *Laser beams with phase singularities*, Opt. Quantum Electron. **24**, S951 (1992).

[43] J. Verbeeck, P. Schattschneider, S. Lazar, M. Stöger-Pollach, S. Löffler, A. Steiger-Thirsfeld, and G. Van Tendeloo, *Atomic scale electron vortices for nanoresearch*, Appl. Phys. Lett. **99**, 203109 (2011).

[44] G. Guzzinati, P. Schattschneider, K.Y. Bliokh, F. Nori, and J. Verbeeck, *Observation of the Larmor and Gouy rotations with electron vortex beams*, Phys. Rev. Lett. **110**, 093601 (2013).

[45] K.Y. Bliokh, M.R. Dennis, and F. Nori, *Relativistic electron vortex beams: angular momentum and spin-orbit interaction*, Phys. Rev. Lett. **107**, 174802 (2011).

[46] Y. Iketaki, T. Watanabe, N. Bokor, and M. Fujii, *Investigation of the center intensity of first- and second-order Laguerre-Gaussian beams with linear and circular polarization*, Opt. Lett. **32**, 2357 (2007).

[47] Y. Gorodetski, A. Niv, V. Kleiner, and E. Hasman, *Observation of the Spin-Based Plasmonic Effect in Nanoscale Structures*, Phys. Rev. Lett. **101**, 043903 (2008).

[48] K.Y. Bliokh, A. Aiello, and M. Alonso, in: *The angular momentum of light*, edited by D.L. Andrews and M. Babiker (Cambridge University Press 2013).

[49] L. Allen, V.E. Lembessis, and M. Babiker, *Spin-orbit coupling in free-space Laguerre-Gaussian light beams*, Phys. Rev. A **53**, R2937 (1996).

[50] K.Y. Bliokh, M.A. Alonso, E.A. Ostrovskaya, and A. Aiello, *Angular momenta and spin-orbit interaction of nonparaxial light in free space*, Phys. Rev. A **82**, 063825 (2010).

[51] J.B. Götte and S.M. Barnett, in: *The angular momentum of light*, edited by D.L. Andrews and M. Babiker (Cambridge University Press 2013).

[52] J. Durnin, *Exact solutions for nondiffracting beams. I. The scalar theory*, J. Opt. Soc. Am. **4**, 651 (1987).

[53] J. Durnin, J.J. Miceli Jr., and J.H. Eberly, *Diffraction-free beams*, Phys. Rev. Lett. **58**, 1499 (1987).

[54] D. McGloin and K. Dholakia, *Bessel beams: Diffraction in a new light*, Contemp. Phys. **46**, 15 (2005).

[55] S.K. Tiwari, S.R. Mishra, S.P. Ram, and H.S. Rawat, *Generation of a Bessel beam of variable spot size*, Appl. Opt. **51**, 3718 (2012).

[56] Y. Ismail, N. Khilo, V. Belyj, and A. Forbes, *Shape invariant higher-order Bessel-like beams carrying orbital angular momentum* J. Opt. **14**, 085703 (2012).

[57] A. April, *Bessel-Gauss beams as rigorous solutions of the Helmholtz equation*, J. Opt. Soc. Am. A **28**, 2100 (2011).

[58] V. Grillo, E. Karimi, G.C. Gazzadi, S. Frabboni, M.R. Dennis, and R.W. Boyd, *Generation of Nondiffracting Electron Bessel Beams*, Phys. Rev. X **4**, 011013 (2014).

[59] V. Garcés-Chávez, D. McGloin, H. Melville, W. Sibbett, and K. Dholakia, *Simultaneous micromanipulation in multiple planes using a self-reconstructing light beam*, Nature **419**, 145 (2002).

[60] M. Anguiano-Morales, A. Martínez, M.D. Iturbe-Castillo, S. Chávez-Cerda, and N. Alcalá-Ochoa, *Self-healing property of a caustic optical beam*, Appl. Opt. **46**, 8284 (2007).

[61] F.O. Fahrbach, P. Simon, and A. Rohrbach, *Microscopy with self-reconstructing beams*, Nat. Photonics **4**, 780 (2010).

[62] S. Vyas, Y. Kozawa, and S. Sato, *Self-healing of tightly focused scalar and vector Bessel-Gauss beams at the focal plane*, J. Opt. Soc. Am. A **28**, 837 (2011).

[63] X. Chu, *Analytical study on the self-healing property of Bessel beam*, Eur. Phys. J. D **66**, 259 (2012).

[64] I.S. Gradshtein and I.M. Ryzhik, *Table of Integrals, Series and Products* (Academic Press, 2000).

[65] U.D. Jentschura and V.G. Serbo, *Compton upconversion of twisted photons: backscattering of particles with non-planar wave functions*, Eur. Phys. J. C **71**, 1571 (2011).

[66] A. Messiah, *Quantum Mechanics, Vols. I & II* (Dover publications, New York, 1999).

[67] L.D. Landau and E.M. Lifshitz, *Theoretical Physics: The Classical Theory of Fields* (Vol. 2, Butterworth-Heineman, 2000).

[68] V.B. Berestetskii, E.M. Lifshitz, and L.P. Pitaevskii, *Quantum Electrodynamics* (Pergamon, Oxford, 1982).

[69] A. Bettini, *Introduction to elementary particle physics* (Cambridge University Press, New York, 2008).

[70] L.D. Landau and E.M. Lifshitz, *Theoretical Physics: Quantum Mechanics (Non-relativistic theory)* (Vol. 3, Butterworth-Heineman, 2000).

[71] C. Itzykson and J.-B. Zuber, *Quantum Field Theory* (McGraw-Hill Inc., 1980).

[72] D.M. Wolkow, *Über eine Klasse von Lösungen der Diracschen Gleichung*, Zeit. Phys. **94**, 250 (1935).

[73] J. Schwinger, *On gauge invariance and vacuum polarization*, Phys. Rev.**82**, 664 (1951).

[74] J.D. Jackson and L.B. Okun, *Historical roots of gauge invariance*, Rev. Mod. Phys. **73**, 663 (2001).

[75] J.D. Jackson, *From Lorenz to Coulomb and other explicit gauge transformations*, Am. J. Phys. **70**, 917 (2002).

[76] S. Meuren, C.H. Keitel, and A. Di Piazza, *Polarization operator for plane-wave background fields*, Phys. Rev. D **88**, 013007 (2013).

[77] D.V. Karlovets, *Electron with orbital angular momentum in a strong laser wave*, Phys. Rev. A **86**, 062102 (2012).

[78] A.G. Hayrapetyan, O. Matula, A. Aiello, A. Surzhykov, and S. Fritzsche, *Interaction of relativistic electron vortex beams with few-cycle laser pulses*, Phys. Rev. Lett. **112**, 134801 (2014).

[79] S. Demmler, J. Rothhardt, A.M. Heidt, A. Hartung, E.G. Rohwer, H. Bartelt, J. Limpert, and A. Tünnermann, *Generation of high quality, 1.3 cycle pulses by active phase control of an octave spanning supercontinuum*, Opt. Express **19**, 20151 (2011).

[80] B. Alonso, M. Miranda, Í.J. Sola, and H. Crespo, *Spatiotemporal characterization of few-cycle laser pulses*, Opt. Express **20**, 17880 (2012).

[81] M. Miranda, C.L. Arnold, T. Fordell, F. Silva, B. Alonso, R. Weigand, A. LHuillier, and H. Crespo, *Characterization of broadband few-cycle laser pulses with the d-scan technique*, Opt. Express **20**, 18732 (2012).

[82] A.G. Hayrapetyan and S. Fritzsche, *Bessel beams of laser-driven two-level atoms*, Phys. Scr. **T156**, 014067 (2013).

[83] A.G. Hayrapetyan, O. Matula, A. Surzhykov, and S. Fritzsche, *Bessel beams of two-level atoms driven by a linearly polarized laser field*, Eur. Phys. J. D, **67**, 167 (2013).

[84] *Femtosecond Laser Pulses: Principles and Experiments* edited by C. Rullière (Springer, 2005).

[85] K. Saitoh, Y. Hasegawa, K. Hirakawa, N. Tanaka, and M. Uchida, *Measuring the orbital angular momentum of electron vortex beams using a forked grating*, Phys. Rev. Lett. **111**, 074801(2013).

[86] J. Verbeeck (private communication).

[87] P. Schattschneider, B. Schaffer, I. Ennen, and J. Verbeeck, *Mapping spin-polarized transitions with atomic resolution*, Phys. Rev. B **85**, 134422 (2012).

[88] L. Clark, A. Béché, G. Guzzinati, A. Lubk, M. Mazilu, R. Van Boxem, and J. Verbeeck, *Exploiting lens aberrations to create electron-vortex beams*, Phys. Rev. Lett. **111**, 064801 (2013).

[89] A. Winkelmann and M Vos, *Site-specific recoil diffraction of backscattered electrons in crystals*, Phys. Rev. Lett. **106**, 085503 (2011).

[90] O.L. Krivanek, M.F. Chisholm, V. Nicolosi, T.J. Pennycook, G.J. Corbin, N. Dellby, M.F. Murfitt, C.S. Own, Z.S. Szilagyi, M.P. Oxley, S.T. Pantelides, and S.J. Pennycook, *Atom-by-atom structural and chemical analysis by annular dark-field electron microscopy*, Nature (London) **464**, 571 (2010).

[91] M.O. Scully and M.S. Zubairy, *Quantum Optics* (Cambridge University Press, 2001).

[92] L. Allen and J. Eberly, *Optical Resonance and Two-Level Atoms* (Dover Publications, 1987).

[93] C.J. Foot, *Atomic Physics* (Oxford University Press, 2005).

[94] C. Cohen-Tannoudji and D. Guéry-Odelin, *Advances in Atomic Physics: An overview* (World Scientific, 2011).

[95] V.V. Kozlov, Y. Rostovtsev, and M.O. Scully, *Inducing quantum coherence via decays and incoherent pumping with application to population trapping, lasing without inversion, and quenching of spontaneous emission*, Phys. Rev. A **74**, 063829 (2006).

[96] C. Champenois, G. Hagel, M. Houssin, M. Knoop, C. Zumsteg, and F. Vedel, *Terahertz Frequency Standard Based on Three-Photon Coherent Population Trapping*, Phys. Rev. Lett. **99**, 013001 (2007).

[97] D.A. Cardimona, P.M. Alsing, H. Mozer, and C. Rhodes, *Interference effects in a three-level atom in a cavity beyond the weak-field approximation*, Phys. Rev. A **79**, 063817 (2009).

[98] L-M Duan, A. Sørensen, J.I. Cirac, and P. Zoller, *Squeezing and entanglement of atomic beams*, Phys. Rev. Lett. **85**, 3991 (2000).

[99] H-R Noh and W. Jhe, *Analytical solutions of the time-dependent radiation force for a two-level atom interacting with a continuous-wave single-mode laser*, J. Opt. Soc. Am. B **27**, 1712 (2010).

[100] P. Kumar and A.K. Sarma, *Optical force on two-level atoms by few-cycle-pulse Gaussian laser fields beyond the rotating-wave approximation* Phys. Rev. A **84**, 043402 (2011).

[101] G. Andrelczyk, M. Brewczyk, Ł. Dobrek, M. Gajda, and M. Lewenstein, *Optical generation of vortices in trapped Bose-Einstein condensates*, Phys. Rev. A **64**, 043601 (2001).

[102] L.E. Helseth, *Atomic vortex beams in focal regions*, Phys. Rev. A **69**, 015601 (2004).

[103] X.-J. Liu, H. Jing, X. Liu, and M.-L. Ge, *Generation of two-flavor vortex atom laser from a five-state medium*, Eur. Phys. J. D **37**, 261 (2006).

[104] S.J. van Enk, *Selection rules and centre-of-mass motion of ultracold atoms*, Quant. Opt. **6**, 445 (1994).

[105] C. Cohen-Tannoudji, J. Dupont-Roc, and G. Grynberg, *Photons and Atoms: Introduction to Quantum Electrodynamics* (John Wiley and Sons, 1989).

[106] K. Rzazewski and R.W. Boyd, *Equivalence of interaction Hamiltonians in the electric dipole approximation*, J. Mod. Opt. **51**, 1137 (2004).

[107] J.D. Jackson, *Classical Electrodynamics* (John Wiley and Sons, 2001).

[108] B.H. Bransden and C.J. Joachain, *Physics of Atoms and Molecules* (Longman, London and New York, 1983).

[109] I.I. Rabi, *Space quantization in a gyrating magnetic field*, Phys. Rev. **51**, 652 (1937).

[110] K.J. Meharg, J.S. Parker, and K.T. Taylor, *Beyond the dipole approximation for helium and hydrogen in intense laser fields*, J. Phys. B: At. Mol. Opt. Phys. **38**, 237 (2005).

[111] G.J. Zeng, *Stark splitting of a three-level atom in circularly polarized light*, Phys. Rev. A **63**, 053408 (2001).

[112] V.V. Skobelev, *Photon emission by a neutron in a plane-wave field*, Sov. Phys. JETP **68**, 1322 (1988).

[113] V.V. Skobelev, *The process $n \to n\gamma$ in the field of a circularly polarized plane wave*, Sov. Phys. JETP **68**, 221 (1989).

[114] C. Szymanowski, V. Véniard, R. Taïeb, A. Maquet, and C.H. Keitel, *Mott scattering in strong laser fields*, Phys. Rev. A **56**, 3846 (1997).

[115] A.R. Mkrtchyan, R.M. Avakyan, A.G. Hayrapetyan, B.V. Khachatryan, and R.G. Petrosyan, *Electron-phonon interaction in polar semiconductors under the influence of laser radiation*, Arm. J. Phys. **2**, 258 (2009)

[116] A.R. Mkrtchyan, A.G. Hayrapetyan, B.V. Khachatryan, and R.G. Petrosyan, *On the possibility of high-energy neutron diffraction in a crystal in the field of laser radiation*, Phys. At. Nucl. **73**, 478 (2010).

[117] K.K. Grigoryan, A.G. Hayrapetyan, and R.G. Petrosyan, *On the neutron diffraction in a crystal in the field of a standing laser wave*, Nucl. Instr. & Meth. B **268**, 2539 (2010).

[118] F. Bloch and A. Siegert, *Magnetic resonance for nonrotating fields*, Phys. Rev. **57**, 522 (1940).

[119] J. Tuorila, M. Silveri, M. Sillanpää, E. Thuneberg, Y. Makhlin, and P. Hakonen, *Stark effect and generalized Bloch-Siegert shift in a strongly driven two-level system*, Phys. Rev. Lett. **105**, 257003 (2010).

[120] P. Schattschneider and J. Verbeeck, *Theory of free electron vortices*, Ultramicroscopy **111**, 1461 (2011).

[121] R.G. Parsons and V.F. Weisskopf, *The Spectrum of Alkali-Atoms*, Zeit. Phys. **202**, 492 (1967).

[122] H.J. Metcalf and P. van der Straten, *Laser cooling and trapping* (Springer, New York, Berlin, Heidelberg, 1999).

[123] K.B. Kuntz, B. Braverman, S.H. Youn, M. Lobino, E.M. Pessina, and A.I. Lvovsky, *Spatial and temporal characterization of a Bessel beam produced using a conical mirror*, Phys. Rev. A **79**, 043802 (2009).

[124] K.Y. Bliokh and F. Nori, *Spatiotemporal vortex beams and angular momentum*, Phys. Rev. A **86**, 033824 (2012).